Investigation of mTOR-dependent neuronal markers, gene expression and central metabolism in dopaminergic neurons

Anne-Marie Tricolici

A thesis submitted for the degree of Master of Science (by Dissertation) in Cell and Molecular Biology

Department of Life Sciences

University of Essex

Date of submission for examination: October 2023

Acknowledgements

I would like to thank my supervisor Dr. Charalampos Rallis for all the help, advice and support given during the course of my MSD degree. I would like to express my gratitude to Dr. Kumar Juhi and Dr. Legon Luc for their support, kindness and mentorship. Additionally, I would also like to thank Dr. Islam Rowshan and Dr. Alao John-Patrick, for all their help and advice. Lastly, I would like to express my gratitude to my parents and friends for the encouragement and support through my studies.

Table of contents

Abstract

The mechanistic target of Rapamycin (mTOR) signalling pathway is conserved in all eukaryotes and regulates growth and metabolism in response to environmental cues such as nutrients and growth stimuli. The heart of the pathway is the TOR kinase that operates within two functionally and structurally distinct complexes, TORC1 and TORC2. Analyses of transcriptomics data from previous experiments have identified transcription factors linked to development/metabolism i.e., LHX9 and GATA4, showing significant change in expression following pharmacological inhibition of mTOR via an ATP-competitive inhibitor of both TOR complexes, Torin1. Lim Homeobox 9 (LHX9), a transcription factor, is crucial for nervous system development and is implicated in glycolysis. The purpose of this research was to define the function of the mTOR pathway in controlling gene expression programmes during differentiation, growth and neurodegeneration as well as its implications into glycolysis by implementing a combination of pharmacological interventions in a time course manner using Torin1 (TORC1/2 inhibitor) and RapaLink-1 (TORC1 inhibitor), followed by an investigation into the role of LHX9 in mediating mTOR-dependent effects during growth and neurodegeneration. Western blotting was used to validate RNA-seq derived outputs by examining LHX9 expression in differentiated SH-SY5Y cells. The results show an upregulation of LHX9 in differentiated SH-SY5Y cells after Rapalink-1 and Torin1 treatments, with an increased expression with TORC1 and TORC2 inhibition. All the glycolytic enzymes tested did not have significant changes in differentiated SH-SY5Y cells with Torin1 and RapaLink-1 treatment showing that glycolysis runs normally. Due to these results, we can assume that LHX9 does not have an effect on glycolysis.

List of Abbreviations

4EBP1	Eukaryotic Translation Initiation Factor 4E Binding Protein 1
6-OHDA/AA	Neurotoxin 6-hydroxydopamin/ascorbic acid
AARS1	Alanyl-tRNA Synthetase 1
Akt	Protein kinase B
AlaRS	Cytosolic akanine-tRNA ligase
AMPK	AMP-activated protein kinase
ATP	Adenosine Triphosphate
Aβ	Amyloid β
AβOs	Oligomers of amyloid-β
BAT	Brown adipose tissue
c-Myc	Cellular Myc
CNS	Central nervous system
Curcumin analog C1	mTOR-independent autophagy enhancer
DA neurons	Midbrain dopaminergic neurons
DEG	Differentially expressed genes
Deptor	DEP domain containing mTOR interacting protein

eIF4A	Eukaryotic initiation factor-4A
eIF4E	Eukaryotic translation initiation factor 4E
eIF4G	Eukaryotic initiation factor 4 gamma
ER stress	Endoplasmic reticulum stress
ER	Endoplasmic reticulum
ETC	Electron transport chain
FKBP12	FK506 binding protein (FKBP)12
FOG	Friend of GATA
FoxO	Forkhead box transcription factors class O
FoxO1/3a	Forkhead transcription factor O subfamily member 3a
GAP	GTPase-activating protein
GAPDH	Glyceraldehyde-3-phosphate dehydrogenase
GATA4	GATA Binding Protein 4
GB	Glioblastoma
GBM	Glioblastoma Multiforme
GK	Glucokinase
GO	Gene Ontology
GTP	Guanosine-5’-triphosphate

Hcrt neurons	Hypocretin neurons
HI	Hypoxia/ischemia
HK1	Hexokinase 1
HK2	Hexokinase 2
IF	Immunofluorescence
iPSC	Induced pluripotent stem cells
IRXG	Iroquois Homeobox 6 gene
KO	Knockout
LC3	LC3-phosphatidylethanolamine conjugate
LDHA	Lactate dehydrogenase A
LHX9	LIM Homeobox 9
LIM-hd	LIM homeodomain
LiRiKO	Liver-specific rictor knockout
LMO	LIM only proteins
MLN0128	Sapanisertib, mTOR inhibitor
mLST8	Mammalian lethal with SEC13 protein 8
mSin1	Mammalian stress-activated protein kinase-interacting protein 1

mTOR	Mammalian/Mechanistic Target of Rapamycin
mTORC1	Mammalian Target of rapamycin complex 1
mTORC2	Mammalian Target of rapamycin complex 2
Myc	MYC Proto-Oncogene
NADH	Nicotinamide Adenine Dinucleotide (NAD) + Hydrogen (H)
NRVMs	Neonatal Rat Ventricular myocytes
OA	Okadaic Acid
OS	Oxidative Stress
Oxphos	Oxidative phosphorylation
PD	Parkinson's disease
PDH	Pyruvate dehydrogenase
PDK1	Pyruvate Dehydrogenase Kinase 1
PDK-1	3-phosphoinositide-dependent protein kinase-1
PFKP	Platelet-type phosphofructokinase
PGK1	Phosphoglycerate kinase 1
PI3K	Phosphoinositide 3-kinase
PIKK	Phosphatidylinositol kinase-related kinase
PIP2	Phosphatidylinositol (4,5)-bisphosphate

PIP3	Phosphatidylinositol (3,4,5)-trisphosphate
PKCα	Protein kinase C alpha
PKM1/2	Pyruvate kinase isozymes M1/M2
PKM2	Pyruvate kinase M2
PRAS40	Proline rich Akt substrate of 40 kDa
Protor	Protein observed with Rictor-1
PTEN	Phosphatase and tensin homolog
PTMs	Posttranslational modifications
RA	Retinoic acid
RAFT1	Rapamycin and FK506-binding protein (FKBP)-target 1
RAG	Ras-related GTPase
Raptor	Regulatory-associated protein of mTOR
Ras	Reticular activating system
RCC	Renal cell carcinoma
Rheb	Ras homolog enriched in brain
Rictor	Rapamycin-insensitive companion of mTOR
Rig-1	Retinoic acid-inducible gene I
ROS	Reactive oxygen species

RPTC	Renal Proximal Tubular Cells
S6K	Ribosomal S6 kinase
SH2	Src homology 2
siRNA	Small interfering RNA
SLC7A5	Solute Carrier family 7 member 5
SREBP1c	Sterol regulatory element-binding protein 1c
TCA	Tricarboxylic acid cycle
TOR	Target of rapamycin
TORC1	Target of rapamycin complex 1
TORC2	Target of rapamycin complex 2
TSC1	Tuberous sclerosis 1
TSC2	Tuberous sclerosis 2
Tti1	TELO2 Interacting Protein 1
Tti2	TELO2 Interacting Protein 1
UBF	Upstream Binding Factor
UPR	Unfolded Protein Response

1. Introduction

1.1. Target of Rapamycin (TOR) discovery

Rapamycin was discovered by the purification of an antifungal metabolite that was found in a soil sample from Easter Island. Rapamycin was later found to have immunosuppressive and anti-proliferative effects on mammalian cells (Wullschleger *et al.*, 2006). Another step towards understating rapamycin's pharmacological activity was the uncovering of the interaction between rapamycin and FKBP12 (FK506-binding protein 12) (Schreiber, 1991). Following these breakthrough discoveries, in yeast it was shown that disruption of *TOR1* and *TOR2* genes mimicked the effects of rapamycin by inducing cell growth arrest (Kunz *et al.*, 1993). In a study conducted by Heitman *et al.* (1991), target of rapamycin (TOR) was identified by the TOR1-1 and TOR2-1 mutations in the budding yeast *Saccharomyces cerevisiae* that confer resistance to rapamycin's growth inhibitory properties. Moreover, it was demonstrated that rapamycin toxicity is dependent on FKBP12. Therefore, a complex is formed between rapamycin and FKBP12 which then binds and inhibits TOR. Mammalian TOR (mTOR) was discovered after RAFT1 protein (rapamycin and FK506-binding protein (FKBP)-target 1) also known as FRAP was isolated and shown to interact with FKBP12-rapamicyn complex. Furthermore, it was established that FKBP12-rapamycin directly targets a mammalian TOR homolog (Sabatini *et al.*, 1994). Two TOR genes (*TOR1* and *TOR2*) are present in the budding yeast *Saccharomyces cerevisiae* while in mammals there is only one *mTOR* gene (Wullschleger *et al.*, 2006).

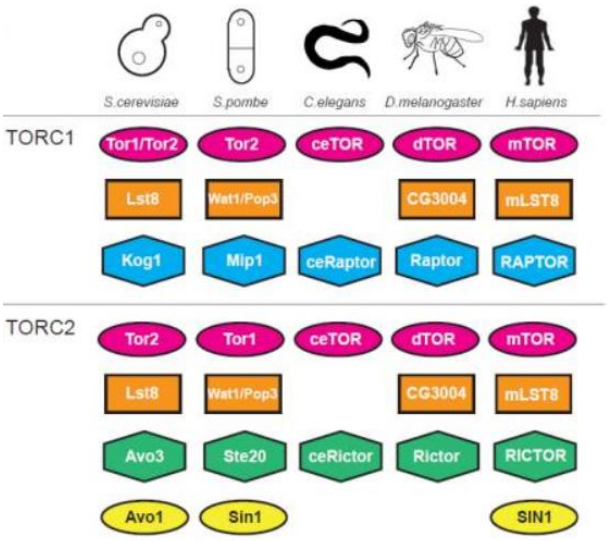

Figure 1: The implication of TOR complexes in different organisms. The subunits of both TORC1 and TORC2 have been found across several model organisms hence showing that within eukaryotes, TOR pathway is highly conserved (Bjedov and Rallis, 2020).

1.2. mTORC complexes

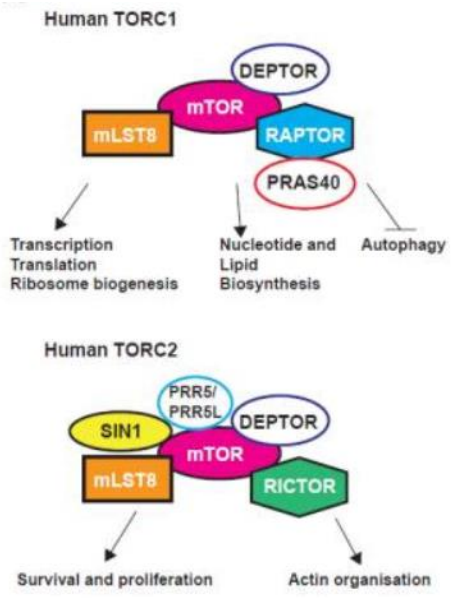

Figure 2: Mammalian Target of Rapamycin complexes. Picture **A** depicts the mammalian target of rapamycin complex 1 (mTORC1) with the components it comprises, as well as the processes the complex controls (shown by the arrows). Picture **B** depicts mTOR complex 2 with the components it comprises, as well as the processes the complex controls (shown by the arrows) (Bjedov and Rallis, 2020).

The idea of TOR forming two different complexes, emerged after findings in yeast and provided evidence that TOR has functions that are both rapamycin-sensitive and rapamycin- insensitive (Zheng *et al.*, 1995). mTOR is a serine/threonine protein kinase which is a member of the phosphatidylinositol kinase-related kinase (PIKK) family and that interacts with diverse proteins to generate unique mTOR complexes, those being mTOR complex 1 (mTORC1) and mTOR complex 2 (mTORC2) (Laplante and Sabatini, 2012; Wullschleger *et al.*, 2006). TORC2 was shown to be resistant to acute rapamycin treatment because of FKBP-rapamycin inability to bind to it, therefore, it was named rapamycin-insensitive. On the other hand, TORC1 has been proven to be rapamycin-sensitive, due to FKBP-rapamycin binding to TORC1 therefore implying that rapamycin inhibits TORC1 signalling only (Loewith *et al.*, 2002). The following catalytic mTOR subunits: the DEP domain containing mTOR interacting protein (Deptor) (Peterson *et al.*, 2009), the mammalian lethal with SEC13 protein 8 (mLST8) (Jacinto *et al.*, 2004), and the Tti1/Tel2 complex (Kaizuka *et al.*, 2010), are all shared by both mTOR complexes. Apart from these shared substrates, each mTORC complex contains other unique substrates that are specific to it. For instance, mTORC1 consists of the Akt substrate 40 kDa

(PRAS40) and the mTOR regulatory-associated protein (Raptor). However, mTORC2 comprises of Rictor which is known to be the mTOR rapamycin-insensitive companion, Protor that is the protein seen along with Rictor and mSin1 also named the mammalian stress-activated MAP kinase-interacting protein 1 (Laplante and Sabatini, 2012; Takei and Nawa, 2014).

1.3. Regulation of mTORC1

mTORC1 responds to several variations in cells and regulates numerous cell activities therefore being a critical integrator of stimuli, such as nutrients, growth factor availability and stress (Zhang *et al.*, 2021). Growth factors, particularly insulin and insulin-like growth factor 1, have powerful anabolic effects and are essential in promoting cell growth, metabolism, and survival (Laplante and Sabatini, 2013). mTORC1 promotes protein synthesis, lipid biosynthesis, and metabolism when is active, while decreasing autophagy in order to start cell growth and proliferation (Laplante and Sabatini, 2013).

A significant upstream regulator of mTORC1 is the TSC1/TSC2 (hamartin–tuberin) protein complex (Huang and Manning, 2008). The functional complex is formed by the gene products of TSC1 and TSC2 which prevents S6K and 4EBP1, two important translational regulators, from being phosphorylated (Inoki *et al.*, 2003b). TSC2 is a TSC complex component that mostly modulates the mTORC1 signal and acts as a GTPase-activating protein (GAP) towards Ras homologue enriched in brain (Rheb) which is a Ras family GTPase that stimulates the phosphorylation of S6K and 4EBP1. Rheb's GTP-bound form engages directly with mTORC1 and significantly increases its kinase activity. Considering

that TSC2 functions as a Rheb GAP, it adversely regulates mTORC1 by inactivating Rheb. Furthermore, in order to regulate cell growth, Rheb works upstream of mTOR and downstream of TSC1/TSC2 (Inoki *et al.*, 2003a).

Energy signals and growth factors are the key regulators of the TSC which is a crucial component of the cellular energy response pathway. The AMP-activated protein kinase (AMPK) functions upstream of the TSC1/TSC2 and it phosphorylates TSC2 which increases its activity when energy is lacking (Inoki *et al.*, 2003b). In reaction to energy deprivation, AMPK phosphorylates TSC2 which is necessary for translation regulation and cell size control. Furthermore, the AMPK-dependent phosphorylation of TSC2 primes cells for an adverse growth environment and prevents cell death (Inoki *et al.*, 2003b). The mTOR binding partner, raptor is directly phosphorylated by AMPK on two serine residues that are well conserved, which results in 14-3-3 binding to raptor (Gwinn *et al.*, 2008). The inhibition of mTORC1 and cell cycle arrest which is promoted by energy stress and dependent on raptor’s phosphorylation by AMPK. On the other hand, PRAS40's phosphorylation that is mediated by Akt causes it to bind to 14-3-3 and activate mTORC1. Moreover, AMPK phosphorylation sites located in raptor have been established to be very important in AMPK's function as a metabolic checkpoint (Gwinn *et al.*, 2008).

Due to their ability to catalyse the formation of phosphatidylinositol-3, 4, 5-trisphosphate (PIP3) from phosphatidylinositol-4, 5-bisphosphate (PIP2), the class IA PI3K enzymes are the most important for activation of the PI3K/Akt/mTOR pathway. PI3K is activated by Src homology 2 (SH2) domains interacting with phosphotyrosine residues located on activated growth factor receptors or by direct contact with activated Ras. The essential

downstream kinases PDK-1 and Akt, as well as their activation is dependent on the production of PIP3 and PIP2 (Hassan *et al.*, 2013).

mTORC1 is activated by insulin and growth stimuli via a route involving class I PI3K and Akt, its downstream effector, as well as a protein kinase that phosphorylates directly numerous serine and threonine residues on TSC2 which is found within the TSC complex. Through the PI3K-Akt pathway insulin activates mTORC1 which leads to the inhibition of the TSC complex allowing Rheb, an important mTORC1 stimulator, to be activated. Insulin acutely induces TSC complex separation from Rheb at the lysosomal surface, which necessitates direct phosphorylation of TSC2 by Akt (Menon *et al.*, 2014). mTORC1 activity suppresses growth factor activation of PI3K via negative feedback mechanisms. This is notably apparent in tumours and cells absent of the TSC1-TSC2 complex, where constitutive activation of mTORC1 is at least partially to blame for the severe attenuation of Akt signalling. The effect of mTORC1 signalling upon both PI3K and Akt serves as a negative feedback loop in normal cells to monitor and restrict Akt signalling (Huang and Manning, 2009). Moreover, Akt connects both mTORC1 and mTORC2 as a downstream target of mTORC2 (Huang and Manning, 2009).

There has been identified that mTORC1 has the following direct downstream targets: the ribosomal protein S6 kinase 1 (S6K1) and the eukaryotic translation initiation factor 4E-binding protein 1 (4EBP1). These two targets are phosphorylated by mTORC1 which results in protein synthesis. The following initiation factors: eIF4E, eIF4G, and eIF4A9 are responsible for making up the eIF4F complex. Therefore, eIF4E binds to the 5′ cap and recruits eIF4G and eIF4A to form the eIF4F complex (Ma and Blenis, 2009). When 4E-BP1 is phosphorylated by mTORC1, its separation from eukaryotic translation initiation

factor 4E (eIF4E) occurs. After 4E-BP1 dissociation, eIF4G attaches to eIF4E and triggers 5′ cap-dependent translation (Ghosh and Kapur, 2017). The S6Ks downstream of mTORC1 are activated when they get phosphorylated, while the 4E-BPs are inhibited and released from eIF4E at the 5' cap of mRNAs when they get phosphorylated (Ma and Blenis, 2009). Interestingly enough, even though the activation of S6K and inhibition of 4E-BP promote protein synthesis, it has been suggested that they regulate cell growth and proliferation differently. Ohanna *et al.* (2005) showed in their study that myoblast cell proliferation is unaffected by the deletion of S6K1, but myoblast size is decreased to a similar degree as when mTOR is inhibited by rapamycin. Furthermore, it was also stated that cell cycle is controlled through two distinct paths by Akt and mTOR, but both are independent of S6K. Therefore, this study emphasizes that cell cycle progression is not controlled by S6K, but cell size is. Another study provided evidence on the differences exerted by 4E-BPs on cell proliferation and cell growth. It was shown that despite having no impact on cell size, 4E-BPs prevented cell proliferation by blocking mRNAs translation which have the function to encode proteins that promote proliferation and proteins implicated in cell cycle progression (Dowling *et al.*, 2010). In a study conducted by Hannan *et al.* (2003) it was revealed that mTOR-stimulated ribosomal DNA (rDNA) transcription requires the activity of S6K1 and is predominantly mediated by phosphorylation of the rDNA transcription factor UBF’s carboxy-terminal activation domain. Hence in this study it was stated that, S6K1 activation and UBF phosphorylation are necessary for mTOR to function as a key regulator of ribosome biogenesis. mTORC1’s downstream targets mS6K1 and 4E-BP were shown to have quite a unique influence on the central nervous system (CNS), specifically on axon regeneration. Evidence provided in this study states that axon regeneration promotion requires only S6K1 activation and not 4E-BP inhibition.

Nevertheless, phosphatase and tensin homologue (PTEN) deletion-induced axon regeneration that necessitates the inhibition of 4E-BP (Yang *et al.*, 2014).

1.4. Regulation of mTORC2

In comparison to mTORC1, the mTORC2 pathway is significantly less understood. Nutrients have no effect on mTORC2 signalling, while growth factors like insulin do, but through poorly understood mechanism(s) that necessitate PI3K (Laplante and Sabatini, 2012) mTORC2 works largely as an effector of insulin/PI3K signalling, in contrast to mTORC1. The mTORC2 subunit mSin1, like most PI3K-regulated proteins, includes a phosphoinositide-binding PH domain that is required for insulin-dependent control of mTORC2 activity (Saxton and Sabatini, 2017). PIP3 has been found to be an mTORC2 direct upstream activator (Liu *et al.*, 2015). In the mTORC2 complex, the mTOR active site is predominantly mediated by SIN1's PH domain as well as the attachment of Sin1-PH to mTOR kinase domain under non-stimulated conditions which leads to Akt, an mTORC2 substrate, to have restricted access to the mTOR active site for both phosphorylation and activation. When PI3K is activated by insulin or grow factors, it produces PIP3 which binds to Sin1-PH directly with the help of three different residues. This results in a decreased interaction between Sin1-PH and mTOR kinase domain thus mTOR active site is exposed to Akt for activation (Liu *et al.*, 2015). Another study (Yang *et al.*, 2015) revealed that phosphorylation of SIN1 creates a positive feedback loop between Akt and mTORC2. Thorough analysis conducted on SIN1 phosphorylation in response to Akt, S6K, and mTOR inhibition in different cell lines, identified that Akt is the primary kinase in charge of the SIN1 phosphorylation. Furthermore, the Akt-mTORC2

signalling branch is activated as following: the activity of Akt kinase is increased when Akt is phosphorylated at T308 by PDK1. SIN1 gets phosphorylated at T86 by Akt which increases mTORC2 kinase activity, resulting in mTORC2 phosphorylating Akt S473, enabling full Akt activation (Yang *et al.*, 2015).

An experiment conducted by Zinzalla *et al.* (2011) on melanoma and colon cancer cells found that there is an association between mTORC2 and ribosomes. Insulin-stimulated PI3K signalling promoted the binding of mTORC2 to ribosomes, implying that ribosomes directly activate mTORC2. Adaptor Protein Grb10 has been found to be an insulin signalling negative regulator found upstream of Akt and mTORC2 that gets phosphorylated and activated by mTORC1. This further shows that, because of the existence of a negative feedback loop occurring among mTORC1 and insulin signalling, it results in mTORC2 signalling being regulated by mTORC1 (Yu *et al.*, 2011).

mTORC2 regulates proliferation and survival predominantly through phosphorylating AGC (PKA/PKG/PKC) protein kinase family members (Saxton and Sabatini, 2017). The involvement of mTORC2 in actin cytoskeleton was shown by Sarbassov *et al.* (2004) where they identified that raptor-mTOR complex controls the phosphorylation of Protein Kinase C α (PKCα) as well as the actin cytoskeleton. Nevertheless, another key role of mTORC2 is the activation and phosphorylation of Akt, that is known to be a very important effector of the PI3K signalling (Sarbassov *et al.*, 2006). In a study conducted by Jacinto *et al.* (2006) it was demonstrated that SIN1-rictor-mTOR function in Akt-Ser473 phosphorylation is needed for TORC2 activity but not for TORC1 function in cell survival. Moreover, FoxO1/3a was the only subset of Akt targets in vivo that was negatively impacted by the faulty Ser473 phosphorylation. Additional Akt targets such as TSC2 and

GSK3, as well as S6K and 4E-BP1 which are TORC1 downstream effectors, were unaffected.

1.5. mTORC complexes involvement in glycolysis

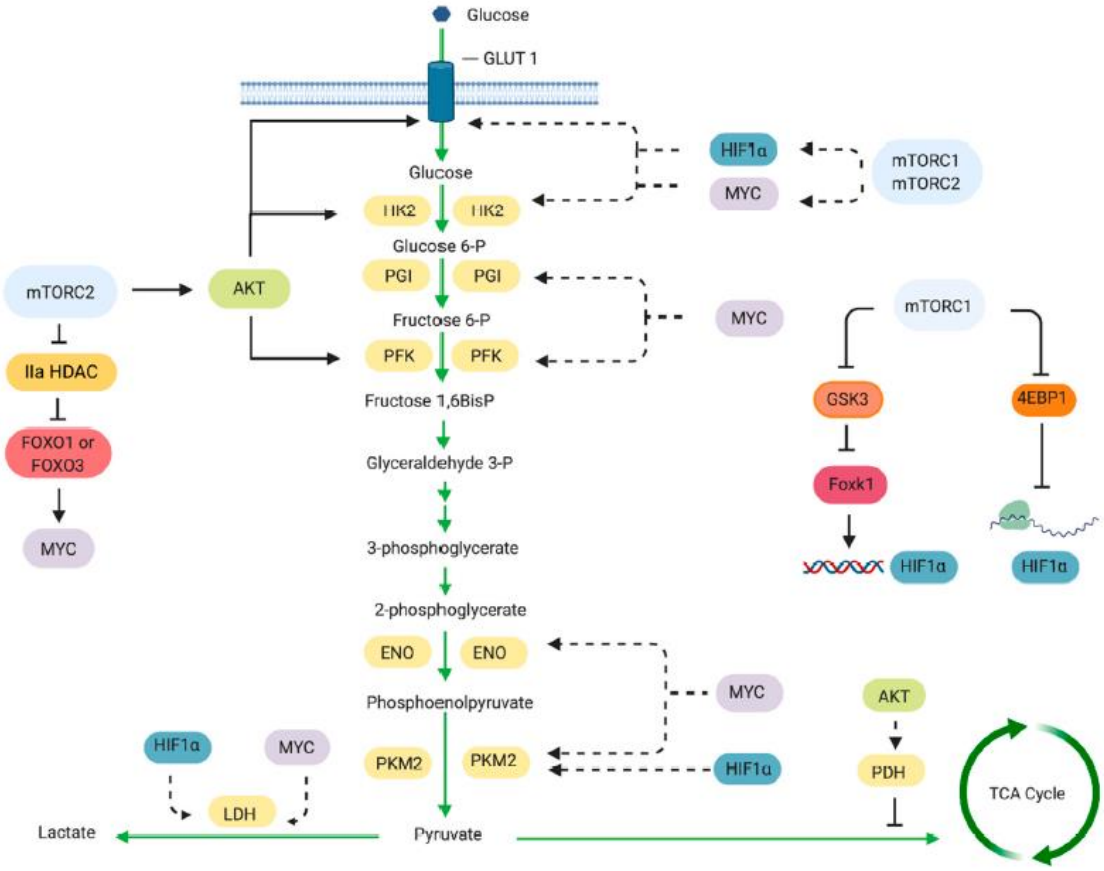

Figure 3: mTORC complexes involvement in glycolysis. Both mTOR complexes regulate glycolysis. mTORC1 controls glycolysis though HIF1 and MYC transcription factors. HIF1 expression is regulated by mTORC1 at both transcriptional and translational level. Therefore, when mTORC1 inhibits GSK3 and represses Foxk1 phosphorylation this leads to the stimulation of HIF1 transcription. Inhibition of the 4E-BP1, a downstream

target of mTORC1, plays a crucial role in the control of HIF1α translation. mTORC1 regulation of MYC has not been characterised yet. mTORC2 regulates glycolysis through the Akt substrate. mTORC2 controls MYC expression by inactivating the Class IIa histone deacetylases, which in turn regulates the acetylation of FoxO1 and FoxO3 transcription factors (Magaway *et al.*, 2019).

Düvel *et al.* (2010) demonstrate that mTORC1 activation is enough to promote particular metabolic pathways such as glycolysis, the oxidative arm of the pentose phosphate pathway, and *de novo* lipid production. mTORC1 signalling elevates HIF1α protein levels by boosting mRNA translation from its 5' UTR, and that the increase occurred is dependent on 4E-BP1 inhibitory phosphorylation. Furthermore, it was revealed that both sterol regulatory element-binding protein (SREBP1 and SREBP2) are necessary for mTORC1-induced expression of fatty acid as well as sterol biosynthesis genes. Additionally, both SREBP1 and SREBP2 were found to increase proliferation downstream of mTORC1, and their activation is mediated by S6K1 (Düvel *et al.*, 2010). mTORC2 has been identified to play an Akt-independent role in controlling glycolytic metabolism in cancer. Additionally, the expression of the cancer cell metabolism regulator c-Myc as well as glycolysis in glioblastoma cells are both regulated by mTORC2 via FoxO acetylation (Masui *et al.*, 2013). mTORC2 maintains thermogenesis in brown adipose tissue (BAT) through uptake of glucose and glycolysis induced by Akt. Furthermore, β-adrenergic stimulation leads to the activation of mTORC2 in brown adipocytes. In BAT, cytosolic hexokinase was particularly activated by mTORC2 and is needed for cold-induced

glucose uptake and glycolysis, as well as for the preservation of energy homeostasis during cold stress. Therefore, mice deficient of mTORC2 were found to be hypothermic, exhibiting enhanced sensitivity to cold and having defective cold induced glucose uptake and glycolysis (Albert *et al.*, 2016). In the liver-specific rictor knockout (LiRiKO) mice, loss of mTORC2 results in increased gluconeogenesis while glycolysis, glycogen synthesis, and lipogenesis in the fed state were decreased. Loss of both FoxO1 inhibition and Akt Ser473 phosphorylation led to constitutively active gluconeogenesis, while decreased glucokinase and uptake of glucose resulted in decreased glycolysis. This study implies that in order to coordinate the glucose and lipid metabolism, mTORC2 has to regulate Akt Ser473 phosphorylation, as well as glucokinase and sterol regulatory element-binding protein 1c (SREBP1c) (Hagiwara *et al.*, 2012).

1.6. mTOR inhibitors

Through the years, several inhibitors were developed to study the mTOR pathway. Rapamycin is a bacterial produced first-generation inhibitor, which is known for its anti-fungal and immunosuppressive properties as well as being an anti-cancer drug (Sehgal, 2003). Through a gain-of-function mechanism, rapamycin inhibits the mTORC1 kinase activity by first binding to the intracellular protein FKBP12 to create a drug-receptor complex (Sarbassov *et al.*, 2006). In contrast mTORC2 kinase is rapamycin insensitive due to FKBP12-rapamycin complex inability to bind to it (Jacinto *et al.*, 2004) while prolonged rapamycin treatment in some cell types has been found to inhibit it’s assembly (Sarbassov *et al.*, 2006).

Historically, rapamycin has been an essential tool in mTOR research. Unfortunately, due to being a rather ineffective inducer of autophagy, it requires to be coupled with another inhibitor such as LY294002, that is known to be an PI3K signalling and autophagy inhibitor, to increase growth inhibition in both rapamycin-sensitive and rapamycin resistant tumour cells (Takeuchi *et al.*, 2005). Moreover, several negative side effects have been associated with rapamycin and it's rapalogs treatments that lead to the restriction of their potential efficacy as anti-aging treatments. Immunosuppression, glucose intolerance, a rise in the incidence of type 2 diabetes, and disturbance of lipid homeostasis are some of these adverse consequences (Schreiber *et al.*, 2019). This led to the development of a more potent second-generation inhibitor named, Torin1. This ATP-competitive inhibitor can directly inhibit both TORC1 and TORC2 and is more effective at impairing cell growth and cell proliferation that its predecessor rapamycin (Thoreen *et al.*, 2009).

In a study conducted by Amin *et al.* (2021), the effect of mTOR inhibitors on glioblastoma (GBM) cells was assessed. Because of their limited mTORC1 inhibition and stimulation of mitogenic pathways via negative feedback loops, rapamycin and its analogues had less efficiency in clinical studies for patients with GBM. In contrast at a higher dose, Torin1 managed to suppress tumour cell migration, proliferation, and entry into S-phase (Synthesis Phase) by inhibiting phosphorylation of the substrates $S6K^{Ser235/236}$ and $4EBP1^{Thr37/46}$ that are part of mTORC1, as well as the substrate AKT^{Ser473} which is part of mTORC2.

Torin1 has been shown to exert a protective role over the neuroblastoma SH-SY5Y cells, against 6-OHDA/AA (Hydroxydopamine/ascorbic acid) that induces cell death and is often utilised to cause oxidative damage to dopaminergic neurons in order to produce

experimental lesions simulating Parkinson's disease (PD). In the 6-OHDA/AA toxicity model, co-treatment with Torin 1 or curcumin analogue C1 significantly boosted cell viability and stopped cell apoptosis. In addition, not only in SH-SY5Y cells but also in iPSC-derived DA neurons, and in mice nigral DA neurons, cell death induced by 6-OHDA/AA was substantially mitigated by autophagy enhancers Torin1 and C1. The findings also suggest that Torin1 and C1 neuroprotection against the toxicity caused by 6-OHDA/AA could revolve around an improvement in mitophagy which removes the damaged mitochondria. This process is very important due to the fact that preservation of neuron survival depends on the proper functioning of the mitochondria (Zhuang *et al.*, 2020).

Rapalink-1, a third generation mTOR inhibitor, has managed to bypass the resistance encountered by the previous generations of inhibitors by linking rapamycin to an ATP competitive inhibitor (MLN0128) (Rodrik-Outmezguine *et al.*, 2016). In human glioblastoma cell lines, RapaLink1 is selective for mTORC1 at lower levels. In this study, tumours treated with RapaLink-1 initially shrunk and showed subsequent tumour size stabilisation, whereas tumour treated with rapamycin and MLN0128 expanded consistently. In addition, RapaLink-1 has a higher in vivo efficacy than earlier generation mTOR inhibitors, which is probably a result of its potent 4EBP1 blockade and its longer residence duration. In the human glioblastoma cell treated with RapaLink-1 the levels of FKBP12 bound to mTOR were registered to be higher than in the rapamycin treated cells. The increased affinity and stability that may result from this dual binding of Rapalink-1 to FRB domain and to the mTORC1 kinase domain are anticipated to improve efficacy which holds great promise for future therapy on GBM (Fan *et al.*, 2017).

Yang *et al.* (2021a) demonstrated that RapaLink-1 selectively and fully suppressed the activity of mTORC1 along with its's substrates that were rapamycin sensitive and resistant, without inhibiting mTORC2 at a low dose. This study also determined that Rapalink-1 outperformed rapamycin in multiple important pathways associated with human disease and ageing such as autophagy, cell proliferation and glycolysis. High dose of RapaLink1 and Torin-1, inhibited both mTORC1 and mTORC2, while low dose RapaLink1 only inhibited mTORC1, therefore showing that both treatments had equal effects on cell size, which further demonstrated that that mTORC2 activity is not necessary for HEK293E cells growth nor size. In the case of treatment with rapamycin, the cell size was reduced similarly to RapaLink1 at a lower dose, even though the prolonged rapamycin administration somewhat inhibited mTORC2 in HEK293E cells. Indicating that S6K is the most likely rapamycin-sensitive substrate through which mTORC1 primarily regulates cell size. A mild effect was registered in autophagy when the cells were treated with rapamycin while Rapalink-1 induced a significant increase in the accumulation of LC3-II, displaying that rapamycin-resistant substrates play a major role in how mTORC1 acutely regulates autophagy. Results based on the treatment with RapaLink-1 also revealed that the insulin-induced glucose uptake was altered only by mTORC2, and that both mTORC1 and mTORC2 have vital roles in aerobic glycolysis (Yang *et al.*, 2021a).

In renal cell carcinoma (RCC), RapaLink-1 successfully inhibited cell proliferation, migration, invasion as well as colony formation by activating apoptosis and G1 arrest. Additionally, in vitro and in vivo therapy of sunitinib-sensitive and sunitinib-resistant RCC cells with RapaLink-1 outperformed the mTOR inhibitor derived from rapamycin known as temsirolimus, in terms of its antitumor effects (Kuroshima *et al.*, 2020).

1.7. LIM domain family and LIM-HD transcription factor LHX9

The LIM domain is a zinc finger structure found in many proteins, such as homeodomain transcription factors, kinases, and proteins with multiple LIM domains. The LIM domain name was acquired from the initials of three homeodomain proteins: Lin11, Isl-1 and Mec-3, in which it was first detected. From ascidians to humans, the LIM domain is a zinc-coordinating, cysteine-histidine-rich domain which is highly conserved. Following that, several LIM homeodomain (LIM-hd) genes were discovered, all of which shared two tandemly repeated LIM domains linked to a conserved homeodomain. LIM motifs were also identified in genes that encode nuclear and cytoplasmic LIM domain proteins. Certain proteins that are found in the nucleus are made up primarily of two LIM domains and are hence referred to be LIM only proteins (LMO). LIM domains are linked to kinases in Lmk1 and Lmk2, and other LIM proteins with various numbers of LIM domains that are primarily found in the cytoplasm have also been identified (Bach, 2000). The focus of this study will be upon the LIM-homeodomain (LIM-hd) transcription factors which are known to play a crucial role in embryonic development (Singh *et al.*, 2022).

Even though, the LIM-hd transcription factors are involved in embryonic development, they have also been found active in the nervous system, where they were shown to exhibit specialised high patterns with particular implications in the specification of the regional and neuronal cell- type. LIM-HD factors interact with Ldb1/Ldb2 (or CLIM1/CLIM2), which are also expressed throughout the developing brain, to exert their transcriptional control on these different characteristics of neuronal differentiation (Mollé *et al.*, 2004). The LIM-HD family of transcription factors have the following characteristics: they contain two

protein zinc finger motifs and the LIM domains that can be found at the N-terminal of a central homeodomain, having the role to bind the TAAT sequence which contains DNA. This LIM-HD transcription factors have the unique capacity to create homomeric or heteromeric complexes with other transcription factors due to the presence of the LIM domains (Balasubramanian *et al.*, 2014).

The LIM-hd proteins have been clearly identified to be classified into six groups: Lhx3/4, Lhx1/5, Lhx2/9, Lhx6/7/8, Islet, and Lmx Failli *et al.* (2000). The transcription factor of interest, LHX9, belongs to the APTEROUS group of LIM-HD transcription factors. Bertuzzi *et al.* (1999) postulated that an LHX2 related gene might exist in order to elucidate the phenotype observed in the LHX2 mutant embryos. Therefore, a LIM/homeobox gene was cloned and named LHX9. In this study it was further shown that LHX2 and LHX9 are closely related and that both are expressed in the developing central nervous system (CNS). Moreover, it was also demonstrated that Lhx9 and Lhx2 bind the LIM domain binding protein Ldb1/Nli1/Clim2. In the developing mouse brain, the highest expression levels exhibited by LHX9 were recorded in the diencephalon, telencephalic vesicles (brain vesicles), and dorsal mesencephalon (midbrain). Additionally, the expression of LHX9 has been also seen in the spinal cord, forebrain, hindlimb mesenchyme and in the genitourinary system. It was assumed that LHX9 encodes a transcription factor involved in cell differentiation control in a range of brain cell types based on its expression pattern and structural properties (Rétaux *et al.*, 1999).

It was reported that LHX9 plays a critical function in controlling somnolence and is expressed in a subset of Hcrt neurons (hypocretin neurons) which are located in the hypothalamus. The appropriate regulation of sleep and wakefulness depends on

hypocretin neurons, which have also been linked to anxiety and depression. In humans and model species, the lack of these neurons causes narcolepsy (Dalal *et al.*, 2013). Absence of LHX9 gene causes a 30% reduction in Hcrt neurons exclusively without affecting the overall hypothalamic development (Dalal *et al.*, 2013). Lhx2 and Lhx9, are expressed by a group of commissural relay neurons (dI1c neurons) and are necessary for dI1c axon projection. Both transcription factors define dI1 neurons and control the midline crossing of dI1c axons, which is a particular component of their developmental programme. Midline crossing by dI1c axons is absent in Lhx2/9 double mutants, therefore being a deficiency caused by the lack of Rig-1 expression from dI1c axons. The activity of Lhx2/9 proteins appears to be mediated by direct transcriptional control of the expression of the Rig-1, an axon guidance receptor (Wilson *et al.*, 2008). Despite the fact that LHX9 has been identified to have a prevalent neuronal expression pattern, Birk *et al.* (2000) demonstrated that when LHX9 was knocked out in mice, animal viability and neural development were unaffected. Therefore, it demonstrated that LHX9 has an indispensable role in early gonadal development by revealing that a null mutation in the murine LHX9 gene has a significant impact on gonadal development. Lhx9 investigation in pineal gland development revealed that it plays an important role in the development of the mouse pineal organ and that the pineal gland is hypoplastic in the absence of this homeobox gene. This study has revealed the impact of Lhx9 deletion on gonadal development and on particular neuronal cell subtypes of the CNS by reporting that severe hydrocephalus arises in the brain of the adult *Lhx9* $^{-/-}$ C57BL/6J mouse (Yamazaki *et al.*, 2015).

Vladimirova *et al.* (2009) showed that LHX9 is frequently hypermethylated in paediatric malignant astrocytoma. According to this studies, LHX9 methylation is present in 29% of

non-diffuse fibroblastic astrogliomas and in 88% of high-grade gliomas (HGGs). Additionally, epigenetic changes of the LHX9 gene are linked to decreased mRNA expression and plays a tumour-specific role in the migratory and invasive phenotype of glioma cells. In paediatric malignant astrocytoma's, recurrent hypermethylation of a CGI-associated area of the LHX9 gene has been found to be linked to decreased LHX9 gene expression. Without directly influencing proliferation or apoptosis, LHX9 reexpression blocked glioma migration and invasion, indicating that the regular epigenetic silencing of the LHX9 gene is responsible for the invasive nature of paediatric high-grade gliomas. A complex is formed between the transcription factor LHX9 and the tumour suppressor p53 in glioma cells. Therefore, p53's interaction with LHX9 was mediated by the DB (DNA binding) domain. In tumour cells p53 plays a very important role because it supresses glycolysis. The impact of LHX9 on glycolysis in glioma cell was investigated due to LHX9's interaction with p53. The results revealed that downregulation of LHX9 showed to boost the expression of glycolysis, which in turn led to the formation of glioma cells, while upregulation of LHX9 led to inhibition of growth in glioma cells. Additionally, the interaction between LHX9 and p53 leads to the inhibition of PGK1 expression which is known to be a central enzyme in glycolysis. Interfering with downstream PGK1 expression in tumour formation almost completely reversed the tumorigenicity driven by the downregulation of LHX9 expression (Vladimirova *et al.*, 2009).

There have been some propositions that entail LHX9 being essential in heart development (Smagulova *et al.*, 2008). This assumption was supported by the finding of the GATA4/FOG2 transcription complex, which is necessary for mouse cardiac development, to control the cardiac expression of LHX9 gene by binding to GATA sites located in Lhx9

regulatory regions. Moreover, the absence of the GATA4/FOG2 relationship caused an overexpression of LHX9 expression in epicardial cells (Smagulova *et al.*, 2008). In this study it was also revealed that the Lhx9 isoform, which encodes a protein with a full homeodomain, is not found in the embryonic heart, whereas the alpha and beta isoforms, which encode a truncated homeodomain, are expressed. The variation seen in LHX9 isoform expression indicates that shortened LHX9 proteins serve a purpose distinct to that of the full-length LHX9 molecule (Smagulova *et al.*, 2008). This observation was reported previously by Mollé *et al.* (2004) where results showed that LHX9 isoforms do not directly contend with each other during neural development but rather function in distinct pathways.

1.8. SH-SY5Y cell line model

The SH-SY5Y cell line originates from the SK-N-SH cell line that was obtained from a 4-year-old female's bone marrow biopsy in 1970 and has gone through three rounds of clonal selection (Xicoy *et al.*, 2017). This neuroblastoma cell line is an immortalised cell line that has been used extensively within *in vitro* models of neurological disorders (Peng *et al.*, 2021). SH-SY5Y has been frequently used in Parkinson's disease (PD) studies because it contains a mechanism that can produce both the dopamine (DA) and basal noradrenaline (NA). Since the cell line is derived from a neuroblastoma cell line, it still contains malignant characteristics that affect its viability, differentiation fate, growth performance, metabolic capabilities, and genomic stability therefore SH-SY5Y cells can’t be dopaminergic neurons (DAergic) entirely (Xicoy *et al.*, 2017).

de Medeiros *et al.* (2019) reported that treatment of differentiated SH-SY5Y cells with sublethal dosages of okadaic acid (OA) and oligomers of amyloid-β (AβOs) creates an in vivo model that closely mirrors the pathophysiology of cholinergic neurons which are originally damaged by Alzheimer disease (AD). Neurotoxicity has also been investigated in this cell line and findings show that Tetramethylpyrazine, that has potent neuroprotective properties against neurotoxicity, was observed to reduce the neurotoxicity of the local anaesthetic Bupivacaine on SH-SY5Y cells (Wang *et al.*, 2019). Another study looked into the potential of the following compounds: Curcumin, piperine, bacoside A, and chebulinic acid; in drugs for prevention and therapy against Alzheimer's disease (Abdul Manap *et al.*, 2019). Curcumin coupled with piperine has been shown *in vitro* to protect SH-SY5Y cells from amyloid β (Aβ) promoted cytotoxicity, fibrillation, and oxidative damage. This protection provided by the two compounds reduced the harmful effects on neuronal cells, preventing the fibrils from aggregating, and by suppressing reactive oxygen species (ROS) from generating (Abdul Manap *et al.*, 2019).

1.9 The hypothesis and aims of the study

Pharmacological inhibition of mTOR, via Torin1 or RapaLink-1, in differentiated SH-SY5Y cells would lead to an upregulation of LHX9 and downregulation of GATA4, which would negatively affect (or inhibit) glycolysis. Alternatively, if GATA4 is found to be upregulated post-treatment, then LHX9 would be downregulated, leading to activation of glycolysis.

The purpose of this research is to define the function of the mTOR pathway in controlling gene expression programmes during differentiation, growth, and neurodegeneration as well as its implications into glycolysis (by utilising pharmacological interventions with dual and TORC1 inhibitors in differentiated SH-SY5Y cells). Additionally, the link between the transcription factor LHX9 and mTOR, as well as their effects in growth, neurodegeneration and glycolysis will be investigated (Western blots to validate the RNA-seq outputs by examining LHX9 expression levels in differentiated SH-SY5Y cells). This study alongside the approaches employed within, will eventually aid us to comprehend the nutrient-response circuits as well as their implications in physiology and disease.

2. Methods

2.1. Cell Culture

The SH-SY5Y neuroblastoma cells were cultured in Dulbecco's modified Eagle's medium (DMEM, 11965092, ThermoFisher) containing high glucose (25 mM), l-glutamine (4 mM), and sodium pyruvate (1 mM). The DMEM media was supplemented with 1% penicillin streptomycin (P/S, 15140122, ThermoFisher) and 10% (v/v) heat-inactivated fetal bovine serum (FBS, A4766801, ThermoFisher). T75 flasks were used for the cell maintenance and were kept in the incubator, at 37 °C with 5% CO2 at saturated humidity. Cells were split at 80–90% confluency.

2.2. Serum starvation experiment

Undifferentiated SH-SY5Y were used for the serum starvation experiment which was conducted over a period of 3 days. The media utilised for the serum starvation experiment was Dulbecco's modified Eagle's medium (DMEM) containing high glucose (25 mM), l-glutamine (4 mM), and sodium pyruvate (1 mM) supplemented with 1% penicillin streptomycin (P/S). For the control, media with supplemented serum (10% FBS) was utilised. Complete media was removed from the cells then media without serum (0% FBS), or media with serum (10% FBS) was added for 5h and 24h. There were 6 different conditions for this experiment; 5h media with serum (control), 5h media with no serum (starvation), 5h media with no serum followed by addition of media with serum for another 5h (readdition), 24h media with serum (control), 24h media with no serum (starvation), 24h media with no serum followed by addition of media with serum for another 24h (readdition).

2.3. Differentiation protocol and treatment

SH-SY5Y cells differentiation protocol contains two different stages that utilise phase 1 and phase 2 media. Phase 1 media used for the experiment was DMEM (11965092, ThermoFisher) containing high glucose (25 mM), l-glutamine (4 mM), no sodium pyruvate, and 1% P/S. Then the phase 1 media was further supplemented with 10 µM all-trans retinoic acid (RA) before the media was added to the cells. Cells remained in phase 1 media for 3 days. The media used for the second differentiation phase was Neurobasal™-A Medium minus phenol red (11570426, ThermoFisher) with 1% (v/v) L-

glutamine and 1% P/S. The phase 2 media was further supplemented with N-2 and BDNF before the addition of media to the cells. Cells were incubated with phase 2 media for 3 days. Following the SH-SY5Y differentiation, cells were treated with mTOR inhibitors: Torin1 (250nM) and RapaLink-1 (25nM) for 5 h. DMSO was used as a control. After the treatment cells were washed with PBS, pellets were collected and stored at -80°C.

2.4. Protein Quantification/Bradford assay

Pellets were supplemented with 49 µL of RIPA buffer (89900, Thermo Fisher), 0.5 µL of protease inhibitor (PPC2020, Sigma-Aldrich), 0.5 µL of phosphatase inhibitor (PPC2020, Sigma-Aldrich) each and were left for 10 minutes at room temperature. The eppendorf tubes containing the lysed pallets were centrifuged at 12000 RPM for 10 minutes, then the supernatant was collected and the pellets were thrown away. Standards for the Bradford assay were prepared by diluting bovine serum albumin (BSA, 5217, Tocris) using PBS. In a 96-well plate 5 µL of each standard and 5 µL of protein were added to the wells, then 250 µL of Bradford dye reagent was added to each one of the wells. The 96-well plate was incubated for 5 minutes. Using the CLARIOstar Plus, the absorbance was measured at 595 nm and the values given were used to determine the protein concentrations.

2.5 Western Blots

For the sample preparation 10 µg of protein per sample was utilised, then supplemented with NuPAGE LDS Sample Buffer (4x), NuPAGE Reducing Agent (10x) and Deionized Water to make up a total loading volume of 20 µL. For the electrophoresis step, MES SDS running buffer (1X) (NP0002, Invitrogen™) was prepared after which samples were loaded into an SDS-PAGE (4%-12%, Bis-Tris) gel and ran at 200V for 45 min. The next step conducted was the electrotransfer of the gel onto a PVDF nitrocellulose membrane by utilising transfer buffer (NuPAGE Transfer Buffer (1X)) at 30V for 1 hour. When the transfer was completed, the membrane was blocked for 1 hour at room temperature in 5% skimmed milk in PBST. Primary antibody was diluted in 5% bovine serum albumin (BSA) in PBST and incubated overnight at 4°C. In order to discard any remaining primary antibody, the membrane was washed with PBST 5 times for 5 minutes each wash. Secondary antibody with a dilution of 1:10000 was added in 5% skimmed milk in PBST and incubated at room temperature for 1 hour. The membrane was then washed as specified earlier. SuperSignal™ West Pico PLUS Chemiluminescent Substrate (34580, Thermo Fisher Scientific™) was added to the membrane and incubated for 5 minutes then chemiluminescence was determined by Fusion Fx (Peqlab). Following this step, the membrane was washed 2 times with PBST for 5 minutes and the membrane was probed with β-Actin primary antibody which was used as a loading control/housekeeping. From here onwards the same steps stated above were followed. Afterwards, the relative protein expression was measured by ImageJ. Table of antibodies used can be found below.

Antibody	Organism derived	Company	Cat number	Dilution used
LHX9	Rabbit pAb	ABclonal	A12717	1:1000
GATA-4	Rabbit mAb	Cell Signalling Technology	D3A3M	1:1000
Phospho-4E-BP1(Thr37/46)	Rabbit mAb	Cell Signalling Technology	236B4	1:1000
PGK1	Rabbit mAb	Cell Signalling Technology	E9R7O	1:1000
Glycolysis Antibody Sampler Kit (8337, Cell Signalling Technology)				
Antibody	**Organism derived**	**Company**	**Cat number**	**Dilution used**
PKM2	XP® Rabbit mAb	Cell Signalling Technology	D78A4	1:1000
GAPDH	XP® Rabbit mAb	Cell Signalling Technology	D16H11	1:1000
Pyruvate Dehydrogenase	Rabbit mAb	Cell Signalling Technology	C54G1	1:1000
Hexokinase I	Rabbit mAb	Cell Signalling Technology	C35C4	1:1000
Hexokinase II	Rabbit mAb	Cell Signalling Technology	C64G5	1:1000
LDHA	Rabbit mAb	Cell Signalling Technology	C4B5	1:1000
PKM1/2	Rabbit mAb	Cell Signalling Technology	C103A3	1:1000
PFKP	Rabbit mAb	Cell Signalling Technology	D4B2	1:1000
HRP-linked Antibody	Anti-rabbit IgG	Cell Signalling Technology	7074	1:10000

2.6 Immunofluorescence staining

For this experiment both differentiated SH-SY5Y with pharmacological treatment as well as undifferentiated cells were used. Cover slips were coated with 0.01% (w/v) Poly-D-Lysine and were left to dry in the incubator for 24h prior to the cell seeding. The cover

slips were placed into 6-well plates and 250,000 cells were added to each well then left to grow in the incubator for 3 days. When the cells reached 80-90% confluence, they were differentiated and treated following the protocol stated before. Post-treatment, the cells were washed 2 times with PBS. In order to fixate the cells, 4% of Paraformaldehyde (PFA) diluted in PBS was used then the 6-well plates were incubated at room temperature for 10 minutes. To remove any remaining PFA, the wells were washed 2 times with PBS. For cytoplasmic/nuclear staining, cell permeabilization was conducted with 0.1% Triton-X diluted in PBS followed by 10 minutes incubation at room temperature. To remove any remaining Triton-X, cells were washed 2 times with PBS. Afterwards, cells were blocked for 1 hour at room temperature in 5%BSA diluted in PBS. Blocking buffer was removed and LHX9 (primary antibody) with the antibody ratio of 1:1000 diluted in 5% BSA w/ PBS was added on the wells and incubated overnight at 4°C. When primary antibody incubation was completed, cells were washed two times with PBS to remove any remaining antibody. Cells were probed with Goat Anti-Rabbit IgG H&L (Alexa Fluor® 488, ab150077, Abcam) secondary antibody followed by the plates being covered with foil and incubated at room temperature for 2 hours. For the removal of any remaining fluorophore, cells were washed 3 times with 0.1% PBS-Tween20. 1.5 µL of 4',6-diamidino-2-phenylindole (DAPI, ab228549, Abcam) florescent staining solution was dissolved in 15 mL of H_2O and added onto the cover slips for 10 minutes at RT. This type of staining was conducted in order to visualise the nucleus. Following DAPI staining the wells were washed with PBS two times then the cover slips were extracted and attached to slides using ProLong™ Glass Antifade Mountant medium (P36982, Thermo Fisher Scientific™). Images were taken with EVOS M5000 imaging system at 60x magnification.

2.7 RNA-seq

The SH-SY5Y cells were differentiated and treated as previously explained in the differentiation section. The pallets from each sample contained 1 x 10^6 cells. Total RNA was prepared by using the RNA isolation kit (74104, Qiagen) according to the manufacture's protocol. On average the total amount of RNA per sample ≥ 200 ng. After RNA extraction, the samples (Control, Torin1, RapaLink-1) were sent to Novogene (in Cambridge) for quality control of sample purity and for the RNA-seq to be run on them. The Sequencing platform used by Novogene is Illumina NovaSeq 6000 Sequencing System, the read length is 150 bp and the data output ≥ 20 million read pairs per sample.

2.8 Statistical analysis

The programme R studio was used for the RNA-seq analysis of both data sets: Torin1 vs Control and RapaLink-1 vs Control. Differential gene expression was done to display the changes in the level of expression in different conditions. In this case, in order to conduct differential expression (DE) analysis, the package DESeq2 was utilised and for the gene ontology analysis (GO), the enrichGO function was used. The cutoff used to determine the significant genes was adjusted P value (q value) of <0.05. The genes were also filtered by log2FoldChange of 0.6 for the RapaLink-1 vs Control data and by log2FoldChange of 1 for the Torin1 vs Control data. The figures containing the Venn Diagrams, were done with Venny 2.1 (Oliveros, J.C. (2007-2015)). Vulcano plots for

both datasets (Torin vs Control and RapaLink-1 vs Control) were created by using ggplot2 package in RStudio. In order to produce the volcano plots, the most significant upregulated and downregulated genes were first determined by filtering them by P value of <0.05 and by log2FoldChange of 0.6 (for the RapaLink-1 vs Control) and by log2FoldChange of 1 for the (Torin1 vs Control data). Tables of the most significant genes form both data sets after the filtering can be found in the Appendix. The density of the western blot bands was measured by Image J software. The histogram graphs were created in Excell and depict the data extracted from ImageJ software after it was normalised with the control and housekeeping. In the histograms containing data with several repeats, the standard deviation of all the replicates was calculated in Excel. Heat map was created with the Spyder software by utilising the following packages: pandas, seaborn and matplotlib.pyplot. Statistical analysis was conducted on the experiments with several repeats in order to identify if the data is statistically significant ($P \leq 0.05$). The software used to determine the statistical significance was GraphPad Prism and the test performed was one-way ANOVA for every experiment with several repeats.

3. Results

3.1 Differentiation of the SH-SY5Y cells

Through the differentiation period, the SH-SY5Y cells go through morphological changes, therefore both differentiation phases were presented in **Figure 4** and **Figure 5**. After the addition of phase 1 media, the neurites were elongated, forming axonal projections linking them to other neurites (**Figure 4**). Once phase 2 differentiation has ended, the cells were evenly spread out and shown to be interconnected demonstrating substantial elongated neuritic projections. After differentiation, the SH-SY5Y cells showed to have a pyramidal shaped cell body which is highlighted by the white arrows in **Figure 5**.

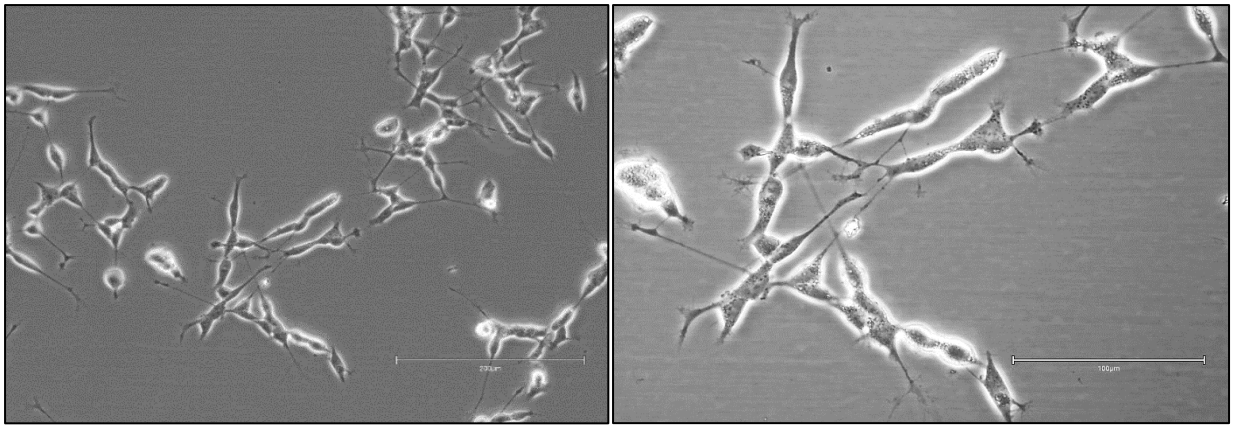

Figure 4: Phase 1 of SH-SY5Y differentiation

Images of SH-SY5Y cells showing the phase 1 stage of the differentiation process. For the first phase of differentiation, cells were treated with 10 µM of retinoic acid (RA). Both images were obtained using EVOS M5000 imaging system at 40x (left) with a 200 µm scale bar and at 20x (right) with a 100 µm scale bar.

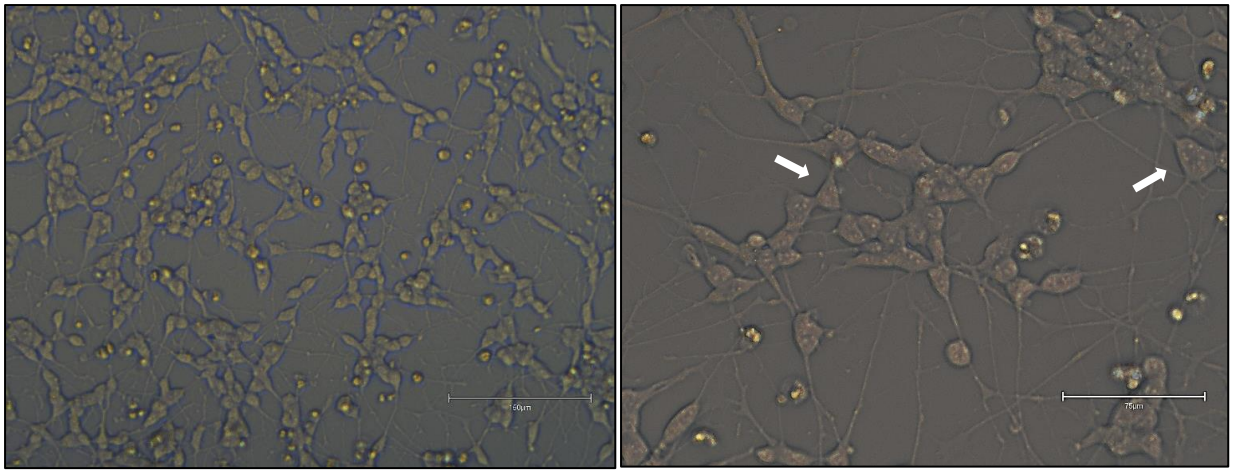

Figure 5: Phase 2 of SH-SY5Y differentiation

Images of SH-SY5Y cells showing the phase 2 stage of the differentiation process. For the second phase of differentiation, cells were treated with BDNF (50 ng/mL) and 1%N2 supplement. Both images were obtained using EVOS M5000 imaging system at 40x (left) with a 150 µm scale bar and at 20x (right) with a 75 µm scale bar.

3.2. Differentially expressed genes

Two data sets were analysed, one being RapaLink-1 vs Control and the other Torin1 vs Control, by utilising RStudio in order to identify the most significant differentially expressed genes (DEGs). When analysing these data sets, we were particularly looking for changes in the expression but also at the transcriptional responses that occur with Torin1 and RapaLink-1 treatment in the differentiated SH-SY5Y cells. One of the DEGs that caught our attention was LHX9 due to its high upregulation in the Torin1 vs Control data set. Another DEGs that we wanted to explore was GATA4. Firstly, because it has

been linked to LHX9, secondly because GATA transcription factors have been associated to mTOR pathway before. Therefore, we were interested to investigate LHX9's transitional response in comparison to its expression at the protein level as well as its implication into glycolysis which will be discussed later in this paper.

3.2.a. Differentially expressed genes in the Torin1 vs Control RNA-seq data

DEseq analysis was performed in order to examine the differentially expressed genes in the Torin vs Control dataset. The volcano plot in **Figure 6** displays the differential expression of all genes, where the threshold in the volcano plot was p-adjusted < 0.05 and $\log_2$FC cut-off of 1. Based on the cut-off, a total of 4493 genes were found to be differentially expressed, this including 203 upregulated and 251 downregulated differentially expressed genes. As it can be observed from **Figure 6**, LHX9 is present within the upregulated genes. More information regarding the genes in the Torin1 vs Control data set after filtering can be found in the Appendix 1 at page 122 and Appendix 2 at page 127.

A.

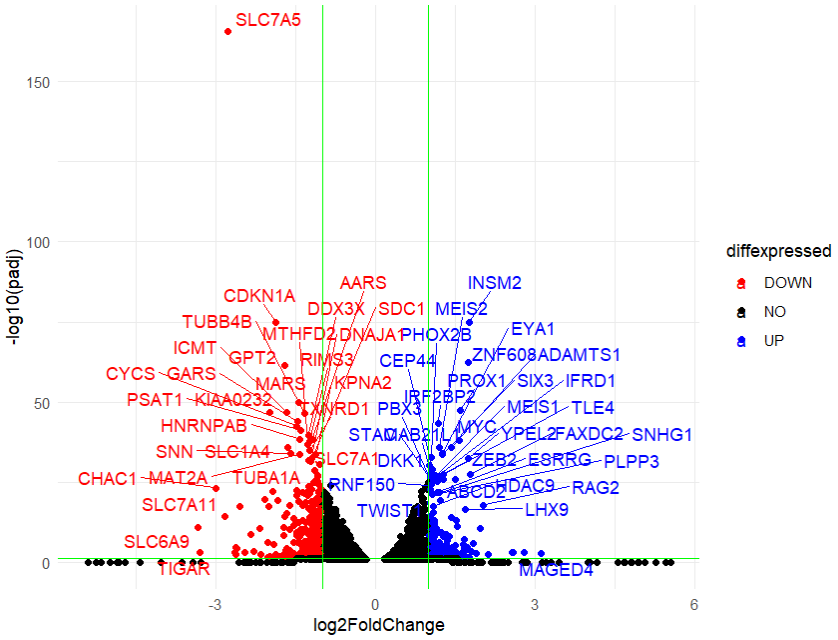

B.

DEG in the Torin1 vs Control	
No. of Upregulated genes	203
No. of Downregulated genes	251
Total number of the differentially expressed genes	4493

Figure 6: Differentially expressed genes in the Torin vs Control RNA-seq data. Volcano Plot portraying differentially expressed genes between Torin1 and Control in SH-SY5Y cells treated for 5h, assessed based on p-adjusted value (padj < 0.05) and log_2FoldChange cut-off (log_2FoldChange > 1 for upregulated genes and log_2FoldChange < -1 for the downregulated

genes). The blue dots indicate the upregulated genes, the red dots indicate the downregulated genes, and the black dots represent the genes that are not differentially expressed. **B)** Table displaying the total number of differentially expressed genes and the number of up or downregulated genes in the Torin1 vs Control data set after filtering by p-value and log_2FoldChange.

3.2.b. Differentially expressed genes in the RapaLink-1 vs Control RNA-seq data

DEseq analysis was performed in order to examine the differentially expressed genes in the RapaLink-1 vs Control dataset. The volcano plot in **Figure 7** displays the differential expression of all genes, where the threshold in the volcano plot was p-adjusted < 0.05 and log2 FC cut-off of 0.6. Based on the cut-off, a total of 1014 genes were found to be differentially expressed, this including 128 upregulated and 41 downregulated differentially expressed genes. More information regarding the genes in the RapaLink-1 vs Control data set after filtering can be found in the Appendix 3 at page 134 and in Appendix 4 at page 137.

A.

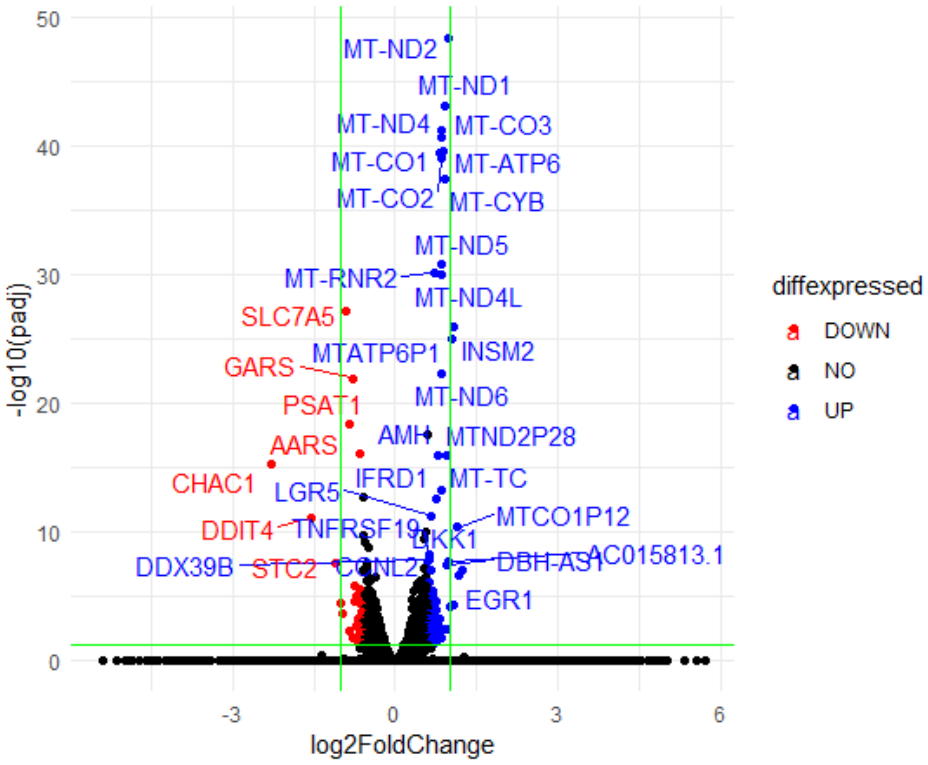

B.

DEG in the RapaLink-1 vs Control	
Number of Upregulated genes	128
No. of Downregulated genes	41
Total number of the differentially expressed genes	1014

Figure 7: Differentially expressed genes in the RapaLink-1 vs Control RNA-seq data. Volcano Plot portraying differentially expressed genes between RapaLink-1 and Control in SH-SY5Y cell treated for 5h, assessed based on p-adjusted value (padj < 0.05) and $\log_2$FoldChange cut-off

(log_2FoldChange > 0.6 for upregulated genes and log_2FoldChange < -0.6 for the downregulated genes). The blue dots indicate the upregulated genes, the red dots indicate the downregulated genes, and the black dots represent the genes that are not differentially expressed. **B)** Table displaying the total number of differentially expressed genes and the number of up or downregulated genes in the RapaLink-1 vs Control data set after filtering by p-value and log_2FoldChange.

3.2.c. Venn Diagram of the differentially expressed genes in Torin1 vs Control and RapaLink-1 vs Control RNA-seq datasets.

As previously stated, DEseq was used to identify the differentially expressed genes in both Torin1 vs Control and RapaLink-1 vs Control RNA-seq datasets. **Figure 8** displays a four-way Venn diagram of the significant differentially expressed genes overlapping. In this figure, it can be observed that there is one common gene in RvsC UP and TvsC DOWN, 14 common genes in RvsC DOWN and TvsC DOWN, 13 common genes in RvsC UP and TvsC UP. More information regarding the common genes between data sets can be found in the Appendix 5 at page 139.

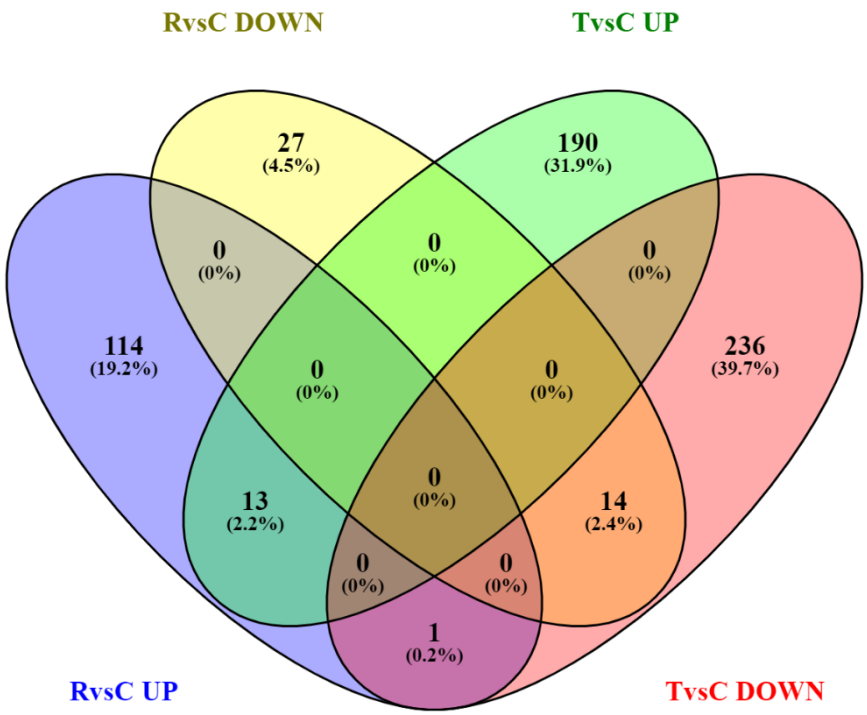

Figure 8: Venn diagrams illustrating the differentially expressed genes in both Torin1 vs Control and RapaLink-1 vs Control datasets. Each dataset is split into upregulated and downregulated differentially expressed genes.

3.3 Gene ontology (GO) analysis on differentially expressed genes

Gene ontology analysis was conducted to identify the Biological Processes (BP) and Molecular Functions (MF) of the most significant DEGs in both datasets.

3.3.a. Gene ontology analysis on the upregulated genes in the RapaLink-1 vs Control dataset

The bar plot depicts the enrichment scores (adjusted p values) against the upregulated genes count. The GO results in the biological process analysis indicate that all the upregulated differentially expressed genes in the RapaLink-1vsControl were mainly associated with oxidative phosphorylation and aerobic respiration (**Figure 9A**). The molecular functions associated with the most upregulated DEGs in the RapaLink-1vsControl dataset are displayed in **Figure 9B** where the results indicate that active transmembrane transporter activity, primary active transmembrane transporter activity, electron transfer activity and oxidoreduction-driven active transmembrane transporter activity, are the most significant molecular functions.

A. **B.**

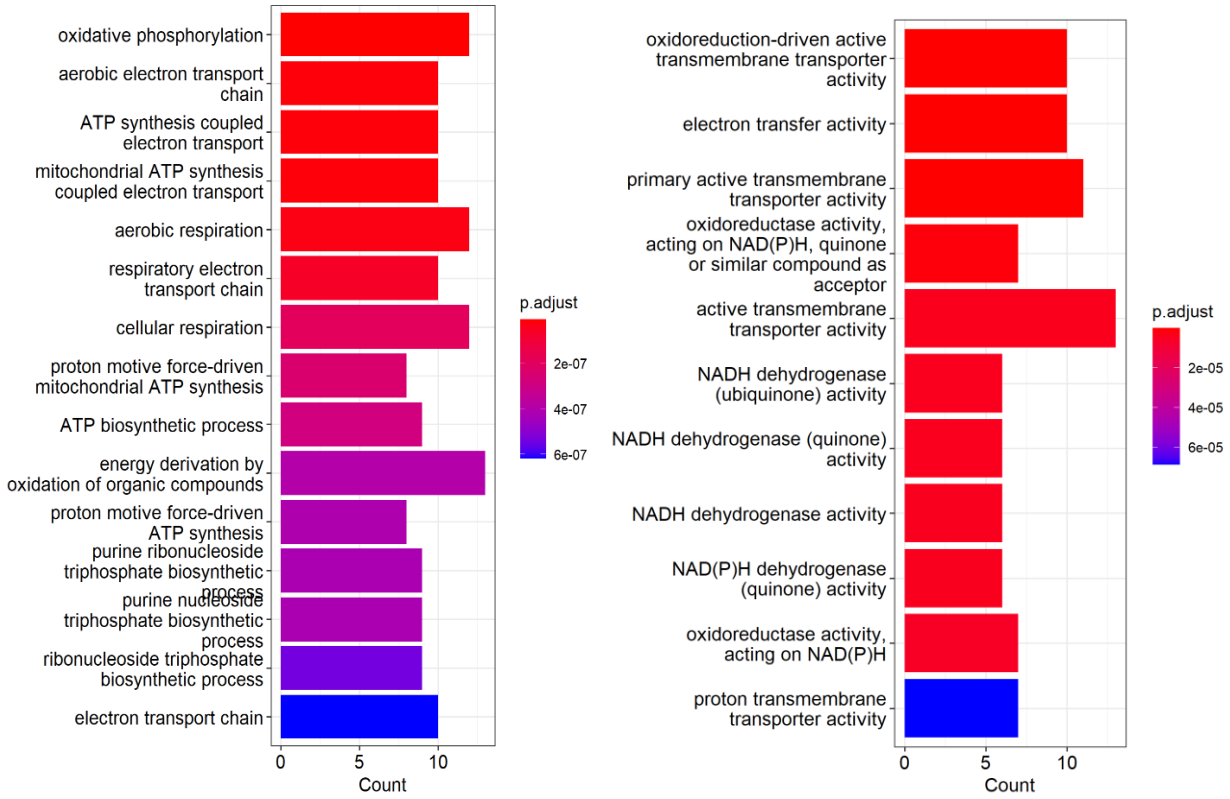

Figure 9: Gene Ontology analysis results. A. Biological Processes of the upregulated genes in the RapaLink-1 vs Control dataset. **B.** Molecular functions of the upregulated genes in the RapaLink-1 vs Control dataset.

3.3.b Gene ontology analysis on the downregulated genes in the RapaLink-1 vs Control dataset.

The bar plot depicts the enrichment scores (adjusted p values) against the downregulated genes count in the RapaLink-1 vs Control dataset. GO results shown in **Figure 10A**, display the biological processes analysis which indicates that all the

downregulated DEGs were mainly associated with response to endoplasmic reticulum stress (ER stress), cellular response to glucose starvation and positive regulation of extrinsic apoptotic signalling pathway via death domain receptors. Based on the molecular function analysis (**Figure 10B**), the downregulated genes were mostly enriched in terms of protein heterodimerization activity.

A. **B.**

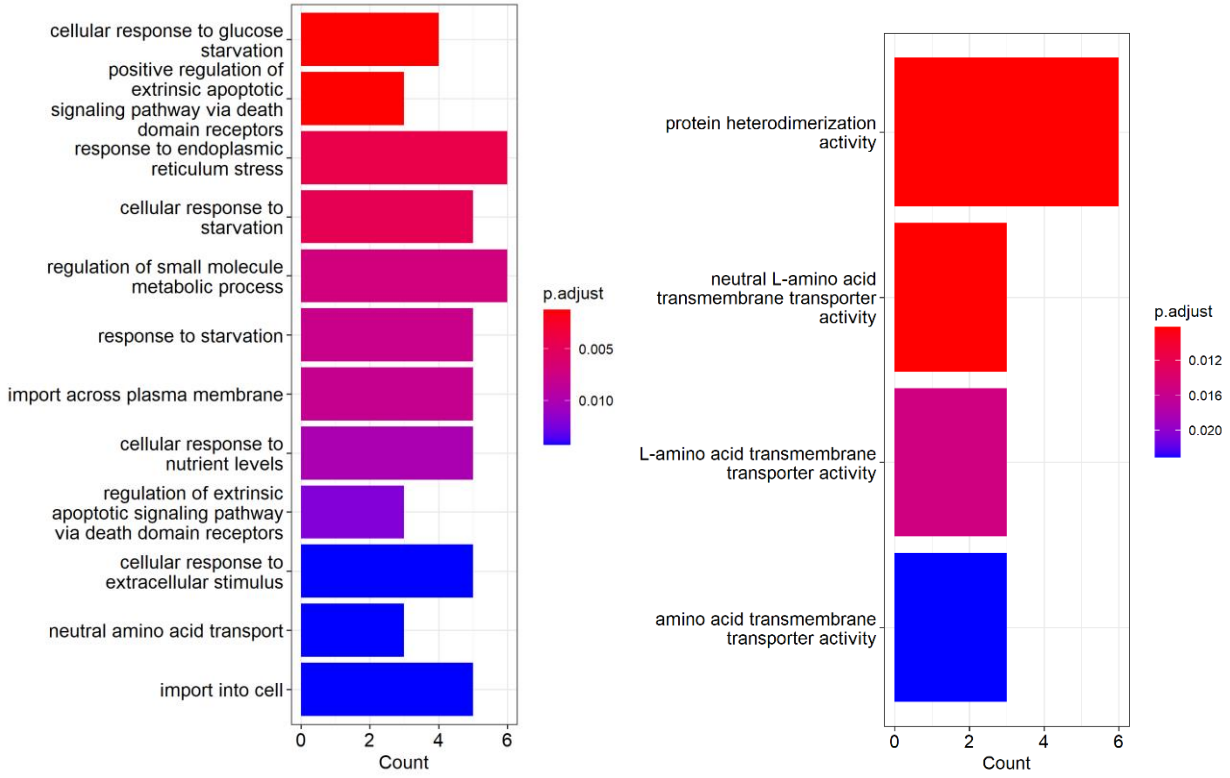

Figure 10: Gene Ontology analysis results. A. Biological Processes of the downregulated genes in the RapaLink-1 vs Control dataset. **B.** Molecular functions of the downregulated genes in the RapaLink-1 vs Control dataset.

3.3.c. Gene ontology analysis on the upregulated genes in the Torin1 vs Control dataset.

The bar plot depicts the enrichment scores (adjusted p values) against the upregulated genes count from the Torin1 vs Control dataset. GO results shown in **Figure 11A**, display the biological processes analysis which indicates that all the upregulated DEGs were mainly associated with regulation of neuron differentiation. The top enriched GO terms for the molecular function were DNA-binding transcription activator activity, RNA polymerase II-specific and DNA-binding transcription activator activity (**Figure 11B**).

A.

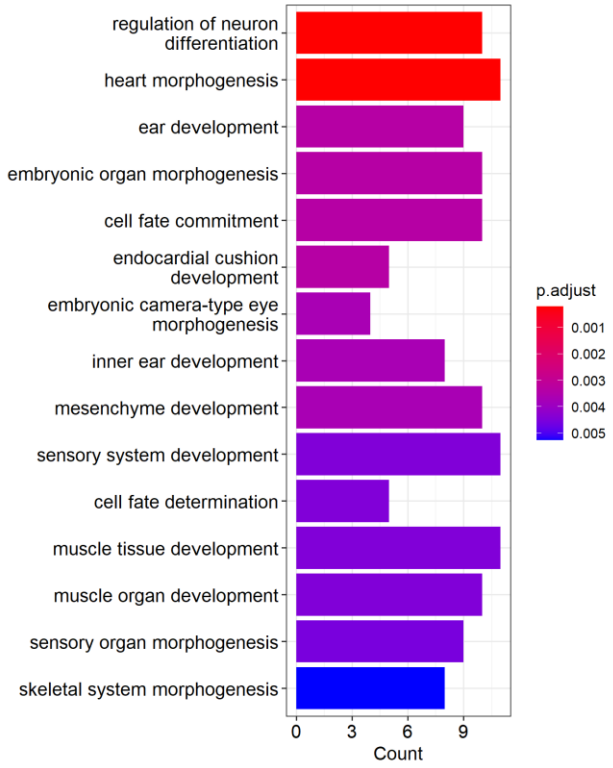

B.

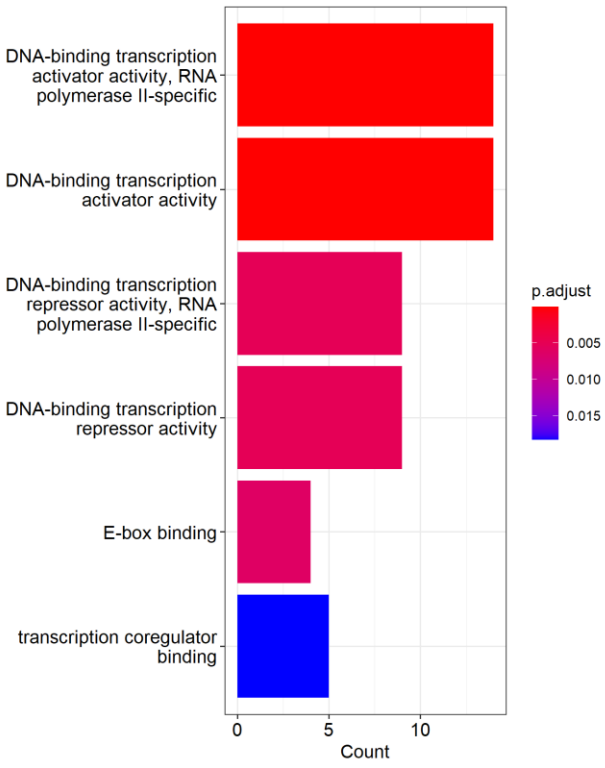

Figure 11: Gene Ontology analysis results. A. GO enrichment results of the biological processes of upregulated genes in the Torin1 vs Control dataset. **B.** Molecular functions of the upregulated genes in the Torin1 vs Control dataset.

3.3.d. Gene ontology analysis on the downregulated genes in the Torin1 vs Control dataset.

The bar plot depicts the enrichment scores (adjusted p values) against the downregulated genes count from the Torin1 vs Control dataset. GO results shown in **Figure 12A** display the BP analysis which indicates that all the downregulated DEGs were mainly associated with the amino acid metabolic process and intrinsic apoptotic signalling pathway. The top enriched GO terms for the molecular function were amino acid transmembrane transporter activity, carboxylic acid transmembrane transporter activity and organic acid transmembrane transporter activity (**Figure 12B**).

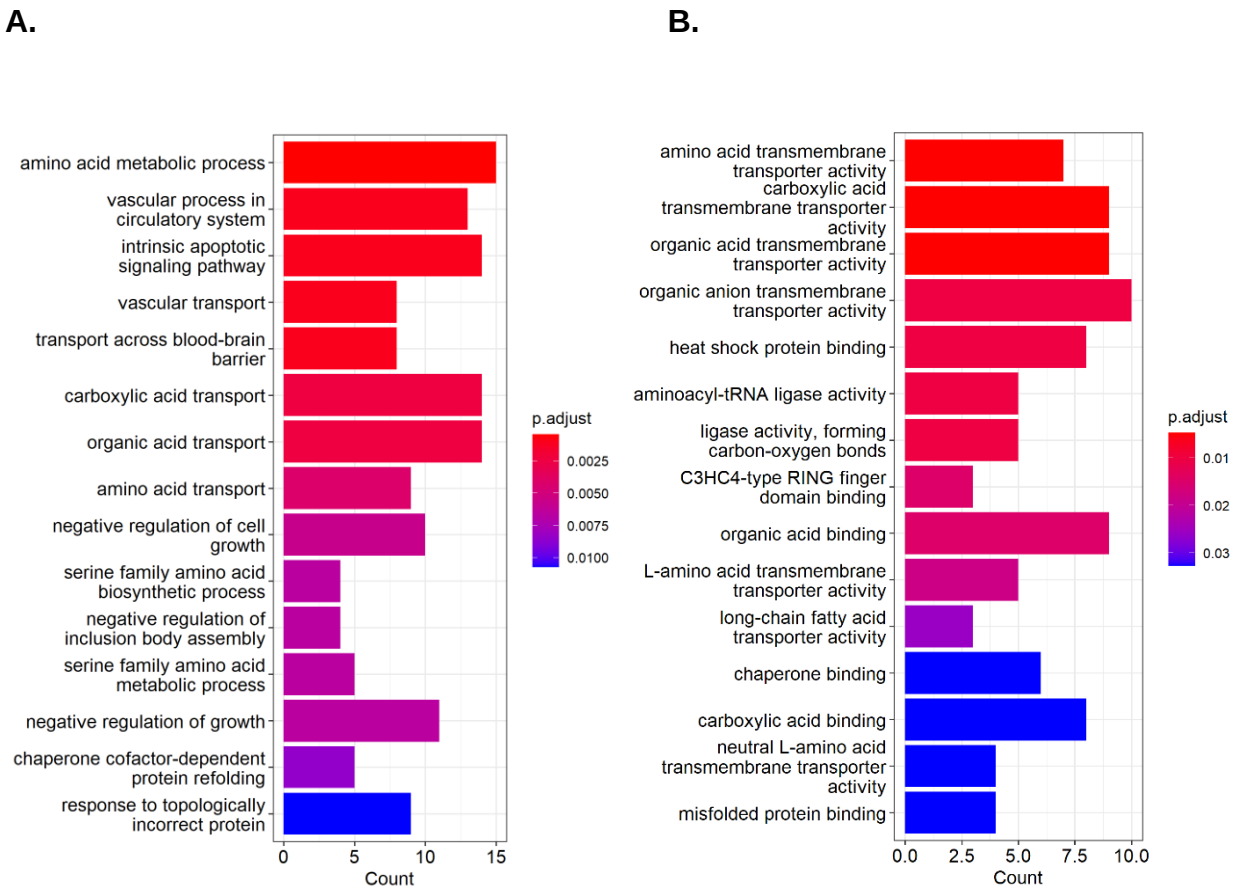

Figure 12: Gene Ontology analysis results. A. Biological Processes of the downregulated genes in the Torin1 vs Control dataset. **B.** Molecular functions of the downregulated genes in the Torin1 vs Control dataset.

3.4. Immunofluorescence staining of LHX9 in differentiated SH-SY5Y cells

Immunofluorescence (IF) staining was performed to visualise the location of LHX9 in the cell and to examine LHX9's expression in differentiated cells with pharmacological treatment (Torin-1 and RapaLink-1). The SH-SY5Y cells were differentiated and treated for 5h then IF was conducted on them. The cells were incubated with LHX9 as primary antibody then stained with Alexa Flour 488-conjugated Goat Anti-rabbit IgG secondary antibody(green). **Figure 13A** shows the DAPI staining (blue) in differentiated SH-SY5Y with no treatment (control) and **Figure 13B** displays LHX9 staining (green) in differentiated SH-SY5Y with no treatment. **Figure 13C** shows the merged channels. Positive staining of LHX9 was localised in the nucleus which can be observed in **Figure 13B**. In the image displaying the merged channels (**Figure 13C**), LHX9 expression seems to be present in the cytoplasm as well.

A. DAPI

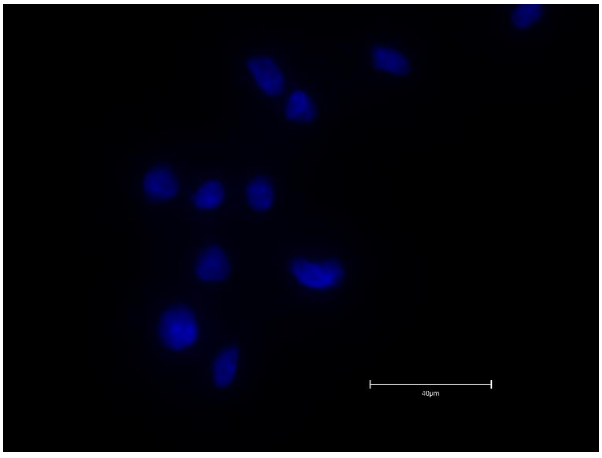

B. LHX9

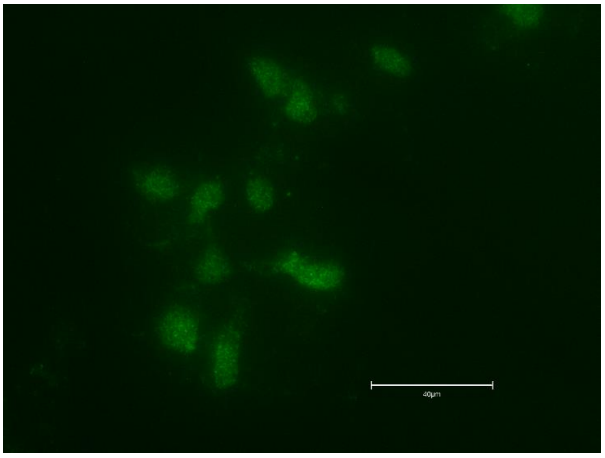

C. Merge

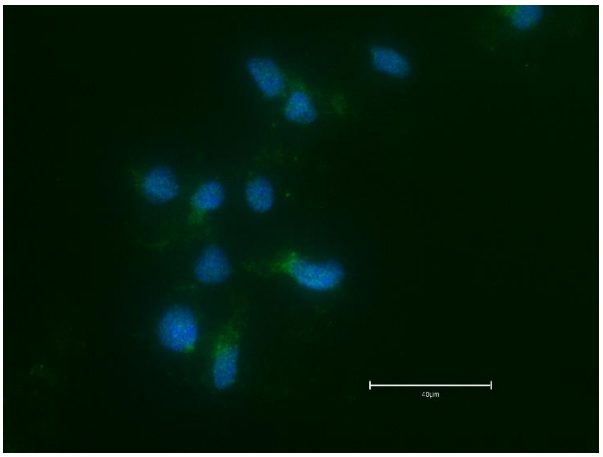

Figure 13: Immunofluorescence staining of LHX9 in differentiated SH-SY5Y without treatment (A) Nuclei of the differentiated SH-SY5Y with no treatment were stained with DAPI (blue). **(B)** Differentiated SH-SY5Y cells were stained with LHX9 antibody at a 1:1000 dilution then conjugated with Alexa flour 488 (green) in order to view the location of LHX9 in the cell. **(C)** Merging of both channels. Images taken at ×60 magnification with EVOS M5000 imaging system with a scale bar of 40 µm for all the images.

3.4.a. Immunofluorescence staining of LHX9 in differentiated SH-SY5Y cells treated with Torin1

Images showing immunofluorescence staining of LHX9 in differentiated SH-SY5Y with Torin1 treatment. **Figure 14A** shows the DAPI staining (blue), and **Figure 14B** displays LHX9 staining (green) in differentiated SH-SY5Y with Torin1 treatment while **Figure 14C** shows the merged channels. Despite the SH-SY5Y cells treatment with Torin-1, LHX9 is

still highly expressed in the nucleus (**Figure 14B**). However, as it was previously observed in the control, LHX9 is also slightly expressed in the cytoplasm (**Figure 14C**).

A. DAPI

B. LHX9

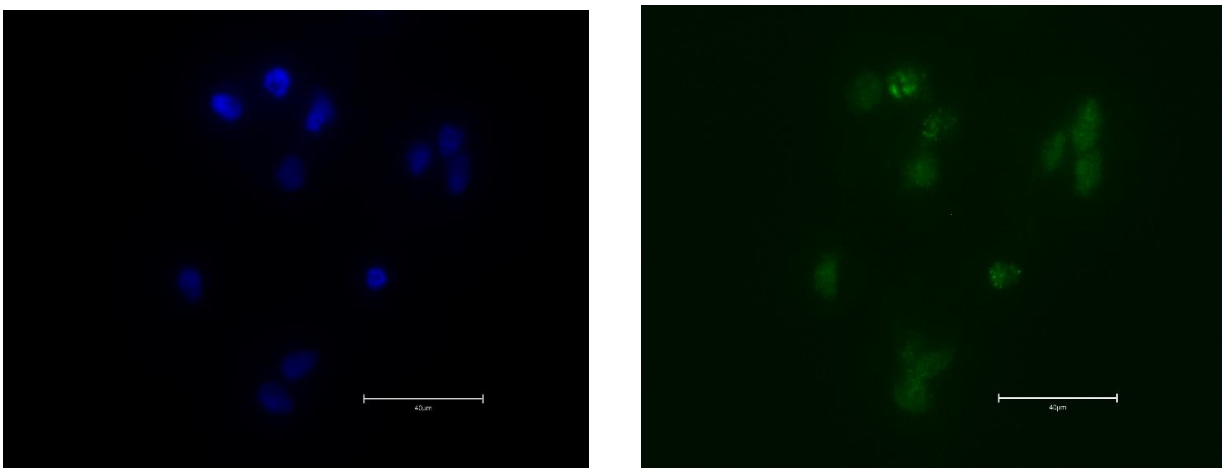

C. Merge

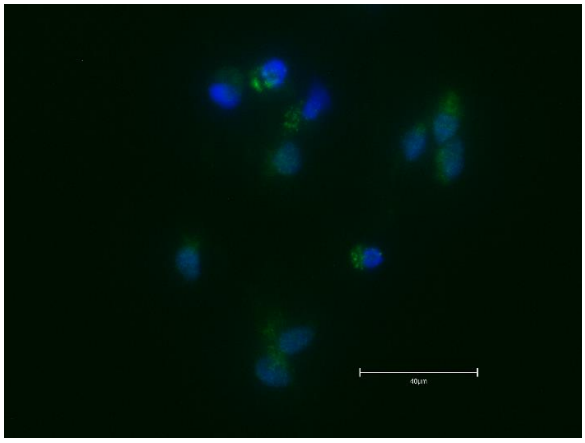

Figure 14: Immunofluorescence staining of LHX9 in differentiated SH-SY5Y with Torin1 treatment (A) Nuclei of the differentiated SH-SY5Y with Torin1 treatment were stained with DAPI (blue). **(B)** Differentiated SH-SY5Y cells were stained with LHX9 antibody at a 1:1000 dilution then conjugated with Alexa flour 488 (green) in order to view the location of

LHX9 in the cell. **(C)** Merging of both channels. Images taken at ×60 magnification with EVOS M5000 imaging system with a scale bar of 40 µm for all the images.

3.4.b. Immunofluorescence staining of LHX9 in differentiated SH-SY5Y cells treated with RapaLink-1

Images showing immunofluorescence staining of LHX9 in differentiated SH-SY5Y with RapaLink-1 treatment. **Figure 15A** shows the DAPI staining (blue) and **Figure 15B** displays LHX9 staining (green) in differentiated SH-SY5Y with RapaLink-1 treatment. **Figure 15C** shows the merged channels. Regardless of the RapaLink-1 treatment on differentiated SH-SY5Y cells, LHX9 was still found to be expressed in the nucleus (**Figure 15B**). However, as it was previously observed in both the control and the Torin1 treatment, LHX9 was also found to be slightly expressed in the cytoplasm (**Figure 15C**).

A. DAPI

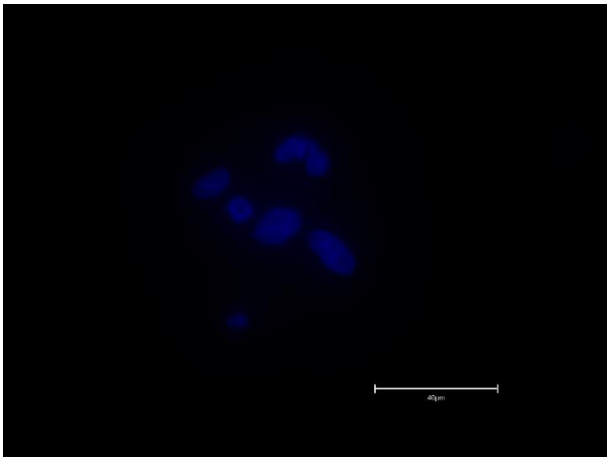

B. LHX9

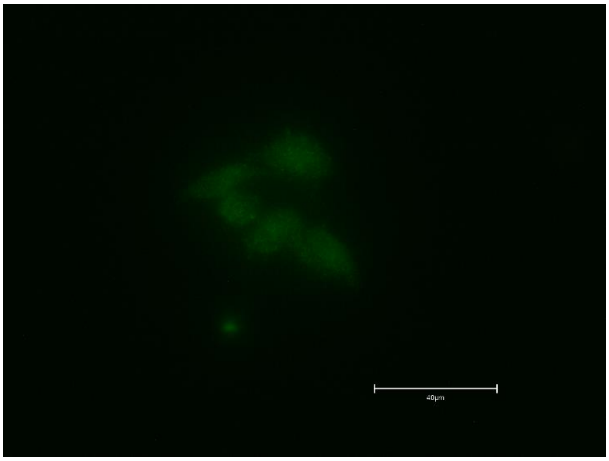

C. Merge

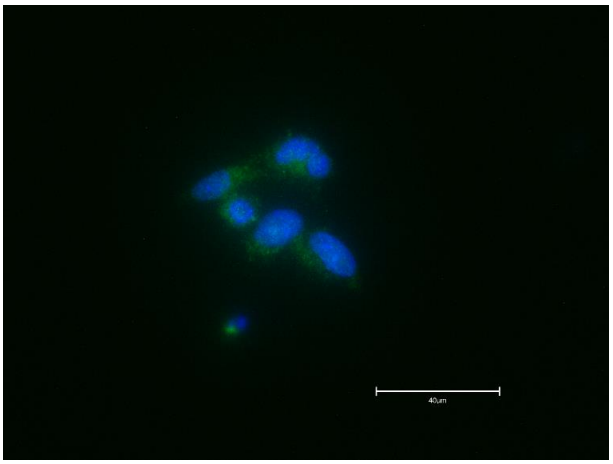

Figure 15: Immunofluorescence staining of LHX9 in differentiated SH-SY5Y with RapaLink-1 treatment (A) Nuclei of the differentiated SH-SY5Y with RapaLink-1 treatment were stained with DAPI (blue). **(B)** Differentiated SH-SY5Y cells were stained with LHX9 antibody at a 1:1000 dilution then conjugated with Alexa flour 488 (green) in order to view the location of LHX9 in the cell. **(C)** Merging of both channels. Images taken at ×60 magnification with EVOS M5000 imaging system with a scale bar of 40 µm for all the images.

3.4c. Differentiated SH-SY5Y nucleocytoplasmic ratio difference from control to treatments

The images were analysed by utilising ImageJ, after which the nuclear to cytoplasm (N/C) ratios were determined (**Figure 16**). The N/C ratios were measured in order to look into the relative size of the nucleus to the cytoplasm as well as to assess if there are any differences between the control and the treatments (Torin1 and RapaLink-1) used on the differentiated SH-SY5Y cells. In comparison to the control (mean value of 1.50), both treatments were recorded to have reduced N/C ratios. The lowest N/C ratio value was in the RapaLink-1 treatment (mean value of 1.30) compared to the Torin1 treatment (mean value of 1.39) which has a minor increase in the N/C ratio. These results suggest that in RapaLink-1 treatment, LHX9 is predominantly expressed in the nucleus with a lower expression in the cytoplasm.

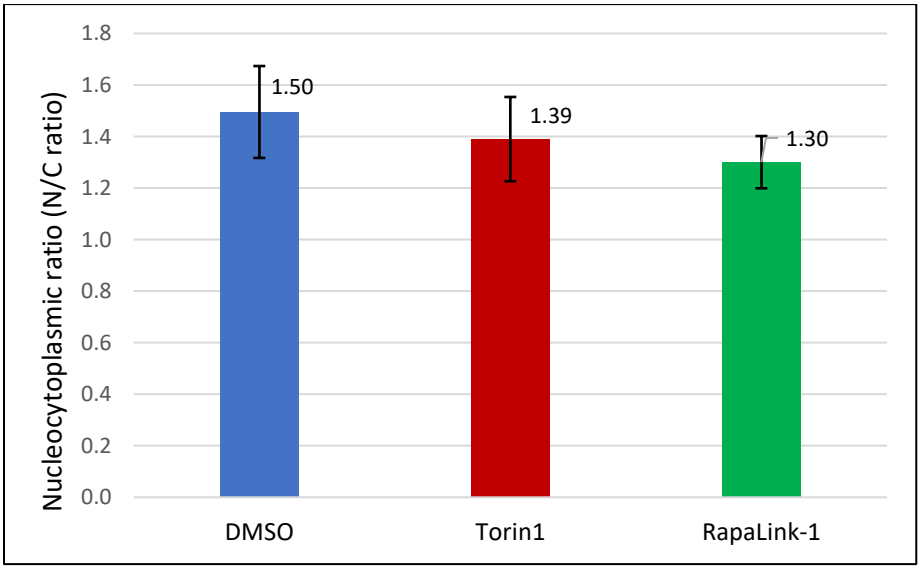

Figure 16: Differentiated SH-SY5Y cells N/C ratios. Histogram displaying the N/C ratios of the control, Torin1 and RapaLink-1 treatments.

By selecting the regions of interest, the nucleocytoplasmic ratio values were calculated for approximately 3-26 cells using the ImageJ software. For this experiment 5 images per each condition were analysed for better accuracy and the analysis contains the standard deviation of all replicates. A one-way ANOVA statistical test was performed by using GraphPad Prism software and the result showed no statistical significance (p-value = 0.24).

3.5. Validating the expression level of LHX9 and GATA4 in differentiated SH-SY5Y

The following western blots were performed on differentiated SH-SY5Y cells with pharmacological treatment. These experiments were conducted to validate the expression levels of both LHX9 and GATA4 in the SH-SY5Y cells as well as to observe if there were any differences between the protein levels expression and transcriptional levels. After differentiation cells were treated with the following inhibitors: Torin1 and RapaLink-1. In this study, DMSO was used as a control.

3.5.a. LHX9 expression in differentiated SH-SYSY

To invstigate the expression level of LHX9 in differetiated SH-SY5Y after pharmacological treatment, western blots were performed. As shown in **Figure 17A**, LHX9 was found to be highly expressed in both the RapaLink-1 and Torin1 treatments in comparison to the control. To measure the expression level of LHX9, ImageJ was used to determine the relative desity (fold change) of LHX9 in each condition that was

normalised against the Control and against β-Actin. LHX9's expression was upregulated in RapaLink-1 and slightly upregulated in Torin1 which can be observed from **Figure 17A.** In the histogram shown in **Figure 17B**, treatment with RapaLink-1 indicated that LHX9 has 1.88-fold change increase whereas treatment with Torin1 revealed that LHX9 has a 1.83-fold change. These results suggest that LHX9 expression was upregulated in SH-SY5Y cells after treatment with both Torin1 and Rapalink-1.

A.

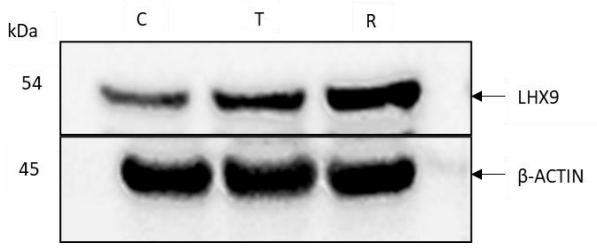

B.

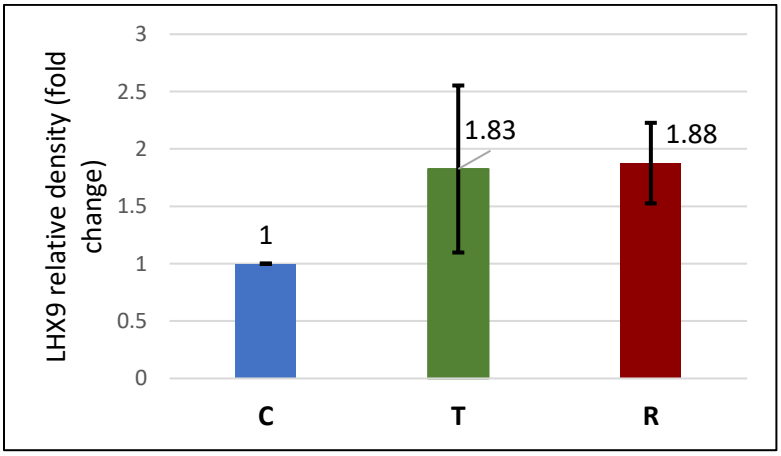

Figure 17: LHX9 level of expression in differentiated SH-SY5Y. (A) The expression level of LHX9 with β-Actin serving as the control in differentiated SH-SY5Y cells treated with Torin1 and RapaLink1 for 5h were detected by Western blot. **(B)** Histogram is representative of the fold

changes of LHX9 protein levels. Each column represents a normalized ratio (fold-changes) to β-actin and to controls. For this experiment triplicates were conducted for better accuracy and the analysis contains the standard deviation of all three replicates. **Legend:** DMSO treated cells are labelled with (C). Torin1 treated cells are labelled with (T) and the RapaLink-1 treated cells are labelled with (R).

3.5.b. GATA4 expression in differentiated SH-SY5Y

In order to test our hypothesis, the level of expression of the transcription factor, GATA4 has to be investigated in differetiated SH-SY5Y cell after pharmacological treatment with Torin1 and RapaLink-1 by utilising Western Blot technique. To measure the expression level of GATA4, ImageJ was used to determine the relative desity (fold change) of GATA4 in each condition that was normalised against the Control and against β-Actin. As it is shown in **Figure 18A**, GATA4 level of expression seems to be consistent in all the conditions without showing any significant upregulation/downregulation. In the histogram displayed in **Figure 18B**, treatment with Torin1 indicates that GATA4 is slightly upregulated with 1.26-fold change than treatment with RapaLink-1 which reveals that GATA4 has 1.05-fold change. These results suggest that GATA4 level of expression does not have a significant change in SH-SY5Y cells after treatment with both Torin1 and Rapalink-1.

A.

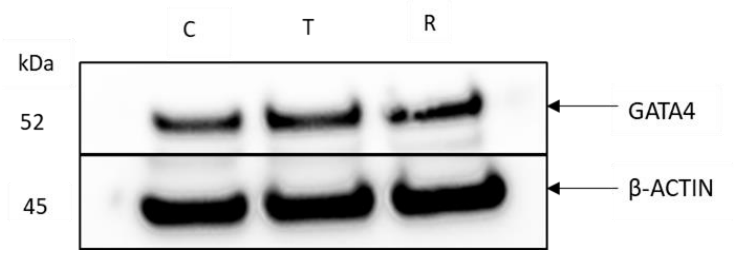

B.

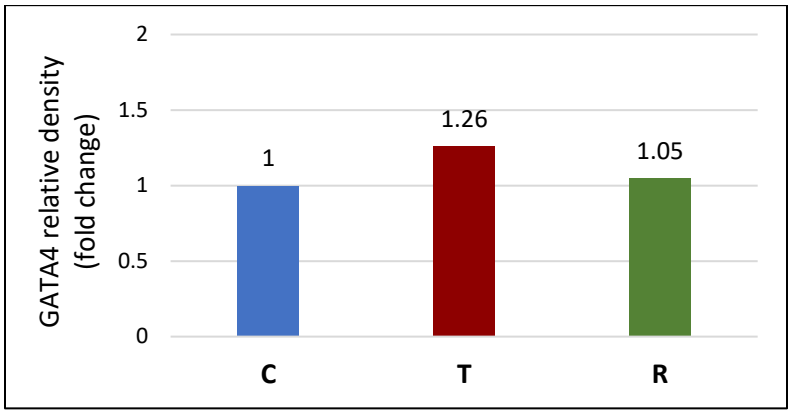

Figure 18: GATA4 level of expression in differentiated SH-SY5Y. **(A)**The expression level of GATA4, with β-Actin serving as the control in differentiated SH-SY5Y cells which were treated with Torin1 and RapaLink-1 for 5h were detected by Western Blot. **(B)** Western blot quantification represented by a histogram showing the fold changes of GATA4 protein levels. Each column represents a normalized ratio (fold-change) to β-Actin and to controls. **Legend:** DMSO treated cells are

labelled with (C). Torin1 treated cells are labelled with (T) and the RapaLink-1 treated cells are labelled with (R).

3.6. Serum starvation experiment on undifferentiated SH-SY5Y

The purpose of this serum starvation experiment was to identify the state of activity or inactivity of mTOR in undifferentiated SH-SY5Y as well as to determine the timeline of mTOR reactivation after the serum starvation occurred. Western blots with the antibodies of interest were tested in this experiment namely, LHX9 and GATA4 to validate their expression patterns in undifferentiated SH-SY5Y. Phospho-4E-BP1 was also tested to establish the state of activity or inactivity of mTOR upon starvation as well as addition of serum. The undifferentiated cells in this experiment were not probed with any treatment.

3.6.a. GATA4 expression in undifferentiated SH-SY5Y

As it can be observed from **Figure 19A**, GATA4 expression is much more prominent in the S condition after the cells were starved for 5h than in the other treatments. In the case of serum readdition (R) for both timepoints (5h and 24h), GATA4's level of expression seemed to be slightly down. The histogram in **Figure 19B** reveals that for both time points the starvation conditions (S) had similar fold changes to the control. The expression level of GATA4 has been registered to be slightly down in the 5h serum readdition (R) condition with a 0.65-fold change while in the 24h serum readdition (R) condition a 0.45-fold change was recorded. These results suggest that GATA4 does not

have a significant change apart from the serum readdition conditions, both timepoints, where it is slightly downregulated in undifferentiated SH-SY5Y cells.

A.

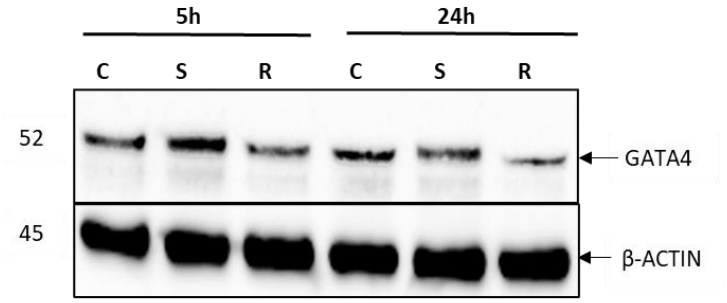

B.

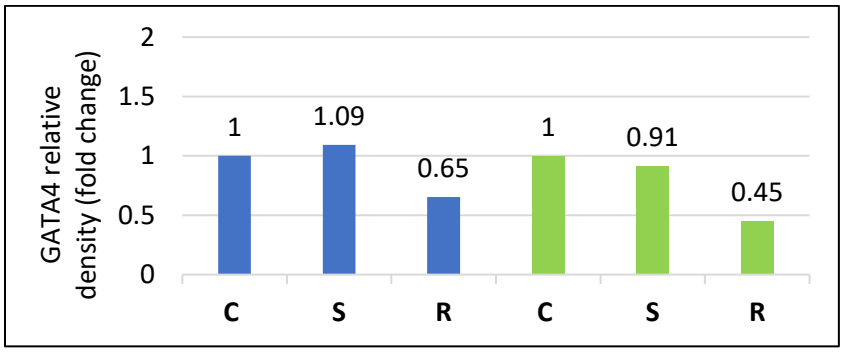

Figure 19: GATA4 expression in undifferentiated SH-SY5Y cells (A) Western blot analyses of GATA4 and loading control (β-Actin) levels in undifferentiated SH-SY5Y cells grown in DMEM with and without serum for 5h and 24h. This experiment was performed one time. **(B)** Histogram is representative of the fold changes of GATA4 protein levels, which were analysed using ImageJ. Each column represents a normalized ratio (fold-changes) to the loading control (β-Actin) and to controls. The blue columns represent the 5h treatments while the green ones represent the 24h

treatments. **Legend**: C represents 5h/10h with complete media (controls); S represents media with no serum for 5h/10h; R represents media with no serum for 5h/24h followed by addition of complete media for another 5h/24h. C= Control, S= Starvation, R= Readdition.

3.6.b. LHX9 expression in undifferentiated SH-SY5Y

After looking at LHX9's expression in differentiated SH-SY5Y cells with treatment previously shown (Figure 4A, B), we were interested to investigate if LHX9's level of expression would be similar in undifferentiated SH-SY5Y with no treatment. As it can be observed from **Figure 20A**, in the 5h treatments, LHX9 has a similar level of expression in the control (C), in the serum starvation condition (S), and in the readdition condition (R). In the 24h treatment, LHX9 was slightly more expressed in the serum starvation condition (S) than in the 5h treatment. In the case of serum readdition (R) for the 24h timepoint, LHX9's level of expression seemed to be slightly down then in the 24h timepoint serum starvation condition. The histogram in **Figure 20B** reveals that LHX9 has a 1.51-fold change for the S condition in the 5h timepoint while in the 24h time point it has a 1.34-fold change. The expression level of LHX9 has been registered to be slightly down in the 5h serum readdition (R) condition with a 0.84-fold change while in the 24h serum readdition (R) condition a 1.11-fold change was recorded. These results suggest that LHX9 is expressed in undifferentiated SH-SY5Y cells with higher levels of expression in the serum starvation conditions for both timepoints than in the serum readdition conditions. However, there is no statistical significance.

A.

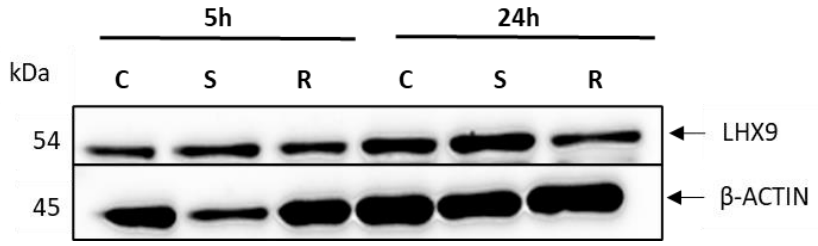

B.

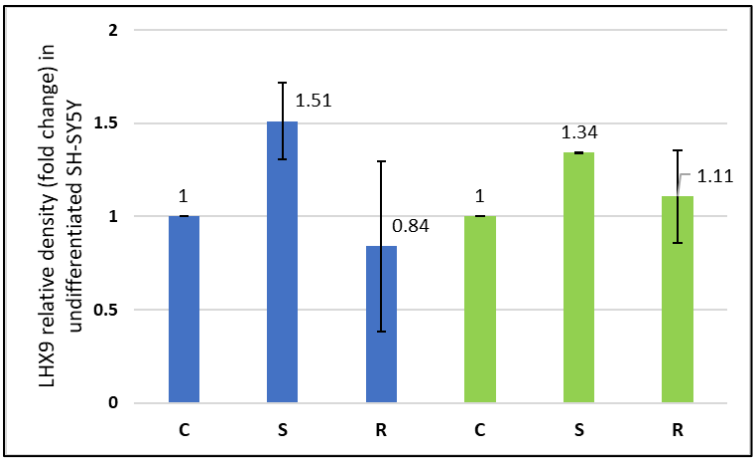

Figure 20: LHX9 expression in undifferentiated SH-SY5Y cells (A) Western blot analyses of LHX9 and loading control (β-Actin) levels in undifferentiated SH-SY5Y cells grown in DMEM with and without serum for 5h and 24h. **(B)** Histogram is representative of the fold changes of LHX9 protein levels, which were analysed using ImageJ. Each column represents a normalized ratio (fold-changes) to the loading control (β-Actin) and to controls. The blue columns represent the 5h treatments while

the green ones represent the 24h treatments. For this experiment duplicates were conducted for better accuracy and the analysis contains the standard deviation of all three replicates**. Legend**: C represents 5h/10h with complete media (controls); S represents media with no serum for 5h/10h; R represents media with no serum for 5h/24h followed by addition of complete media for another 5h/24h. C= Control, S= Starvation, R= Readdition.

3.6.c. Phospho-4E-BP1 expression in undifferentiated SH-SY5Y

Phospho-4E-BP1 was tested on undifferentiated SH-SY5Y to visualise the state of activity or inactivity of mTOR under the serum starvation condition as well as after the addition of serum. The expression of Phospho-4E-BP1 in the 5h serum stravation (S) condition and the serum readdion condition (R) is much more prominent than its expression in the 24h serum stravation (S) condition and the serum readdion condition (R) which is shown in **Figure 21A**. Moreover, the relative desity of Phospho-4E-BP1 in all conditions presented in the histogram **Figure 21B** reveals that Phospho-4E-BP1 had a 3.57-fold change under the 5h serum readdion condition (R) while in the other conditions the level of expression did not change substatially. The results displayed earlier suggest that Phospho-4E-BP1 level of expression in undifferentiated SH-SY5Y cells is upregulated only in the 5h serum readdion condition (R).

A.

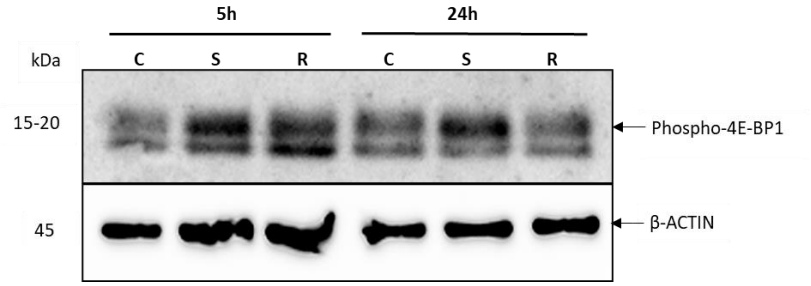

B.

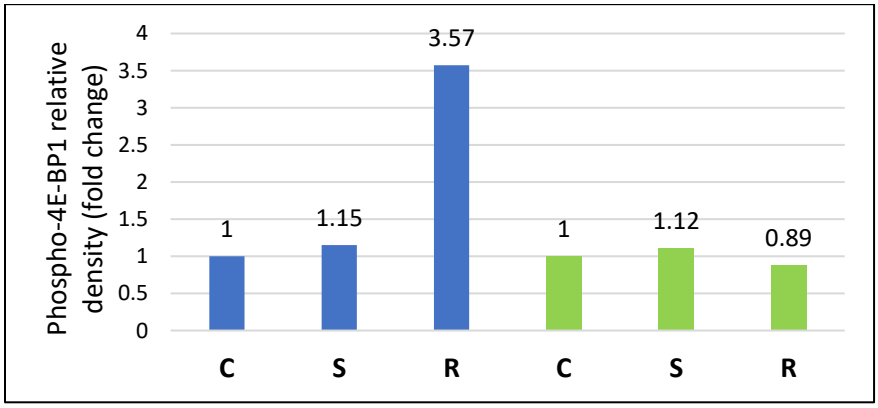

Figure 21: Phospho-4E-BP1 expression in undifferentiated SH-SY5Y. **(A)** Western blot analyses of Phospho-4E-BP1 and loading control (β-Actin) expression in undifferentiated SH-SY5Y cells grown in DMEM with and without serum for 5h and 24h. This experiment was performed one time. **(B)** Histogram is representative of the fold changes of Phospho-4E-BP1 protein levels, which were analysed using ImageJ. Each column

represents a normalized ratio (fold-changes) to the loading control (β-Actin) and to controls. The blue columns represent the 5h treatments while the green ones represent the 24h treatments. **Legend**: C represents 5h/10h with complete media (controls); S represents media with no serum for 5h/10h; R represents media with no serum for 5h/24h followed by addition of complete media for another 5h/24h. C= Control, S= Starvation, R= Readdition.

3.7. Glycolysis assay

The transciption factor of interst LHX9 has been found to be inplicate in glycolysis. It is postulated that when LHX9 is overexpressed it inhibits the PGK1 induction by knockdown of the tumour supressor p53 thereby inhibiting glycolysis (Luo *et al.*, 2021). A glycolysis assay was conducted in this study to investigate particular enzymes which are key regulators of glycolysis in differentiated SH-SY5Y cells treated with pharmacological treatments namely Torin1 and RapaLink-1. Differences between the transcriptome data showing their transcriptional level and the level of protein expression shown in the Western Blods were investigated.

3.7.a. Hexokinase 1

Hexokinase1 (HK1) catalyses the conversion of D-glucose into glucose-6-phosphate, this being the first step of glycolysis. In this experiment the expression of Hexokinase1 seems to be similar in all the conditions, shown in **Figure 22A**. To further analyse if

there are any significant fold changes in HK1, ImageJ was used to determine the relative desity (fold change) of HK1 in each condition that was normalised against the control and against β-Actin. The histogram in **Figure 22B** reveals that there are no significant fold changes in HK1 expression. These results suggest that HK1 expression does not have a significant change after pharmacological treatment with Torin1 and RapaLink-1 in differentiated SH-SY5Y.

A.

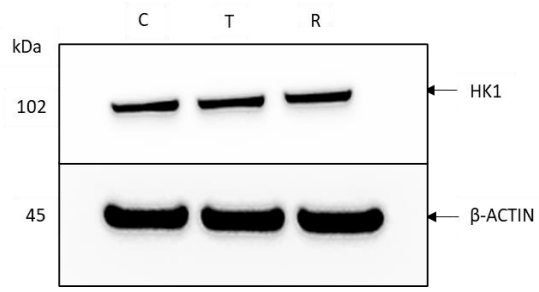

B.

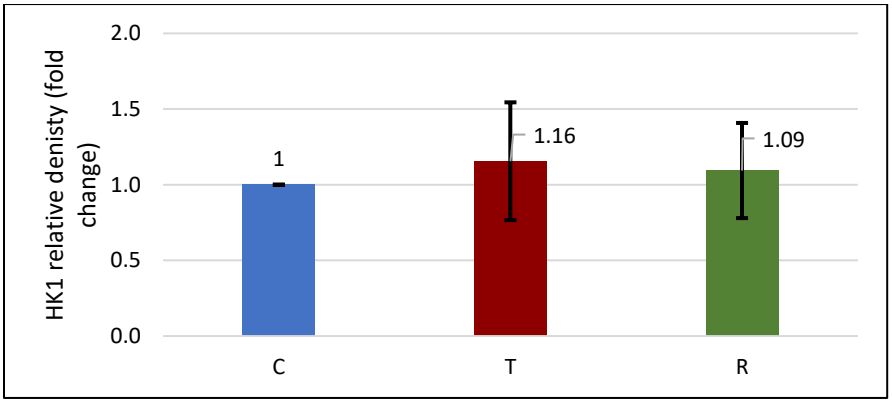

Figure 22: HK1 expression in differentiated SH-SY5Y after pharmacological treatment. A) Western blot analyses of HK1 and loading control (β-Actin) expression in differentiated SH-SY5Y cells treated with DMSO, Torin1(250nM) and RapaLink-1(25nM) for 5h. **B**) Histogram is

representative of the fold changes of HK1 protein levels, which were analysed using ImageJ. Each column represents a normalized ratio (fold-changes) to the loading control (β-Actin) and to controls. For this experiment triplicates were conducted for better accuracy and the analysis contains the standard deviation of all three replicates. **Legend:** DMSO/Control treated cells are labelled with C. Torin1 treatment cells are labelled with T and the RapaLink-1 treated cells are labelled with R.

3.7.b. Hexokinase 2

As in the case of HK1, Hexokinase2 (HK2) also regulates the conversion of D-glucose into glucose-6-phosphate. In **Figure 23A**, it can be observed that in differentiated SH-SY5Y cells with pharmacological tratment, the expression of HK2 does not change in all the conditions. To further analyse if there are any significant fold changes in HK2, ImageJ was used to determine the relative desity (fold change) of HK2 in each condition that was normalised against the control and against β-Actin. The histogram in **Figure 23B** reveals that in all the treatments the fold changes are negligible. Therefore, these results show that HK2 expression does not have a significant change in differentiated SH-SY5Y after treatment with Torin1 and RapaLink-1.

A.

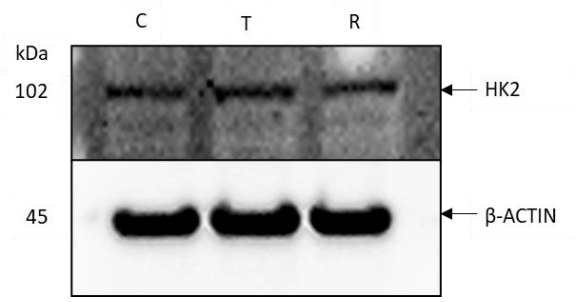

B.

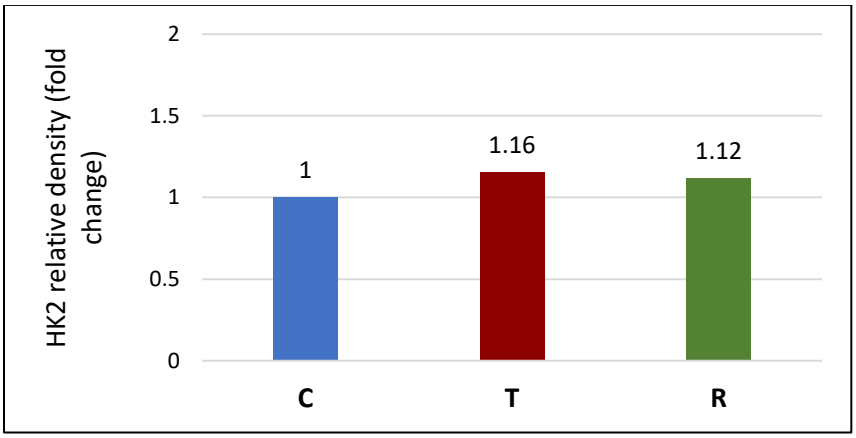

Figure 23: HK2 expression in differentiated SH-SY5Y after pharmacological treatment.A) Western blot analyses of HK2 and loading control (β-Actin) expression in differentiated SH-SY5Y cells treated with DMSO, Torin1(250nM) and RapaLink-1(25nM) for 5h. **B**) Histogram is representative of the fold changes of HK2 protein levels, which were analysed using ImageJ. Each column represents a normalized ratio (fold-changes) to the loading control (β-Actin) and to controls. **Legend:** DMSO/Control treated cells are labelled with C. Torin1 treatment cells are labelled with T and the RapaLink-1 treated cells are labelled with R.

3.7.c. PFKP

Phosphofructokinase (PFK) is an enzyme implicated in glycolysis that catalyses the phosphorylation of fructose-6-phosphate. Platelet-type phosphofructokinase (PFKP) is a subunit of PFK (Morrison *et al.*, 1992). In **Figure 24A,** PFKP's level of expression in differentiated SH-SY5Y cells with pharmacological tratment, is quite faint and does not change in any of the conditions. In order to determine the significance of PFKP expresssion, ImageJ was utilised to determine the relative desity (fold change) of PFKP in each condition that was normalised against the control and against β-Actin.The histogram in **Figure 24B** revals that in all the treatments PFKP does not have a significant increase or decrease in fold change. Therefore, these results show that PFKP expression does not change in differentiated SH-SY5Y following treatment with Torin1 and RapaLink-1**.**

A.

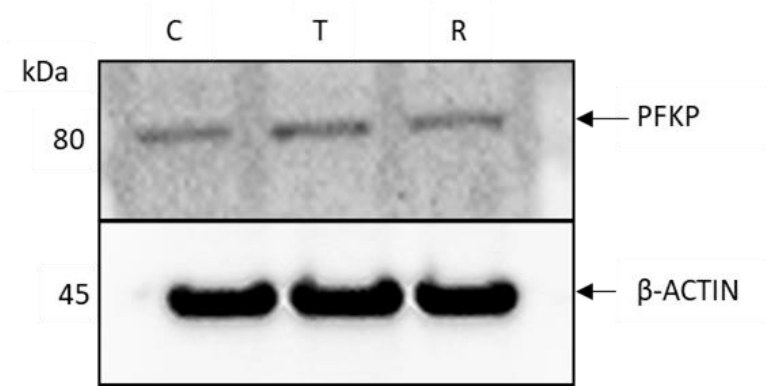

B.

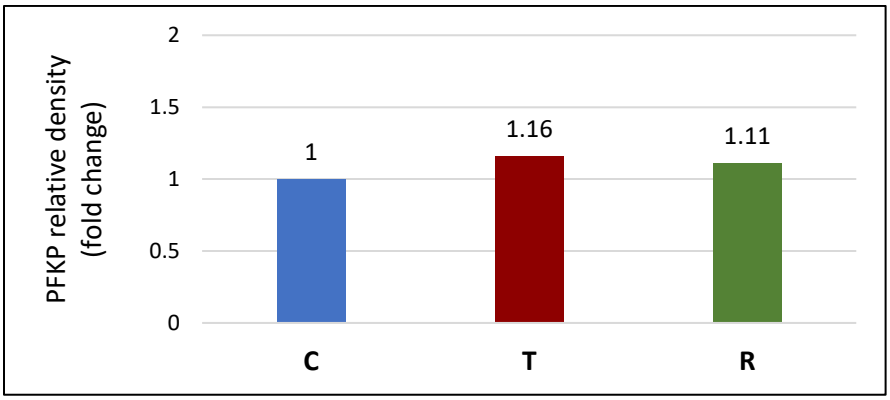

Figure 24: PFKP expression in differentiated SH-SY5Y after pharmacological treatment. A) Western blot analyses of PFKP and loading control (β-Actin) expression in differentiated SH-SY5Y cells treated with DMSO, Torin1(250nM) and RapaLink-1(25nM) for 5h. **B**) Histogram is representative of the fold changes of HK1 protein levels, which were analysed using ImageJ. Each column represents a normalized ratio (fold-changes) to the loading control (β-Actin) and to controls. **Legend:** DMSO/Control treated cells are labelled with C. Torin1 treatment cells are labelled with T and the RapaLink-1 treated cells are labelled with R**.**

3.7.d. GAPDH

Another key regulator in glycolysis is glyceraldehyde-3-phosphate dehydrogenase (GAPDH) which is an enzyme that catalyses the phosphorylation of glyceraldehyde-3-phosphate (Barber *et al.*, 2005). GAPDH level of expression in differentiated SH-SY5Y cells after treatment seems to be constant in all the conditions (**Figure 25A**). In order to determine the significance of GAPDH expresssion, ImageJ was utilised to determine the relative desity (fold change) of GAPDH in each condition that was normalised against the control and against β-Actin. As it can be observed in **Figure 25B**, RapaLink-1 treatment has a 1.24-fold change while the Torin1 treatment has a 1.19-fold change. Therefore, these results suggest that GAPDH expresion in differentiated SH-SY5Y with pharmacolgical treatement, does not have a significant change.

A.

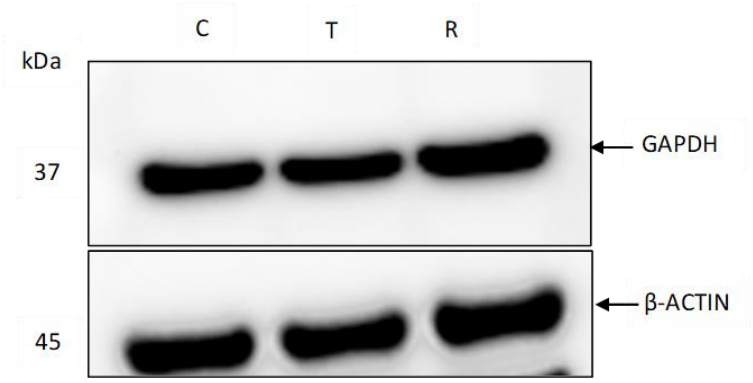

B.

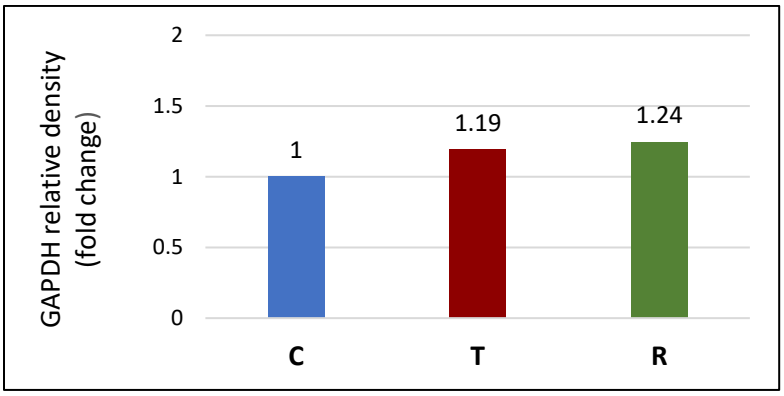

Figure 25: GAPDH expression in differentiated SH-SY5Y after pharmacological treatment. A) Western blots showing the level of GAPDH protein, with β-actin serving as the control in differentiated SH-SY5Y cells treated with DMSO, Torin1(250nM) and RapaLink-1(25nM) for 5h. GAPDH antibody was not used as a loading control, it is part of glycolysis assay kit. **B**) Histogram is representative of the fold changes of GAPDH protein levels using ImageJ. Each column represents a normalized ratio (fold-changes) to β-actin and to control. **Legend:** DMSO/Control treated cells shown in the first lane are labelled with C. Torin1 treatment cells shown in the second lane are labelled with T and the RapaLink-1 treated cells shown in the last lane are labelled with R.

3.7.e. LDHA

Lactate dehydrogenase A (LDHA) is a key effector in the glucose metabolism because it converts pyruvate into lactate (Semenza, 2007). The expression of LDHA can be observed in **Figure 26A**, where in all the conditions LDHA seems to have similar levels of expression. In order to further analyse if there is any significance in LDHA expression in differentiated SH-SY5Y cells, ImageJ analysis on the Western Blot was perforemed to determine the relative desity (fold change) of LDHA. Each condition was normalised against the control and against β-Actin. LDHA fold changes displayed in **Figure 26B** show that in the RapaLink-1 treatment a 1.26-fold change was registered while the Torin1 treatment had a 1.19-fold change. Furthermore, the analysis reveals that in differentiated SH-SY5Y cells with pharmacological treatment, LDHA expression does not have a significant change.

A.

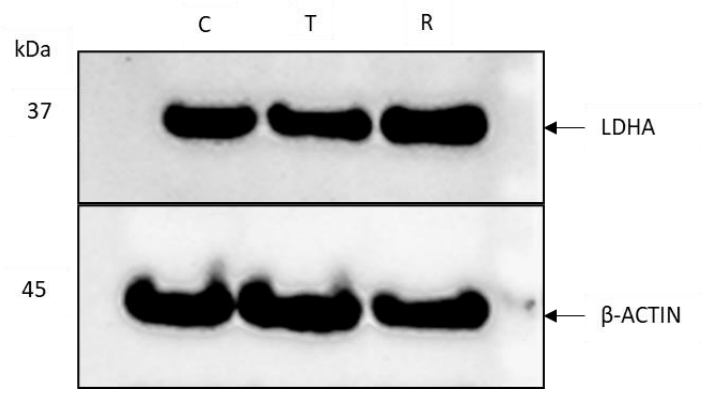

B.

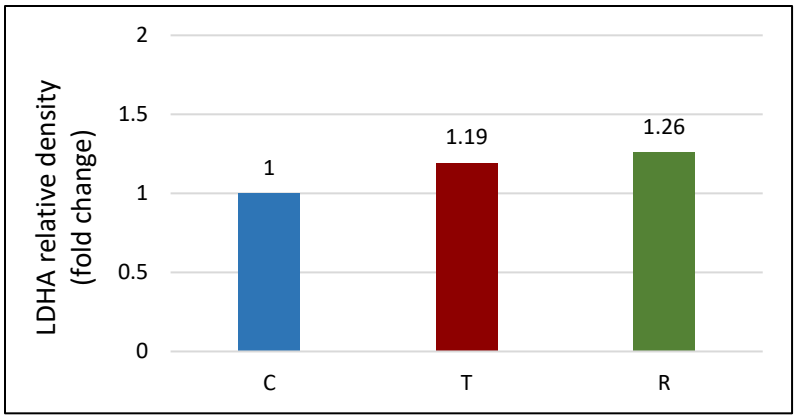

Figure 26: LDHA expression in differentiated SH-SY5Y after pharmacological treatment. A) Western blots showing the level of LDHA protein, with β-Actin serving as the control in differentiated SH-SY5Y cells treated with DMSO, Torin1(250nM) and RapaLink-1(25nM) for 5h. **B**) Histogram is representative of the fold changes of LDHA protein levels using ImageJ. Each column represents a normalized ratio (fold-changes) to β-actin and to the control. **Legend:** DMSO/Control treated cells shown in the first lane are labelled with C. Torin1 treatment cells shown in the second lane are labelled with T and the RapaLink-1 treated cells shown in the last lane are labelled with R.

3.7.f. PKM1/2

Another glycoytic enzyme is Pyruvate kinase which regulates the last step of glycolysis by catalysing the conversion of phosphoenolpyruvate to pyruvate (Christofk *et al.*, 2008). In mammals there are four pyruvate kinase izoforms but the ones revelevat for this study are M1 and M2. Most adult tissues express the M1 isoform, and during embryonic development, a splice variation of M1 called the M2 isoform is expressed (Christofk *et al.*, 2008). As it can be observed from **Figure 27A**, PKM1/2 in differentiated SH-SY5Y with pharmacologycal treatment has a similar level of expression in all the conditions. In order to further analyse if there is any significance in PKM1/2 expression in differentiated SH-SY5Y cells, ImageJ analysis on the Western Blot was perforemed to determine the relative desity (fold change) of PKM1/2. Each condition was normalised against the control and against β-Actin. In both Torin1 and RapaLink-1 treatments PKM1/2 is shown to have identical fold changes and not a sigificat chage to the control (**Figure 27B**). The analysis reveals that in differentiated SH-SY5Y cells with pharmacological treatment, PKM1/2 expression does not have a significant change.

A.

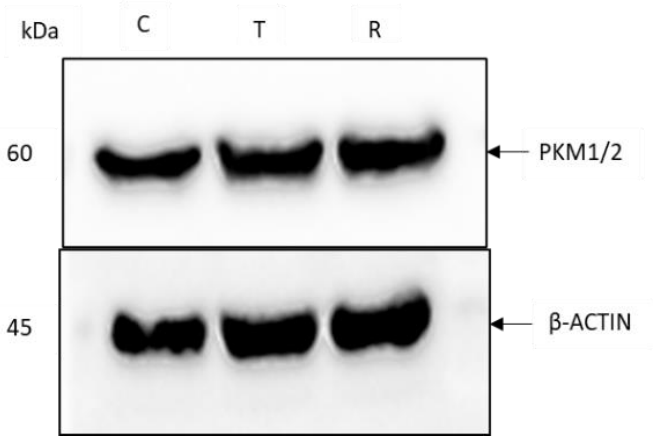

B.

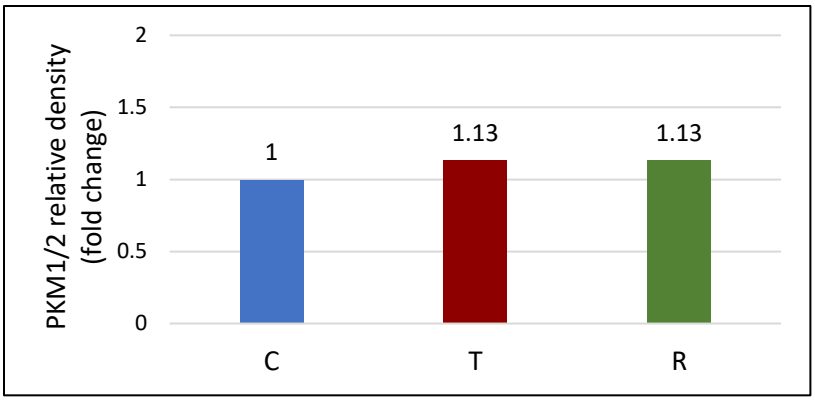

Figure 27: PKM1/2 expression in differentiated SH-SY5Y after pharmacological treatment. A) Western blots showing the level of PKM1/2 protein, with β-Actin serving as the control in differentiated SH-SY5Y cells treated with DMSO, Torin1(250nM) and RapaLink-1(25nM) for 5h. **B**) Histogram is representative of the fold changes of PKM1/2 protein levels using ImageJ. Each column represents a normalized ratio (fold-changes) to β-actin and to the control. **Legend:** DMSO/Control treated cells shown in the first lane are labelled with C. Torin1 treatment cells shown in the second lane are labelled with T and the RapaLink-1 treated cells shown in the last lane are labelled with R.

3.7.g. PKM2

As previously stated pyruvate kinase M2 (PKM2) is an izoform of pyruvate kinase. In this study both PKM1/2 and PKM2 were tested in order to identify which one of the pyruvate kniase izoforms is present in differentiated SH-SY5Y with pahracologycal treatment. PKM2 is shown to be highly expressed in all the treatment conditions as well as control in differentiated SH-SY5Y which are displayed in **Figure 28A**. In order to further analyse if there is any significance in PKM2 expression in differentiated SH-SY5Y cells, ImageJ analysis on the Western Blot was perforemed to determine the relative desity (fold change) of PKM2. Each condition was normalised against the control and against β-Actin. The analysis result is shown in **Figure 28B**, where the fold changes of PKM2 in both paramcological treatents are shown to be similar to the control condition. These results suggest that out of all the pyruvate kinase izoforms tested in this experiment, PKM2 is the izoform expressed in differentiated SH-SY5Y cells with pharmacologycal treamtnet. In addition, these resuls also display that PKM2 level of exrepssion does not have a significant change in diffrerentiated SH-SY5Y cells with Torin1 and RapaLink-1 treatment.

A.

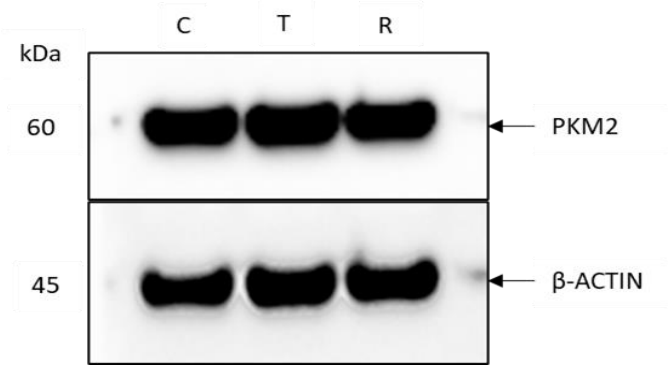

B.

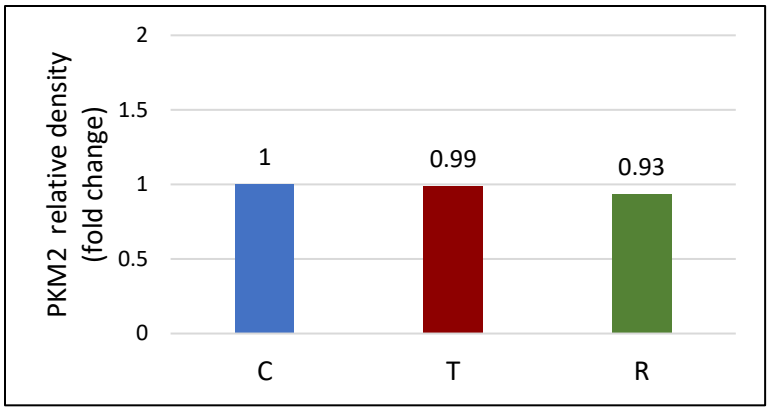

Figure 28: PKM2 expression in differentiated SH-SY5Y after pharmacological treatment. A) Western blots showing the level of PKM2 protein, with β-Actin serving as the control in differentiated SH-SY5Y cells treated with DMSO, Torin1(250nM) and RapaLink-1(25nM) for 5h. **B**) Histogram is representative of the fold changes of PKM2 protein levels using ImageJ. Each column represents a normalized ratio (fold-changes) to β-actin and to the control. **Legend:** DMSO/Control treated cells shown in the first lane are labelled with C. Torin1 treatment cells shown in the second lane are labelled with T and the RapaLink-1 treated cells shown in the last lane are labelled with R.

3.7.h. Pyruvate Dehydrogenase

In the presence of NAD+ (Nicotinamide adenine dinucleotide), pyruvate dehydrogenase complex initiates the change of pyuvate and CoA (Coenzyme A) into acetyl-CoA (acetyl coenzyme A) and CO2 (Strumiło, 2005). As it can be observed in **Figure 29A**, pyruvate dehydrogenase (PDH) is highly expressed in all treatments. In order to further analyse if there is any significance in pyruvate dehydrogenase expression in differentiated SH-SY5Y cells, ImageJ analysis on the Western Blot was perforemed to determine the relative desity (fold change) of pyruate dehydrogenase. The results of this analysis are dysplayed in **Figure 29B** where pyruvate dehydrogenease has a 1.46-fold change in the RapaLink-1 treated cells and a 1.26- fold change in the Torin1 treated cells. A one way ANOVA test was also conducted in order to determine if PDH increase in the treatments is statistically significant. The results displayed by the ANOVA test revealed that PDH's fold changes are not statistically significant.Therefore, in diffrerentiated SH-SY5Y cells with Torin1 and RapaLink-1 treatment, PDH was found not to have a significant change.

A.

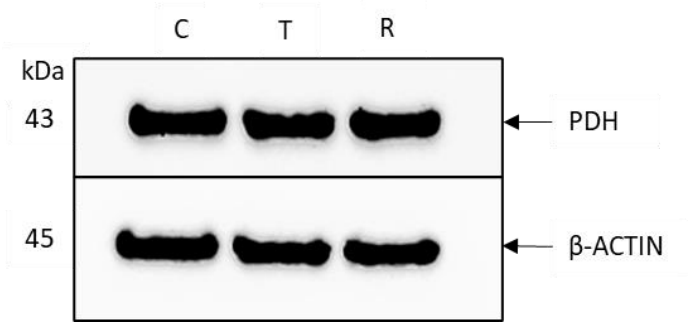

B.

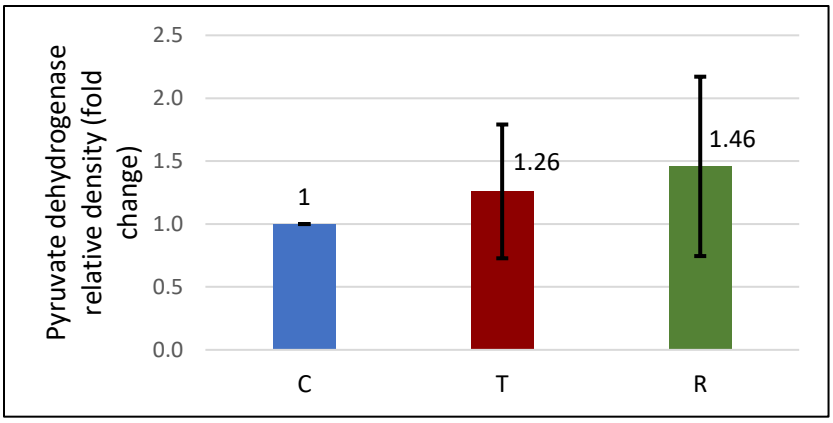

Figure 29: Pyruvate dehydrogenase expression in differentiated SH-SY5Y after pharmacological treatment. A) Western blots showing the level of pyruvate dehydrogenase protein, with β-Actin serving as the control in differentiated SH-SY5Y cells treated with DMSO, Torin1(250nM) and RapaLink-1(25nM) for 5h. **B**) Histogram is representative of the fold changes of pyruvate dehydrogenase protein levels using ImageJ. Each column represents a normalized ratio (fold-changes) to β-actin and to the control. For this experiment triplicates were conducted for better accuracy and the analysis contains the standard deviation of all three replicates. One-way ANOVA statistical test was conducted and the p-value found was 0.66, therefore showing that PDH expression was not statistically significant. **Legend:** DMSO/Control treated cells shown in the first lane are labelled with C. Torin1 treatment cells shown in the second lane are labelled with T and the RapaLink-1 treated cells shown in the last lane are labelled with R.

3.7.i. PGK1

In order to generate 3-phosphoglycerate (3-PGA), phosphoglycerate kinase (PGK) catalyses a phospho-transfer process from 1,3-diphosphoglycerate (1,3-DPG) to ATP (Beutler, 2007). PGK1 expression in SH-SY5Y cells with pharmacological tretment is very prominenet in all the condinitions including control which can be seen in **Figure 30A**. In order to further analyse if there is any significance in PGK1 expression in differentiated SH-SY5Y cells, ImageJ analysis on the Western Blot was perforemed to determine the relative desity (fold change) of PGK1 in each condition. The results of this analysis are dysplayed in **Figure 30B**, showing that with Torin1 and RapaLink-1 treament, PGK1 fold changes do not have a significant chage. Additionally, these resuls also display that PGK1 level of expression does not have a significant change in diffrerentiated SH-SY5Y cells with Torin1 and RapaLink-1 treatment.

A.

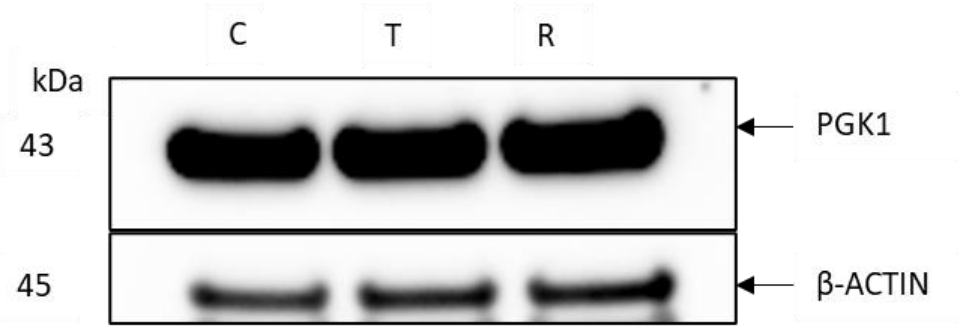

B.

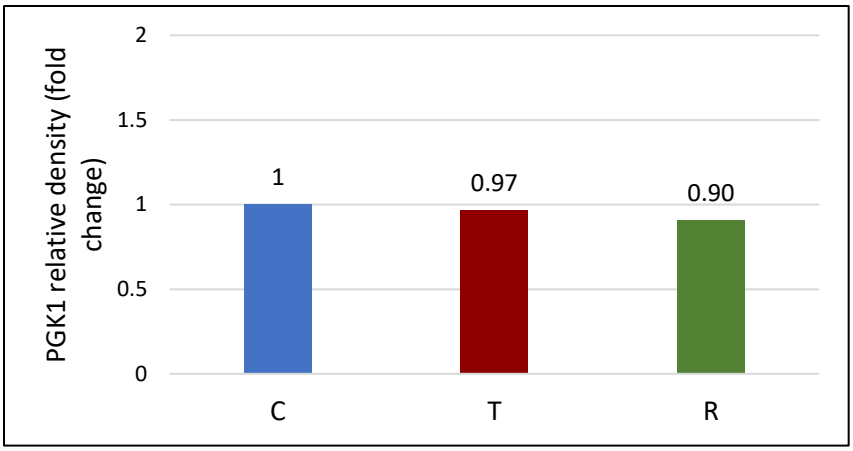

Figure 30: PGK1 expression in differentiated SH-SY5Y after pharmacological treatment. A) Western blots showing the level of PGK1 protein, with β-Actin serving as the control in differentiated SH-SY5Y cells treated with DMSO, Torin1(250nM) and RapaLink-1(25nM) for 5h. **B**) Histogram is representative of the fold changes of PGK1 protein levels using ImageJ. Each column represents a normalized ratio (fold-changes) to β-actin and to the control. **Legend:** DMSO/Control treated cells shown in the first lane are labelled with C. Torin1 treatment cells shown in the second lane are labelled with T and the RapaLink-1 treated cells shown in the last lane are labelled with R

3.7.j. Glycolysis pathway and the glycolytic enzymes of interest

In order to ilustrate the placement of the glycolytic enzymes of interest previously tested by Western Blot techinque in the glycolysis pathway, **Figure 31** was produced. As it can be observed from **Figure 31**, all the glycolytic enzymes tested did not show any significant changes at the protein level in differentiated SH-SY5Y cells with pharmacological treatment.

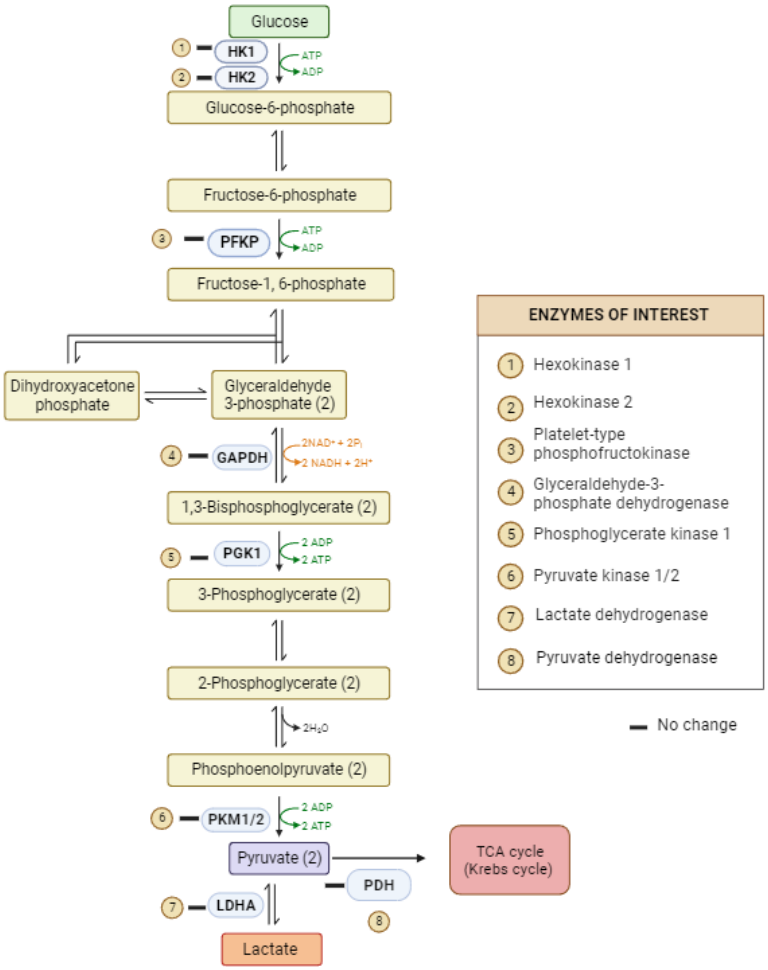

Figure 31: Glycolysis pathway and glycolytic enzymes. Schemtic diagram of the glycolytic metabolism with the enzymes of interest, each shown in the light blue round boxes. Next to each of the enzymes tested,

there is a black line representative of their level of expression in the SH-SY5Y differentiated cells with treatment. Their level of expression was determined by Western Blots previously performed and by ImageJ analysis. This diagram was made with the help of BioRender app.

3.8 Transcriptional level of the glycolytic enzymes and the transcription factors tested

After conducting Western blots in order to determine the level of expression of each enzyme and transcription factor of interest in this experiment, we wanted to establish if there were any differences between the protein levels observed and the transcriptional levels found in the RNA-seq data. Therefore, as it can be observed in **Figure 32A**, in the treatment with Rapalink-1, all the genes seem to have an unchanged expression. In contrast in the Torin1 treatment, LHX9 is upregulated, HK2 is downregulated and LDHA is slightly downregulated.

A.

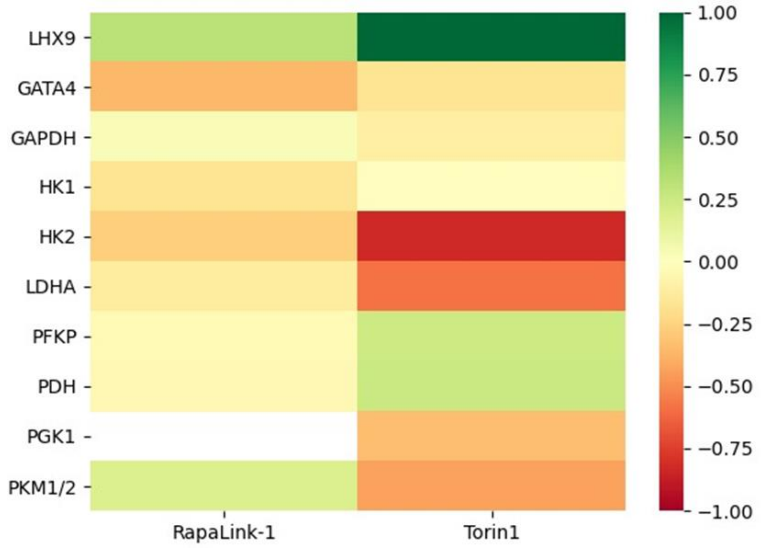

B.

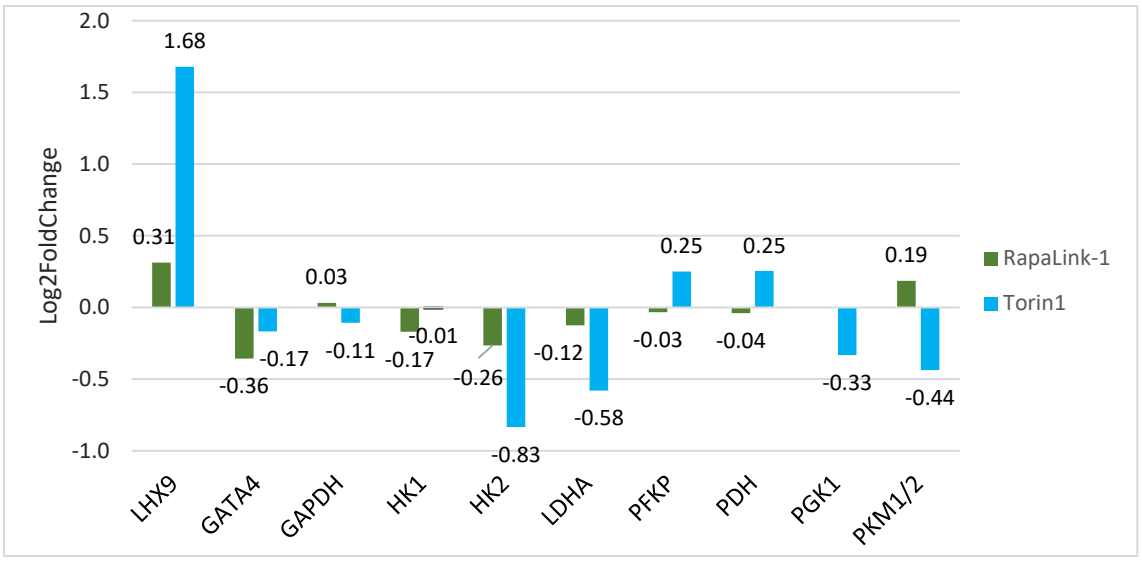

Figure 32: The significance of the genes of interest at the transcriptional level. A. Heatmap showing the gene expression of the genes of interest in Torin-1 and RapaLink-1 treated SH-SY5Y cells. The red boxes represent down-regulated genes and green

boxes represents up-regulated genes. Yellow represents the genes with an unchanged expression. **B.** Histogram displaying the comparison of the Log2FoldChange of all the genes of interest in two different pharmacological treatments.

4. Discussions

4.1. LHX9 upregulation in differentiated SH-SY5Y cell after pharmacological treatment with mTOR inhibitors.

It has been already established that mTOR is a very complex pathway that regulates vital cellular processes and has been associated with a multitude of diseases including cancer, neurodegeneration, insulin resistance, type 2 diabetes, and many more (Laplante and Sabatini, 2012). In the current study, we provide evidence that LHX9 was found to be upregulated in differentiated SH-SY5Y cells after pharmacological treatment with the mTOR inhibitors Torin1 and RapaLink-1. Additionally, we show that LHX9 does not have an effect on glycolysis as per conditions examined. LHX9 is a LIM/homeobox transcription factor, known to be primarily implicated into the development of the central nervous system but until now, it has not been studied in the context of the mTOR pathway (Bertuzzi *et al.*, 1999). The RapaLink-1 inhibitor is known to suppress mTOR complex 1 activity whereas Torin1 is known to inhibit both mTORC complexes, therefore, this would indicate that LHX9 has an increased expression with mTORC1 and mTORC2

inactivation. Interestingly enough, mTOR is known to be highly expressed in the brain, predominantly in the neurons but also in glial cells. In the brain, in response to signals such as growth factors, nutrients, hormones and stress, mTOR regulates neuronal survival and division (Perluigi *et al.*, 2015). Both mTORC complexes have been established to play very important roles in the brain development. In a study conducted by Carson *et al.* (2013) on mice that were knockout (KO) of Rictor, which is a subunit of mTORC2, it was observed that these mice had smaller neurons in the cerebral cortex which supported their assumption that mTORC2 in implicated in the neuronal size. Additionally, in this study it was also observed that impairment of mTOR2 activity led to the disruption of the normal brain development but without affecting mTORC1 signalling. Normally, mTORC1 activation in the brain can also be done by Akt which is activated by mTORC2. Therefore, if mTORC2 activity is inhibited then this would lead to downregulation of mTORC1, but this was not the case in this study because the Rictor knockout mice had a normal mTORC1 activity (Carson *et al.*, 2013).

mTOR has also been implicated in dendritic development. This observation was tested by (Jaworski *et al.*, 2005) in hippocampal neurons where mTOR was inhibited by rapamycin which led to substantial reduction of dendritic branches therefore showing that the complex implicated is mTORC1. Another publication (Jossin and Goffinet, 2007) looked into Reelin, a glycoprotein involved in the mature brain development, connected to PI3K and mTOR. In this paper they showed in hippocampal neurons that Reelin activates the mTOR-S6K1 pathway (mTORC1 downstream effector), however this activation is dependent on the activation of PI3K and Akt as well as Dab1 phosphorylation. Additionally, inhibition of PI3K, Akt, and mTOR prevented the growth

and branching of dendrites which further shows that mTORC2 may be activated by Reelin which would lead Akt phosphorylation (Jossin and Goffinet, 2007). From the research papers stated above, it can be seen that both mTOR complexes play very important roles in neuronal development (Takei and Nawa, 2014).

As previously stated, LHX9 was found to be upregulated, after treatment with the mTOR inhibitors Torin1 and RapaLink-1. Despite the inactivation of both mTOR complexes, LHX9 is still present in big quantities at the protein level which can be observed in **Figure 17A**. The statistical significance of LHX9's expression in these cells after pharmacological treatment was determined by the Kruskal-Wallis test. The p-value found by this statistical test was 0.06, therefore showing that LHX9's expression is not statistically significant. However, as specified before, LHX9's expression looks upregulated at the protein level and there are differences in the fold changes seen between the treatments and control **(Figure 17B)**. In our case, the statistical power was very small due to the actual number of repeats conducted on LHX9 protein levels, although triplicates are standard for such experiments. Furthermore, in order to assess better LHX9's expression in SH-SY5Y cells with mTOR inhibitors, several repeats should be conducted. In addition, the biological significance of small intracellular amount changes for a transcription factor cannot be easily evaluated through western blots. Further functional experiments will be required towards this goal. Until now, this transcription factor has not been linked to mTOR but in this study we provide evidence that LHX9 might be linked to both mTOR complexes. This assumption was made due to the fact that LHX9 had an increased expression after treatment with both mTOR inhibitors (Torin1 and RapaLink-1).

4.2. Evidence of possible LHX9 isoforms in SH-SY5Y cells.

While testing LHX9 expression in differentiated SH-SY5Y cells with pharmacological treatment, we observed that in every Western Blot (WB) conducted, LHX9 presented multiple bands. One of the bands was found at the kDa specified by the supplier (55 kDa) but other nonspecific bands were also found on the blot. For the analysis of LHX9 expression in all the WB, the band encountered at the right kDa was examined. LHX9 expression has been tested in the following glioma cells: U87, SK-N-SH, SHG44 and A172 cells (Luo *et al.*, 2021), but it has not been tested in the SH-SY5Y cell line until now. In the literature, double bands were not reported in other cell lines where LHX9 was tested. With this result, we can make the assumption that the protein of interest exhibits multiple bands either because it has multiple isoforms or because of posttranslational modifications (PTMs). In a study conducted by Failli *et al.* (2000), Lhx9α cDNA, a splicing variation of the gene Lhx9, was isolated and cloned. The expression of both Lhx9 and its isoform was observed in the brain, but with lower expression values of Lhx9α. Differences between Lhx9 and Lhx9α were also recorded in this study, where it was observed that regardless of their expression patterns in the brain, Lhx9 was expressed in the hippocampus and in the first generated neurons of the neocortex while Lhx9α was found to be expressed only in the hippocampus. Furthermore, in another paper (Oshima *et al.*, 2007) LHX9 and four isoforms named Lhx9α, β, γ and δ were tested in the frog *Rana rugosa* in order to identify if LHX9 is expressed in the developing gonads of amphibians. In this study Lhx9 and Lhx9α were found predominantly expressed in the ovary, testis, brain, and heart while Lhx9γ and Lhx9δ were observed in the brain but with a lower expression. The isoform that was

barely detected was Lhx9β (Oshima *et al.*, 2007). We previously assumed that the multiple bands found on the WB may be caused by Lhx9's isoforms. While this assumption may be true, due to the existence of isoforms proven by the studies stated above, none of these papers conducted WB analysis. Therefore, in order to validate the assumption previously made, further approaches such as mass spectrometry-based proteomics should be conducted in order to observe if the nonspecific bands encountered are LHX9's isoforms. Alternatively, gene-specific RT-PCRs designed to target or detect possible isoforms could be conducted.

The other presumption made was that the multiple bands encountered could be caused by post-transcriptional modifications. In order for this to be tested several methods to detect PTMs could be used in further research. One of them is colloidal Coomassie staining, followed by florescent tagging which then results in immunodetection of the PTMs. This method is easy and inexpensive but it also has its limitations therefore another method that could be conducted is Mass Spectrometry. This method can detect known and unknown PTMs, it can find PTMs in complex matrices and it can also show the site where the PTM is situated in the protein molecule.

4.3. LHX9 localisation in both nucleus and cytoplasm in treated SH-SY5Y cells

After validating LHX9's protein expression in the SH-SY5Y cells with pharmacological treatment, we wanted to look into the localisation of this transcription factor therefore, immunofluorescence staining was conducted. In our experiment we observed that LHX9

is located in the nucleus **(Figure 13A)**, however, we also detected LHX9 in the cytoplasm **(Figure 13C, Figure 14C, Figure 15C)**. The results we found match with the results found by Mollé *et al.* (2004) where they investigated both LHX9 and LHX9α localization in the PC12 cells. In this experiment they observed that LHX9 was located in both nucleus and cytoplasm while LHX9α was located only in the nucleus. Furthermore, they also showed that LHX9 and LHX9α have different but significant roles in neuronal differentiation. In PC12 cells, LHX9 was found to promote neuronal differentiation while LHX9α affected the cellular morphology. Thus, they came to the suggestion that LHX9 and LHX9α are not dependent on one another and function in distinct pathways. In our study we also looked into the N/C ratios of the treated SH-SY5Y cells in order to assess if there are any differences between the control and treatments (Torin1 and RapaLink-1). We observed that RapaLink-1 treated cells **(Figure 16)** had a lower N/C ratio (mean value of 1.30) than the control (mean value of 1.50) and the Torin1 treated cells (mean value of 1.39). This result further shows that in RapaLink-1 treated cells, LHX9 is more localised in the nucleus than in the cytoplasm, but less in comparison to the other treatments. For future research, in order to assess better the N/C ratios of the treated SH-SY5Y cells with Torin-1 and RapaLink-1, more replicates should be conducted. Nevertheless, these should be coupled with experiments that would point to the function of LHX9 as a transcription factor and its possible recruitment to specific genomic loci.

4.4. GATA4 expression in differentiated SH-SY5Y cells and link to LHX9

When analysing both of the RNA-seq data sets we came across GATA4 transcription factor which picked our interest for two reasons. Firstly, it has been linked to LHX9 and

secondly, because GATA factors are associated with mTOR function or dietary restriction in other systems (Dobson *et al.*, 2018; Rodriguez-Lopez *et al.*, 2020). GATA4 is known to be primarily involved in cardiac development but it has also been found expressed in the normal brain, playing important roles in the neural inflammatory responses and senescence (Xu *et al.*, 2019). FOG (Friend of GATA) proteins are known to interact and regulate the activity of the GATA transcription factors (Chang *et al.*, 2002). In a study conducted by Smagulova *et al.* (2008) they identified that the GATA4/FOG2 complex, which is required for cardiac development, regulates the cardiac expression of LHX9. Moreover, they also showed that LHX9 is found to be over-expressed if the GATA4/FOG2 complex is lost. However, they also identified that LHX9 α/β are the only truncated isoforms of LHX9 that are expressed in the developing mouse heart. Their discovery on LHX9's isoforms pattern of expression in heart development supports the previous report by Mollé *et al.* (2004), in which it is stated that LHX9's isoforms function in different pathways without having direct competition with each other. In this study, due to this link found between LHX9 and GATA4, we hypothesised that pharmacological inhibition of mTOR, via Torin1 or RapaLink-1, in differentiated SH-SY5Y cells would lead to an upregulation of LHX9 and downregulation of GATA4, which would negatively affect (or inhibit) glycolysis. Alternatively, if GATA4 is found to be upregulated post-treatment, then LHX9 would be downregulated, leading to activation of glycolysis. Therefore, in order to confirm our hypothesis, we validated GATA4 expression in SH-SY5Y cells with Torin1 and RapaLink-1 treatments and we observed that GATA4 does not have a significant change in expression at the protein level **(Figure 18 A, B)**. As a result, we can assume that LHX9 might not be a direct target of GATA4 in this cell line but further studies should be conducted in order to validate this assumption. One approach that

could determine if GATA4 has a specific role and function in the SH-SY5Y cells could be done by conducting knockdown experiments.

4.5. mTOR activity in serum starved SH-SY5Y cells

Serum starvation experiments were conducted in order to investigate the activity/inactivity state of mTOR in undifferentiated SH-SY5Y cells with no treatment. In order to evaluate mTOR's activity/inactivity in serum starved SH-SY5Y cells, Phospho-4E-BP1 was tested. mTORC1 controls several processes yet, protein synthesis is the most well characterised process and is promoted by two downstream effectors of mTORC1 known as 4E-BP1 and S6K1. mTORC1 phosphorylates and inhibits 4E-BP1 in order to enable the initiation of the cap-dependant translation (Laplante and Sabatini, 2012). In this study we provide evidence that reactivation of mTOR after serum starvation took 24h **(Figure 21 A)**. Phospho-4EBP1 was highly expressed in the 5h serum readdition condition (R) with a 3.57-fold change which further shows that mTOR did not manage to reactivate after 5h of serum starvation followed by 5h of serum readdition. However, mTOR was observed to be active in the 24h serum readdition condition (R) where the expression levels of phosphor-4EBP1 were considerably low (0.89- fold change). After looking into the expression levels of LHX9 and GATA4 in differentiated SH-SY5Y cells with treatment, we wanted to examine their expression patterns in undifferentiated SH-SY5Y cell with no treatment. LHX9 was found to be expressed in all the conditions with higher levels of expression in the serum starvation conditions (S) in both timepoints (5h and 24h) **(Figure 20A)**. Interestingly enough, Okutomo *et al.* (2022) noticed that in serum starved alveolar epithelial type 2 (A549)

cells, LHX9 had a decreased expression in comparison to the culture containing medium with serum. In this study they also showed that LHX9 knockdown via siRNA in serum starved A549 cells led to an increased ratio of viable to necrotic cells, indicating that LHX9 boosted the sensitivity to cell death. Our results on LHX9's expression in serum starved SH-SY5Y cells do not match with the findings displayed in the study previously stated. Furthermore, these differences encountered between our results and what is reported in the literature, could be due to changes in LHX9's expression in various cell lines as well as the roles and functions this transcription factor plays in each model of study. However, further investigations should be conducted to validate this assumption. Additionally, we tested GATA4's level of expression in undifferentiated SH-SY5Y cells and we observed that there is no significant change **(Figure 19 B).** As far as our results show, there is no link found between GATA4 levels of expression and mTOR, as shown by the unchanged expression of GATA4 at protein level in both differentiated and undifferentiated SH-SY5Y cells with or without treatment. Furthermore, this means that GATA4 might not be involved in neuronal differentiation.

4.6. Glycolysis runs normally in SH-SY5Y cells with Torin-1 and RapaLink-1 treatment

Previously, we hypothesised that upregulation of LHX9 would lead to inhibition of glycolysis. We detected an upregulation of LHX9 with mTORC1 and mTORC2 inhibition. Therefore, we tested the expression of several enzymes involved in glycolysis in differentiated SH-SY5Y cell with pharmacological treatment to validate our hypothesis **(Figure 22A - Figure30A)**. Both mTORC complexes have been found to be implicate in

glycolysis, mTORC2 through activation of Akt and mTORC1 through the shift of oxidative phosphorylation to glycolysis (Saxton and Sabatini, 2017). In a study (Yang *et al.*, 2021b), it was shown that Ras homolog enriched in brain (RHEB) a GTP-binding protein that activated mTORC1, was found to regulate pyruvate dehydrogenase (PDH) activity without relying on mTORC1. Additionally, this study looked into the effect of mTOR inhibition with both Rapamycin and Torin1 inhibitors on PDH phosphorylation. The result observed by them were that inhibition with both treatments lead to mTORC1 prolonged reduction without affecting PDH phosphorylation nor acetyl-CoA level (Yang *et al.*, 2021b). Our results match with the findings displayed in this study. All the glycolytic enzymes tested (including PDH) in our study did not show significant changes in expression **(Figure31)**, therefore we can assume that glycolysis runs normally after inhibition of both mTOR complexes in differentiated SH-SY5Y cell. There is not much reported in the literature regarding LHX9's involvement in glycolysis, however in a study conducted by Luo *et al.* (2021), it was shown that overexpression of LHX9 inhibited the glycolytic enzyme PGK1 thereby inhibiting glycolysis. They found that LHX9 interacted with p53 therefore inhibiting PGK1's expression ultimately leading to the repression of glioma progression. Our results don't match with the findings reported in the previous study even though a part of our hypothesis was based on it. As far as our results show, LHX9 upregulation did not lead to inhibition of glycolysis thus we can presume that LHX9 does not have an effect on glycolysis in differentiated SH-SY5Y cells treated with mTOR inhibitors. Nevertheless, while the enzymes involved in glycolysis seem unchanged, a metabolomic analysis on central carbon-related metabolites might be worth assessing. This is because of the sensitivity of the approach utilised here.

4.7. Differences between the transcriptional level and the protein level

Western Blots were performed in order to identify the level of expression of the transcription factors and the glycolytic enzymes of interest. We wanted to examine if what we observed at the protein level corresponds with what we see at the transcriptional level in the RNA-seq data sets and if there are any differences. At the transcriptional level, in the RapaLink-1 treatment, the genes of interest did not have significant fold-changes which corelates with what we found at the protein level **(Figure 32 B)**. However, one of the differences encountered was in the RapaLink-1 vs Control data set where LHX9 was found to have a 0.31-fold change **(Figure 32 B)** while at the protein level LHX9 had a 1.88-fold change **(Figure 17 B)**. In the Torin1 vs Control data set, LHX9 fold change is very similar with the fold change found at the protein level. The biggest differences encountered between what is found at the transcriptional level vs what we see at the protein level is in the Torin1 vs Control data set. One of the glycolytic enzymes tested, Hexokinase 2, was found downregulated in the RNA-seq data **(Figure 32 B)** while at the protein level it did not show any significant changes in expression **(Figure 23 B)**. LDHA was also found to be slightly downregulated at the transcriptional level **(Figure 32 B)** while at the protein level it did not change in expression **(Figure 26 B)**. These differences encountered could be due to post-transcriptional regulation which is known to be an important mechanism in controlling gene expression. Furthermore, the amount of protein produced by the cell is controlled by mRNA turnover and translation (Laloo *et al.*, 2009).

4.8. Gene ontology analysis on the upregulated genes in the RapaLink-1 vs Control dataset.

Gene ontology analysis on the significantly enriched DEGs was conducted in order to identify the biological processes as well as the molecular functions associated with the most upregulated or most downregulated genes. In the RapaLink-1 vs Control data set, the biological process analysis showed that the most significant upregulated genes were associated with oxidative phosphorylation (oxphos) and aerobic respiration **(Figure 9A)**. Additionally, we found multiple significant biological processes related to electron transport chain (ETC) (**Figure 9A)**. The majority of differentiated cells generally convert glucose to CO_2 in the presence of oxygen by glycolytic pyruvate oxidation in the mitochondrial TCA cycle. NADH is the byproduct of this reaction that will further stimulate oxidative phosphorylation to enlarge the production of ATP while generating the least amount of lactate. On the other hand, enormous amounts of lactate are produced in cancer cells despite of the availability of oxygen. As such, this metabolism is known as aerobic glycolysis. The Warburg effect is a phenomenon in which cancer cells rely on aerobic glycolysis to generate energy for cellular functions unlike normal cells which predominantly rely on mitochondrial oxidative phosphorylation (Vander Heiden *et al.*, 2009). Mitochondria produces ATP through oxidative phosphorylation and during this process reactive oxygen species (ROS) are created. An imbalance in the concentrations of the ROS can induce oxidative stress (OS) which would lead to cellular death (Almansa-Ordonez *et al.*, 2020). Mitochondrial biogenesis dynamics and functions are regulated by mTORC1. Therefore, mitochondrial impairment can lead to decreased electron transport chain activity, low ATP production and dysregulated mitophagy

(Papadopoli *et al.*, 2019). Lu *et al.* (2015) reported that mTOR has a very important role in the conversion of aerobic glycolysis to oxidative phosphorylation, by a process named "Warburg-Reversing Effect". In this paper, irradiated cells rapidly shifted from aerobic glycolysis to mitochondrial respiration which subsequently led to increase in tumour resistance. However, mTORC1 inhibitor rapamycin managed to block the shift induced by the radiation and stopped the translocation of mTOR to mitochondria. They also observed that with rapamycin treatment, there was an increase in mitochondrial ATP production. Another study showed that in *Drosophila melanogaster*, rapamycin treatment inhibited hydrogen peroxide while boosting mitochondrial respiration and succinate dehydrogenase activity also known as ETC complex II, an enzyme that TCA cycle and electron transport chain share (Villa-Cuesta *et al.*, 2014). Our results had similar findings to the previous papers stated above, therefore we can assume that inhibition of mTORC1 with RapaLink-1 leads to reduced mitochondrial function which subsequently boosts mitochondrial respiration. Furthermore, the upregulation of ETC, oxidative phosphorylation and aerobic respiration with mTORC1 inhibition matches with what was found in the literature. For the molecular function analysis in the RapaLink-1 vs Control data set (**Figure 9B**), active transmembrane transporter activity, primary active transmembrane transporter activity, electron transfer activity and oxidoreduction-driven active transmembrane transporter activity were the most common characteristics found. These molecular functions are all related to transport within mitochondria as well as presence of NAD+ which is a very important process required by the mitochondria for cellular energy transduction and respiration.

4.9. Gene ontology analysis on the downregulated genes in the RapaLink-1 vs Control dataset.

After looking at the upregulated genes in the RapaLink-1 vs Control data set, we wanted to look at the biological processes and the molecular functions associated with the most significant downregulated DEGs. The biological processes analysis indicates that all the downregulated DEGs were mainly associated with response to endoplasmic reticulum stress (ER stress), cellular response to glucose starvation and positive regulation of extrinsic apoptotic signalling pathway via death domain receptors (**Figure 10A**). ER stress is caused when there is an accumulation of misfolded proteins in the ER lumen, resulting in the activation of the unfolded protein response (UPR) which is an adaptive stress response. In order to reduce the buildup of unfolded proteins, the UPR boosts ER-resident chaperone levels, inhibits protein translation and promotes the degradation of unfolded proteins (Lim and Yue, 2015). mTORC1 is a key regulator of protein synthesis. However, if mTORC1 signalling is hyperactivated then this would lead to an increase in translation which would cause an increase in the production of secreted proteins. This hyperactivation of mTORC1 would subsequently triggers endoplasmic reticulum stress and the unfolded protein response (UPR) activation. Additionally, the ER stress caused by the hyperactivation of mTORC1 signalling would result in increased apoptosis (Polak and Hall, 2009). It has been established that there is a bidirectional cross-talk that occurs between ER stress and mTOR. Therefore, ER stress can act downstream of mTORC1, which was briefly explained earlier, but also upstream of mTORC1 (Appenzeller-Herzog and Hall, 2012). In a study it was shown that under conditions of glucolipotoxicity, rapamycin (an mTORC1 inhibitor) managed to

significantly decrease the ER stress response and apoptosis (Bachar *et al.*, 2009). Furthermore, mTORC1 is a negative regulator of autophagy following which mTORC1 inhibition by pharmacological treatment would lead to the upregulation of autophagy which would increase clearance of protein aggregates (Bartolome *et al.*, 2012).

Carloni *et al.* (2014) showed that after neonatal hypoxia/ischemia (HI), ER stress is decreased by the increase of autophagy. Additionally, this study also showed that Rapamycin administration significantly reduced HI that was induced by the UPR as well as that reduced brain damage was due to an increase in autophagy after mTORC1 inhibition. This study solidifies the cross-talk that occurs between ER and the autophagy. We could assume, that in our study, downregulation of ER stress could be due to the inhibition of mTORC1 which would lead to activation of autophagy but further research should be conducted in the SH-SY5Y cells with RapaLink-1 treatment in order to validate this assumption. When a particular ligand attaches to its associated death receptor on the cell surface, the extrinsic is initiated (Huang *et al.*, 2011). Extrinsic apoptotic pathway has been found to be linked to ER stress (Zhang *et al.*, 2016). In renal proximal tubular cells (RPTC), tunicamycin induced ER stress which led to apoptosis. However, when Rapamycin was added, to the RPTC this led to inhibition of apoptosis (Dong *et al.*, 2015). Therefore, we can assume that downregulation of the ER stress with RapaLink-1 inhibition leads to downregulation of apoptosis. One of the other biological processes found to be associated with the downregulated DEGs was cellular response to glucose starvation (**Figure 10A**). In normal glucose conditions, mTORC1 is found to be attached to the lysosomal surface by Ras-related GTPase (RAG) and Ras homolog enriched in brain (Rheb). However, in conditions of glucose starvation, aldolase

promotes the shift of LKB1 (Liver kinase B1) to the surface of the lysosome. Subsequently, AMP-activated protein kinase (AMPK) gets activated and inhibits RAGs which results in the separation of mTORC1 from the lysosome which leads to its inhibition (Li *et al.*, 2023). Furthermore, under glucose depravation AMPK can inhibit mTORC1 through two different mechanisms. AMPK will phosphorylate tuberous sclerosis complex 2, a negative regulator of mTOR, which will lead to its activation, resulting in mTORC1 inhibition. On the other hand, to inhibit mTORC1 under glucose depravation, AMPK will phosphorylate and inhibit Raptor (Regulatory-associated protein of mTOR) (Leprivier and Rotblat, 2020). Through the Rag GTPases, mTORC1 detects amino acids; however, in a published study by Efeyan *et al.* (2013), it has been shown that Rag GTPases might additionally assist glucose regulation of mTORC1. Furthermore, this study showed that glucose depravation led to the inhibition of mTORC1 which was mediated by Rag GTPases (Efeyan *et al.*, 2013). Based on our results on the biological processes, we can assume that treatment with RapaLink-1 has led to mTORC1 suppression which subsequently has resulted to the upregulation of autophagy and the downregulation of the cellular response to glucose starvation. However, further studies should be conducted in order to validate this assumption. The molecular function shown to be downregulated was protein heterodimerization activity (**Figure 10B**). The molecular function found by us to be downregulated could relate to Rag GTPases and tuberous sclerosis complex 2 because they are implicated in mTORC1 inactivation under glucose starvation.

4.10. Gene ontology analysis on the upregulated genes in the Torin1 vs Control dataset.

Gene ontology analysis on the significantly enriched DEGs from the Torin1 vs Control dataset was conducted in order to identify the biological processes as well as the molecular functions associated with the most upregulated or most downregulated genes. In the biological processes analysis, the most significant upregulated DEGs were associated with regulation of neuronal differentiation (**Figure 11A**). In the brain mTOR is a key regulator of neuronal development, differentiation and survival. mTOR activity has been established to be crucial for axon development, dendritic arborization and synaptogenesis. Furthermore, modifications of the mTOR activity in brain have been linked to neurodegenerative disorders (Swiech *et al.*, 2008). Although mTORC2 implication in the brain is less known than mTORC1, both complexes have been found to be required for dendritic growth in hippocampal neurons (Urbanska *et al.*, 2012). A study (Urbanska *et al.*, 2012) revealed that both Raptor (mTORC1 subunit) and Rictor (mTORC2 subunit) are needed for dendritic growth induced by insulin and PI3K. Additionally, the knockdown experiment conducted in this study on Rictor or Raptor led to dendrites morphology being more simplified thus showing that both complexes are required for the formation of dendrites. Furthermore, this study also revealed that dendritic growth induced by Akt requires Raptor and manged to rescue mTORC2 knockdown thus suggesting that mTORC1 acts downstream of mTORC2. Therefore, activation of both mTOR complexes is required for dendritic development dependant on PI3K and insulin (Urbanska *et al.*, 2012). Inhibition of both mTOR complexes has been tested in dopaminergic neurons but the outcome observed was different. In this study,

rapamycin treatment was shown to have a neuroprotective role because it did not inhibit Akt (a survival kinase). In contrast, treatment with Torin1 led to inhibition of Akt phosphorylation at both Thr308 and Ser473, therefore leading to the promotion of neuronal cell death (Malagelada *et al.*, 2010). Insulin/IGF stimulation of the PI3K/Akt/mTOR signalling pathway leads to neuronal differentiation (Han *et al.*, 2008). Lee *et al.* (2016) reported that dopaminergic neuronal differentiation is promoted though the PI3K/Akt/mTOR pathway by S6K, an mTORC1 downstream effector. Furthermore, in human embryonic stem cells, treatment with rapamycin led to reduction of neuronal differentiation due p-S6K inhibition. However, rapamycin did not affect cellular proliferation. Another study, looking into human embryonic stem cells, showed that knockdown of Rictor, an mTORC2 subunit, mediated by small interfering RNA (siRNA) led to the activation of ribosomal protein S6 kinase beta-1 (p70 S6K) which induced neuronal differentiation (Easley *et al.*, 2010). In our study, we observed that regulation of neuronal differentiation was upregulated after the inhibition of both mTOR complexes. Based on the previous studies, we could assume that Torin1 inhibition might not affect neuronal differentiation but further research should be conducted in the SH-SY5Y cells with this inhibitor in order to validate this assumption.

4.11. Gene ontology analysis on the downregulated genes in the Torin1 vs Control dataset.

After looking into the Gene ontology analysis on the upregulated genes in this dataset, we also wanted to examine the gene ontology analysis biological processes and molecular functions associated to the most significant downregulated genes. The biological processes analysis indicates that all the downregulated DEGs were mainly associated with intrinsic apoptotic signalling pathway and amino acid metabolic processes (**Figure 12A**).The intrinsic pathway is one of the apoptosis mechanisms which is mitochondria- mediated (Jan and Chaudhry, 2019). A study (Meng *et al.*, 2021) in neonatal rat ventricular myocytes (NRVMs) looked into nicotine influences in mitochondria dynamics. They observed that treatment with Torin1 led to decreased mitochondrial production of superoxide and mitochondrial fission as well as reduced apoptosis (Meng *et al.*, 2021). The results found in this study match our findings. We can assume that treatment with Torin1 in the SH-SY5Y cells inhibited both mTORC leading to reduced mitochondrial activity and reduced apoptosis. Another biological process associated with the downregulated DEGs was the amino acid metabolic process. In a study (Amemiya *et al.*, 2021) it was shown that activation of mTORC1 relies on amino acid mediated boost in intracellular Ca2+, therefore supporting the stimulation of nascent protein synthesis. Additionally, they observed that the increase in protein synthesis induced by amino acids was inhibited by Torin1 (Amemiya *et al.*, 2021). Based on this study, we could assume that inhibition of both mTOR complexes with Torin1 leads to downregulated of amino acid metabolic processes.

4.12. Venn Diagram of the differentially expressed genes in Torin1 vs Control and RapaLink-1 vs Control RNA-seq datasets.

We made a Venn diagram containing the upregulated and the downregulated differentially expressed genes from both the Torin1 vs Control and RapaLink-1 vs Control RNA-seq datasets in order to identify overlapping genes (**Figure 8**). There were not many genes found to overlap between the two data sets, however, we observed that there were 14 common elements in RvsC DOWN and TvsC DOWN, 13 common elements in RvsC UP and TvsC UP as well as one common element in RvsC UP and TvsC DOWN. In the RvsC UP and TvsC UP datasets, one of the common elements that caught our attention was the IRX6 genes. The iroquois homeobox 6 gene (IRXG) was found to be involved in neuronal differentiation (Star *et al.*, 2012). Previously, we assumed that Torin1 inhibition might not affect neuronal differentiation. The finding of this gene (IRX6) being upregulated in both data sets further solidifies that neuronal differentiation might not be affected following inhibition of mTOR with Torin1. In RvsC DOWN and TvsC DOWN the two common elements that drew our attention were SLC7A5 and AARS1. Leucine, phenylalanine, and tryptophan are amino acids that are carried by solute carrier family 7 member 5 (SLC7A5) which is a transporter that also works as an amino acid exchanger. SLC7A5 exchanges the previously specified amino acids into intracellular glutamine (El Ansari *et al.*, 2018). The other gene found by us to be downregulated was the Alanyl-tRNA Synthetase1 (AARS1) which encodes cytosolic alanine-tRNA ligase (AlaRS) that links alanine to its appropriate tRNA (Hoyer *et al.*, 2022). The SLC7A5 and AARS1 genes were found to be downregulated in both datasets

which matches our assumption, further showing that amino acid metabolic processes might be downregulated after inhibition of mTOR with Torin1.

5. Overall conclusions, future perspectives and directions.

Research on LHX9 is very limited and until now it has not been discussed in the context of mTOR pathway in the brain. Our findings suggest that there might be a link between this transcription factor and mTOR due to its upregulation in the SH-SY5Y cells after pharmacological treatment with Torin1 and RapaLink-1. However, it's implication into the mTOR pathway is still to be determined. LHX9's upregulation in the Torin1 treated (inhibition of both mTOR complexes) SH-SY5Y cells raised the question if this transcription factor links to both or just one of the mTOR complexes and to what extent. It has been established that mTORC2 is less understood than mTORC1 which could also be due to lack of drugs targeting this complex specifically. It would be interesting to see if LHX9 has a link to mTORC2 because it could bring a better understating of its regulation in the brain. When we were testing our hypothesis, we also looked into LHX9 link to GATA4 and glycolysis but, as far as our results show, LHX9 might not be a direct target of GATA4 in these cells and LHX9 did not have an effect on glycolysis. In order to better understand this transcription factor, further studies should be conducted. ChIP-seq could be used in order to identify the binding sites of LHX9 in pharmacologically treated SH-SY5Y cells. Another approach could be conducting knockdown experiments on LHX9 to study its function but also to observe what effect it has in pharmacologically treated SH-SY5Y cells.

6.References

Abdul Manap, A. S., Wei Tan, A. C., Leong, W. H., Yin Chia, A. Y., Vijayabalan, S., Arya, A., Wong, E. H., Rizwan, F., Bindal, U., Koshy, S. and Madhavan, P. (2019) Synergistic Effects of Curcumin and Piperine as Potent Acetylcholine and Amyloidogenic Inhibitors With Significant Neuroprotective Activity in SH-SY5Y Cells via Computational Molecular Modeling and in vitro Assay. *Frontiers in Aging Neuroscience,* **11**, 206.

Albert, V., Svensson, K., Shimobayashi, M., Colombi, M., Muñoz, S., Jimenez, V., Handschin, C., Bosch, F. and Hall, M. N. (2016) mTORC2 sustains thermogenesis via Akt-induced glucose uptake and glycolysis in brown adipose tissue. *EMBO molecular medicine,* **8**, 232-246.

Almansa-Ordonez, A., Bellido, R., Vassena, R., Barragan, M. and Zambelli, F. (2020) Oxidative Stress in Reproduction: A Mitochondrial Perspective. *Biology (Basel),* **9**.

Amemiya, Y., Nakamura, N., Ikeda, N., Sugiyama, R., Ishii, C., Maki, M., Shibata, H. and Takahara, T. (2021) Amino Acid-Mediated Intracellular Ca(2+) Rise Modulates mTORC1 by Regulating the TSC2-Rheb Axis through Ca(2+)/Calmodulin. *Int J Mol Sci,* **22**.

Amin, A. G., Jeong, S. W., Gillick, J. L., Sursal, T., Murali, R., Gandhi, C. D. and Jhanwar-Uniyal, M. (2021) Targeting the mTOR pathway using novel ATP-competitive inhibitors, Torin1, Torin2 and XL388, in the treatment of glioblastoma. *International Journal of Oncology,* **59**, 83.

Appenzeller-Herzog, C. and Hall, M. N. (2012) Bidirectional crosstalk between endoplasmic reticulum stress and mTOR signaling. *Trends Cell Biol,* **22**, 274-82.

Bach, I. (2000) The LIM domain: regulation by association. *Mechanisms of Development,* **91**, 5-17.

Bachar, E., Ariav, Y., Ketzinel-Gilad, M., Cerasi, E., Kaiser, N. and Leibowitz, G. (2009) Glucose amplifies fatty acid-induced endoplasmic reticulum stress in pancreatic beta-cells via activation of mTORC1. *PLoS One,* **4**, e4954.

Balasubramanian, R., Bui, A., Ding, Q. and Gan, L. (2014) Expression of LIM-homeodomain transcription factors in the developing and mature mouse retina. *Gene expression patterns: GEP,* **14**, 1-8.

Barber, R. D., Harmer, D. W., Coleman, R. A. and Clark, B. J. (2005) GAPDH as a housekeeping gene: analysis of GAPDH mRNA expression in a panel of 72 human tissues. *Physiological Genomics,* **21**, 389-395.

Bartolome, A., Guillen, C. and Benito, M. (2012) Autophagy plays a protective role in endoplasmic reticulum stress-mediated pancreatic beta cell death. *Autophagy,* **8**, 1757-68.

Bertuzzi, S., Porter, F. D., Pitts, A., Kumar, M., Agulnick, A., Wassif, C. and Westphal, H. (1999) Characterization of Lhx9, a novel LIM/homeobox gene expressed by the pioneer neurons in the mouse cerebral cortex. *Mechanisms of Development,* **81**, 193-198.

Beutler, E. (2007) PGK deficiency. *British Journal of Haematology,* **136**, 3-11.

Birk, O. S., Casiano, D. E., Wassif, C. A., Cogliati, T., Zhao, L., Zhao, Y., Grinberg, A., Huang, S., Kreidberg, J. A., Parker, K. L., Porter, F. D. and Westphal, H. (2000) The LIM homeobox gene Lhx9 is essential for mouse gonad formation. *Nature,* **403**, 909-913.

Bjedov, I. and Rallis, C. (2020) The Target of Rapamycin Signalling Pathway in Ageing and Lifespan Regulation. *Genes,* **11**, 1043.

Carloni, S., Albertini, M. C., Galluzzi, L., Buonocore, G., Proietti, F. and Balduini, W. (2014) Increased autophagy reduces endoplasmic reticulum stress after neonatal hypoxia-ischemia: role of protein synthesis and autophagic pathways. *Exp Neurol,* **255**, 103-12.

Carson, R. P., Fu, C., Winzenburger, P. and Ess, K. C. (2013) Deletion of Rictor in neural progenitor cells reveals contributions of mTORC2 signaling to tuberous sclerosis complex. *Hum Mol Genet,* **22**, 140-52.

Chang, A. N., Cantor, A. B., Fujiwara, Y., Lodish, M. B., Droho, S., Crispino, J. D. and Orkin, S. H. (2002) GATA-factor dependence of the multitype zinc-finger protein FOG-1 for its essential role in megakaryopoiesis. *Proc Natl Acad Sci U S A,* **99**, 9237-42.

Christofk, H. R., Vander Heiden, M. G., Harris, M. H., Ramanathan, A., Gerszten, R. E., Wei, R., Fleming, M. D., Schreiber, S. L. and Cantley, L. C. (2008) The M2 splice isoform of pyruvate kinase is important for cancer metabolism and tumour growth. *Nature,* **452**, 230-233.

Dalal, J., Roh, J. H., Maloney, S. E., Akuffo, A., Shah, S., Yuan, H., Wamsley, B., Jones, W. B., de Guzman Strong, C., Gray, P. A., Holtzman, D. M., Heintz, N. and Dougherty, J. D. (2013) Translational profiling of hypocretin neurons identifies candidate molecules for sleep regulation. *Genes & Development,* **27**, 565-578.

de Medeiros, L. M., De Bastiani, M. A., Rico, E. P., Schonhofen, P., Pfaffenseller, B., Wollenhaupt-Aguiar, B., Grun, L., Barbé-Tuana, F., Zimmer, E. R., Castro, M. A. A., Parsons, R. B. and Klamt, F. (2019) Cholinergic Differentiation of Human Neuroblastoma SH-SY5Y Cell Line and Its Potential Use as an In vitro Model for Alzheimer's Disease Studies. *Molecular Neurobiology,* **56**, 7355-7367.

Dobson, A. J., He, X., Blanc, E., Bolukbasi, E., Feseha, Y., Yang, M. and Piper, M. D. W. (2018) Tissue-specific transcriptome profiling of Drosophila reveals roles for GATA transcription factors in longevity by dietary restriction. *NPJ Aging Mech Dis,* **4**, 5.

Dong, G., Liu, Y., Zhang, L., Huang, S., Ding, H. F. and Dong, Z. (2015) mTOR contributes to ER stress and associated apoptosis in renal tubular cells. *Am J Physiol Renal Physiol,* **308**, F267-74.

Dowling, R. J. O., Topisirovic, I., Alain, T., Bidinosti, M., Fonseca, B. D., Petroulakis, E., Wang, X., Larsson, O., Selvaraj, A., Liu, Y., Kozma, S. C., Thomas, G. and Sonenberg, N. (2010) mTORC1-mediated cell proliferation, but not cell growth, controlled by the 4E-BPs. *Science (New York, N.Y.),* **328**, 1172-1176.

Düvel, K., Yecies, J. L., Menon, S., Raman, P., Lipovsky, A. I., Souza, A. L., Triantafellow, E., Ma, Q., Gorski, R., Cleaver, S., Vander Heiden, M. G., MacKeigan, J. P., Finan, P. M., Clish, C. B., Murphy, L. O. and Manning, B. D. (2010) Activation of a metabolic gene regulatory network downstream of mTOR complex 1. *Molecular Cell,* **39**, 171-183.

Easley, C. A. t., Ben-Yehudah, A., Redinger, C. J., Oliver, S. L., Varum, S. T., Eisinger, V. M., Carlisle, D. L., Donovan, P. J. and Schatten, G. P. (2010) mTOR-mediated activation of p70 S6K induces differentiation of pluripotent human embryonic stem cells. *Cell Reprogram,* **12**, 263-73.

Efeyan, A., Zoncu, R., Chang, S., Gumper, I., Snitkin, H., Wolfson, R. L., Kirak, O., Sabatini, D. D. and Sabatini, D. M. (2013) Regulation of mTORC1 by the Rag GTPases is necessary for neonatal autophagy and survival. *Nature,* **493**, 679-83.

El Ansari, R., Craze, M. L., Miligy, I., Diez-Rodriguez, M., Nolan, C. C., Ellis, I. O., Rakha, E. A. and Green, A. R. (2018) The amino acid transporter SLC7A5 confers a poor prognosis in the highly proliferative breast cancer subtypes and is a key therapeutic target in luminal B tumours. *Breast Cancer Res,* **20**, 21.

Failli, V., Rogard, M., Mattei, M. G., Vernier, P. and Retaux, S. (2000) Lhx9 and Lhx9alpha LIM-homeodomain factors: genomic structure, expression patterns, chromosomal localization, and phylogenetic analysis. *Genomics,* **64**, 307-17.

Fan, Q., Aksoy, O., Wong, R. A., Ilkhanizadeh, S., Novotny, C. J., Gustafson, W. C., Truong, A. Y.-Q., Cayanan, G., Simonds, E. F., Haas-Kogan, D., Phillips, J. J., Nicolaides, T., Okaniwa, M., Shokat, K. M. and Weiss, W. A. (2017) A Kinase Inhibitor Targeted to mTORC1 Drives Regression in Glioblastoma. *Cancer Cell,* **31**, 424-435.

Ghosh, J. and Kapur, R. (2017) Role of mTORC1–S6K1 signaling pathway in regulation of hematopoietic stem cell and acute myeloid leukemia. *Experimental Hematology,* **50**, 13-21.

Gwinn, D. M., Shackelford, D. B., Egan, D. F., Mihaylova, M. M., Mery, A., Vasquez, D. S., Turk, B. E. and Shaw, R. J. (2008) AMPK phosphorylation of raptor mediates a metabolic checkpoint. *Molecular Cell,* **30**, 214-226.

Hagiwara, A., Cornu, M., Cybulski, N., Polak, P., Betz, C., Trapani, F., Terracciano, L., Heim, M. H., Rüegg, M. A. and Hall, M. N. (2012) Hepatic mTORC2 activates glycolysis and lipogenesis through Akt, glucokinase, and SREBP1c. *Cell Metabolism,* **15**, 725-738.

Han, J., Wang, B., Xiao, Z., Gao, Y., Zhao, Y., Zhang, J., Chen, B., Wang, X. and Dai, J. (2008) Mammalian target of rapamycin (mTOR) is involved in the neuronal differentiation of neural progenitors induced by insulin. *Mol Cell Neurosci,* **39**, 118-24.

Hannan, K. M., Brandenburger, Y., Jenkins, A., Sharkey, K., Cavanaugh, A., Rothblum, L., Moss, T., Poortinga, G., McArthur, G. A., Pearson, R. B. and Hannan, R. D. (2003) mTOR-dependent regulation of ribosomal gene transcription requires S6K1 and is mediated by phosphorylation of the carboxy-terminal activation domain of the nucleolar transcription factor UBF. *Molecular and Cellular Biology,* **23**, 8862-8877.

Hassan, B., Akcakanat, A., Holder, A. M. and Meric-Bernstam, F. (2013) Targeting the PI3-kinase/Akt/mTOR signaling pathway. *Surgical Oncology Clinics of North America,* **22**, 641-664.

Heitman, J., Movva, N. R. and Hall, M. N. (1991) Targets for cell cycle arrest by the immunosuppressant rapamycin in yeast. *Science (New York, N.Y.),* **253**, 905-909.

Hoyer, H., Busk, O. L., Esbensen, Q. Y., Rosby, O., Hilmarsen, H. T., Russell, M. B., Nyman, T. A., Braathen, G. J. and Nilsen, H. L. (2022) Clinical characteristics and proteome modifications in two Charcot-Marie-Tooth families with the AARS1 Arg326Trp mutation. *BMC Neurol,* **22**, 299.

Huang, J. and Manning, B. D. (2008) The TSC1-TSC2 complex: a molecular switchboard controlling cell growth. *The Biochemical Journal,* **412**, 179-190.

Huang, J. and Manning, B. D. (2009) A complex interplay between Akt, TSC2 and the two mTOR complexes. *Biochemical Society Transactions,* **37**, 217-222.

Huang, T. T., Liu, F. G., Wei, C. F., Lu, C. C., Chen, C. C., Lin, H. C., Ojcius, D. M. and Lai, H. C. (2011) Activation of multiple apoptotic pathways in human nasopharyngeal carcinoma cells by the prenylated isoflavone, osajin. *PLoS One,* **6**, e18308.

Inoki, K., Li, Y., Xu, T. and Guan, K.-L. (2003a) Rheb GTPase is a direct target of TSC2 GAP activity and regulates mTOR signaling. *Genes & Development,* **17**, 1829-1834.

Inoki, K., Zhu, T. and Guan, K.-L. (2003b) TSC2 mediates cellular energy response to control cell growth and survival. *Cell,* **115**, 577-590.

Jacinto, E., Facchinetti, V., Liu, D., Soto, N., Wei, S., Jung, S. Y., Huang, Q., Qin, J. and Su, B. (2006) SIN1/MIP1 maintains rictor-mTOR complex integrity and regulates Akt phosphorylation and substrate specificity. *Cell,* **127**, 125-137.

Jacinto, E., Loewith, R., Schmidt, A., Lin, S., Rüegg, M. A., Hall, A. and Hall, M. N. (2004) Mammalian TOR complex 2 controls the actin cytoskeleton and is rapamycin insensitive. *Nature Cell Biology,* **6**, 1122-1128.

Jan, R. and Chaudhry, G. E. (2019) Understanding Apoptosis and Apoptotic Pathways Targeted Cancer Therapeutics. *Adv Pharm Bull,* **9**, 205-218.

Jaworski, J., Spangler, S., Seeburg, D. P., Hoogenraad, C. C. and Sheng, M. (2005) Control of dendritic arborization by the phosphoinositide-3'-kinase-Akt-mammalian target of rapamycin pathway. *The Journal of Neuroscience,* **25**, 11300-12.

Jossin, Y. and Goffinet, A. M. (2007) Reelin signals through phosphatidylinositol 3-kinase and Akt to control cortical development and through mTor to regulate dendritic growth. *Molecular and Cellular Biology,* **27**, 7113-24.

Kaizuka, T., Hara, T., Oshiro, N., Kikkawa, U., Yonezawa, K., Takehana, K., Iemura, S.-I., Natsume, T. and Mizushima, N. (2010) Tti1 and Tel2 are critical factors in mammalian target of rapamycin complex assembly. *The Journal of Biological Chemistry,* **285**, 20109-20116.

Kunz, J., Henriquez, R., Schneider, U., Deuter-Reinhard, M., Movva, N. R. and Hall, M. N. (1993) Target of rapamycin in yeast, TOR2, is an essential phosphatidylinositol kinase homolog required for G1 progression. *Cell,* **73**, 585-596.

Kuroshima, K., Yoshino, H., Okamura, S., Tsuruda, M., Osako, Y., Sakaguchi, T., Sugita, S., Tatarano, S., Nakagawa, M. and Enokida, H. (2020) Potential new therapy of Rapalink-1, a new generation mammalian target of rapamycin inhibitor, against sunitinib-resistant renal cell carcinoma. *Cancer Science,* **111**, 1607-1618.

Laloo, B., Simon, D., Veillat, V., Lauzel, D., Guyonnet-Duperat, V., Moreau-Gaudry, F., Sagliocco, F. and Grosset, C. (2009) Analysis of post-transcriptional regulations by a functional, integrated, and quantitative method. *Mol Cell Proteomics,* **8**, 1777-88.

Laplante, M. and Sabatini, D. M. (2012) mTOR signaling in growth control and disease. *Cell,* **149**, 274-293.

Laplante, M. and Sabatini, D. M. (2013) Regulation of mTORC1 and its impact on gene expression at a glance. *Journal of Cell Science,* **126**, 1713-1719.

Lee, J. E., Lim, M. S., Park, J. H., Park, C. H. and Koh, H. C. (2016) S6K Promotes Dopaminergic Neuronal Differentiation Through PI3K/Akt/mTOR-Dependent Signaling Pathways in Human Neural Stem Cells. *Molecular Neurobiology,* **53**, 3771-3782.

Leprivier, G. and Rotblat, B. (2020) How does mTOR sense glucose starvation? AMPK is the usual suspect. *Cell Death Discov,* **6**, 27.

Li, M., Wei, X., Xiong, J., Feng, J.-W., Zhang, C.-S. and Lin, S.-C. (2023) Hierarchical inhibition of mTORC1 by glucose starvation-triggered AXIN lysosomal translocation and by AMPK. *Life Metabolism,* **2**.

Lim, J. and Yue, Z. (2015) Neuronal aggregates: formation, clearance, and spreading. *Dev Cell,* **32**, 491-501.

Liu, P., Gan, W., Chin, Y. R., Ogura, K., Guo, J., Zhang, J., Wang, B., Blenis, J., Cantley, L. C., Toker, A., Su, B. and Wei, W. (2015) PtdIns(3,4,5)P3-Dependent Activation of the mTORC2 Kinase Complex. *Cancer Discovery,* **5**, 1194-1209.

Loewith, R., Jacinto, E., Wullschleger, S., Lorberg, A., Crespo, J. L., Bonenfant, D., Oppliger, W., Jenoe, P. and Hall, M. N. (2002) Two TOR complexes, only one of which is rapamycin sensitive, have distinct roles in cell growth control. *Molecular Cell,* **10**, 457-468.

Lu, C. L., Qin, L., Liu, H. C., Candas, D., Fan, M. and Li, J. J. (2015) Tumor cells switch to mitochondrial oxidative phosphorylation under radiation via mTOR-mediated hexokinase II inhibition--a Warburg-reversing effect. *PLoS One,* **10**, e0121046.

Luo, X., Ge, J., Chen, T., Liu, J., Liu, Z., Bi, C. and Lan, S. (2021) LHX9, a p53-binding protein, inhibits the progression of glioma by suppressing glycolysis. *Aging,* **13**, 22109-22119.

Ma, X. M. and Blenis, J. (2009) Molecular mechanisms of mTOR-mediated translational control. *Nature Reviews. Molecular Cell Biology,* **10**, 307-318.

Magaway, C., Kim, E. and Jacinto, E. (2019) Targeting mTOR and Metabolism in Cancer: Lessons and Innovations. *Cells,* **8**, 1584.

Malagelada, C., Jin, Z. H., Jackson-Lewis, V., Przedborski, S. and Greene, L. A. (2010) Rapamycin protects against neuron death in in vitro and in vivo models of Parkinson's disease. *The Journal of Neuroscience,* **30**, 1166-75.

Masui, K., Tanaka, K., Akhavan, D., Babic, I., Gini, B., Matsutani, T., Iwanami, A., Liu, F., Villa, G. R., Gu, Y., Campos, C., Zhu, S., Yang, H., Yong, W. H., Cloughesy, T. F., Mellinghoff, I. K., Cavenee, W. K., Shaw, R. J. and Mischel, P. S. (2013) mTOR complex 2 controls glycolytic metabolism in glioblastoma through FoxO acetylation and upregulation of c-Myc. *Cell Metabolism,* **18**, 726-739.

Meng, T. T., Wang, W., Meng, F. L., Wang, S. Y., Wu, H. H., Chen, J. M., Zheng, Y., Wang, G. X., Zhang, M. X., Li, Y. and Su, G. H. (2021) Nicotine Causes Mitochondrial Dynamics Imbalance and Apoptosis Through ROS Mediated Mitophagy Impairment in Cardiomyocytes. *Front Physiol,* **12**, 650055.

Menon, S., Dibble, C. C., Talbott, G., Hoxhaj, G., Valvezan, A. J., Takahashi, H., Cantley, L. C. and Manning, B. D. (2014) Spatial control of the TSC complex integrates insulin and nutrient regulation of mTORC1 at the lysosome. *Cell,* **156**, 771-785.

Mollé, B., Père, S., Failli, V., Bach, I. and Rétaux, S. (2004) Lhx9 and lhx9alpha: differential biochemical properties and effects on neuronal differentiation. *DNA and cell biology,* **23**, 761-768.

Morrison, N., Simpson, C., Fothergill-Gilmore, L., Boyd, E. and Connor, J. M. (1992) Regional chromosomal assignment of the human platelet phosphofructokinase gene to 10p15. *Human Genetics,* **89**, 105-106.

Ohanna, M., Sobering, A. K., Lapointe, T., Lorenzo, L., Praud, C., Petroulakis, E., Sonenberg, N., Kelly, P. A., Sotiropoulos, A. and Pende, M. (2005) Atrophy of S6K1(-/-) skeletal muscle cells reveals distinct mTOR effectors for cell cycle and size control. *Nature Cell Biology,* **7**, 286-294.

Okutomo, K., Fujino, N., Yamada, M., Saito, T., Ono, Y., Okada, Y., Ichinose, M. and Sugiura, H. (2022) Increased LHX9 expression in alveolar epithelial type 2 cells of patients with chronic obstructive pulmonary disease. *Respir Investig,* **60**, 119-128.

Oshima, Y., Noguchi, K. and Nakamura, M. (2007) Expression of Lhx9 isoforms in the developing gonads of Rana rugosa. *Zoolog Sci,* **24**, 798-802.

Papadopoli, D., Boulay, K., Kazak, L., Pollak, M., Mallette, F., Topisirovic, I. and Hulea, L. (2019) mTOR as a central regulator of lifespan and aging. *F1000Res,* **8**.

Peng, Y., Chu, S., Yang, Y., Zhang, Z., Pang, Z. and Chen, N. (2021) Neuroinflammatory In Vitro Cell Culture Models and the Potential Applications for Neurological Disorders. *Frontiers in Pharmacology,* **12**, 671734.

Perluigi, M., Di Domenico, F. and Butterfield, D. A. (2015) mTOR signaling in aging and neurodegeneration: At the crossroad between metabolism dysfunction and impairment of autophagy. *Neurobiol Dis,* **84**, 39-49.

Peterson, T. R., Laplante, M., Thoreen, C. C., Sancak, Y., Kang, S. A., Kuehl, W. M., Gray, N. S. and Sabatini, D. M. (2009) DEPTOR is an mTOR inhibitor frequently overexpressed in multiple myeloma cells and required for their survival. *Cell,* **137**, 873-886.

Polak, P. and Hall, M. N. (2009) mTOR and the control of whole body metabolism. *Curr Opin Cell Biol,* **21**, 209-18.

Rétaux, S., Rogard, M., Bach, I., Failli, V. and Besson, M.-J. (1999) Lhx9: A Novel LIM-Homeodomain Gene Expressed in the Developing Forebrain. *The Journal of Neuroscience,* **19**, 783-793.

Rodriguez-Lopez, M., Gonzalez, S., Hillson, O., Tunnacliffe, E., Codlin, S., Tallada, V. A., Bahler, J. and Rallis, C. (2020) The GATA Transcription Factor Gaf1 Represses tRNAs, Inhibits Growth, and Extends Chronological Lifespan Downstream of Fission Yeast TORC1. *Cell Reports,* **30**, 3240-3249 e4.

Rodrik-Outmezguine, V. S., Okaniwa, M., Yao, Z., Novotny, C. J., McWhirter, C., Banaji, A., Won, H., Wong, W., Berger, M., de Stanchina, E., Barratt, D. G., Cosulich, S., Klinowska, T., Rosen, N. and Shokat, K. M. (2016) Overcoming mTOR resistance mutations with a new-generation mTOR inhibitor. *Nature,* **534**, 272-276.

Sabatini, D. M., Erdjument-Bromage, H., Lui, M., Tempst, P. and Snyder, S. H. (1994) RAFT1: a mammalian protein that binds to FKBP12 in a rapamycin-dependent fashion and is homologous to yeast TORs. *Cell,* **78**, 35-43.

Sarbassov, D. D., Ali, S. M., Kim, D.-H., Guertin, D. A., Latek, R. R., Erdjument-Bromage, H., Tempst, P. and Sabatini, D. M. (2004) Rictor, a novel binding partner of mTOR, defines a rapamycin-insensitive

and raptor-independent pathway that regulates the cytoskeleton. *Current biology: CB,* **14**, 1296-1302.

Sarbassov, D. D., Ali, S. M., Sengupta, S., Sheen, J.-H., Hsu, P. P., Bagley, A. F., Markhard, A. L. and Sabatini, D. M. (2006) Prolonged rapamycin treatment inhibits mTORC2 assembly and Akt/PKB. *Molecular Cell,* **22**, 159-168.

Saxton, R. A. and Sabatini, D. M. (2017) mTOR Signaling in Growth, Metabolism, and Disease. *Cell,* **168**, 960-976.

Schreiber, K. H., Arriola Apelo, S. I., Yu, D., Brinkman, J. A., Velarde, M. C., Syed, F. A., Liao, C.-Y., Baar, E. L., Carbajal, K. A., Sherman, D. S., Ortiz, D., Brunauer, R., Yang, S. E., Tzannis, S. T., Kennedy, B. K. and Lamming, D. W. (2019) A novel rapamycin analog is highly selective for mTORC1 in vivo. *Nature Communications,* **10**, 3194.

Schreiber, S. L. (1991) Chemistry and biology of the immunophilins and their immunosuppressive ligands. *Science (New York, N.Y.),* **251**, 283-287.

Sehgal, S. N. (2003) Sirolimus: its discovery, biological properties, and mechanism of action. *Transplantation Proceedings,* **35**, 7S-14S.

Semenza, G. L. (2007) Oxygen-dependent regulation of mitochondrial respiration by hypoxia-inducible factor 1. *The Biochemical Journal,* **405**, 1-9.

Singh, N., Singh, D. and Modi, D. (2022) LIM Homeodomain (LIM-HD) Genes and Their Co-Regulators in Developing Reproductive System and Disorders of Sex Development. *Sexual Development: Genetics, Molecular Biology, Evolution, Endocrinology, Embryology, and Pathology of Sex Determination and Differentiation,* **16**, 147-161.

Smagulova, F. O., Manuylov, N. L., Leach, L. L. and Tevosian, S. G. (2008) GATA4/FOG2 transcriptional complex regulates Lhx9 gene expression in murine heart development. *BMC developmental biology,* **8**, 67.

Star, E. N., Zhu, M., Shi, Z., Liu, H., Pashmforoush, M., Sauve, Y., Bruneau, B. G. and Chow, R. L. (2012) Regulation of retinal interneuron subtype identity by the Iroquois homeobox gene Irx6. *Development,* **139**, 4644-55.

Strumiło, S. (2005) Short-term regulation of the mammalian pyruvate dehydrogenase complex. *Acta Biochimica Polonica,* **52**, 759-764.

Swiech, L., Perycz, M., Malik, A. and Jaworski, J. (2008) Role of mTOR in physiology and pathology of the nervous system. *Biochim Biophys Acta,* **1784**, 116-32.

Takei, N. and Nawa, H. (2014) mTOR signaling and its roles in normal and abnormal brain development. *Frontiers in Molecular Neuroscience,* **7**, 28.

Takeuchi, H., Kondo, Y., Fujiwara, K., Kanzawa, T., Aoki, H., Mills, G. B. and Kondo, S. (2005) Synergistic Augmentation of Rapamycin-Induced Autophagy in Malignant Glioma Cells by Phosphatidylinositol 3-Kinase/Protein Kinase B Inhibitors. *Cancer Research,* **65**, 3336-3346.

Thoreen, C. C., Kang, S. A., Chang, J. W., Liu, Q., Zhang, J., Gao, Y., Reichling, L. J., Sim, T., Sabatini, D. M. and Gray, N. S. (2009) An ATP-competitive mammalian target of rapamycin inhibitor reveals rapamycin-resistant functions of mTORC1. *The Journal of Biological Chemistry,* **284**, 8023-8032.

Urbanska, M., Gozdz, A., Swiech, L. J. and Jaworski, J. (2012) Mammalian target of rapamycin complex 1 (mTORC1) and 2 (mTORC2) control the dendritic arbor morphology of hippocampal neurons. *The Journal of Biological Chemistry,* **287**, 30240-56.

Vander Heiden, M. G., Cantley, L. C. and Thompson, C. B. (2009) Understanding the Warburg effect: the metabolic requirements of cell proliferation. *Science (New York, N.Y.),* **324**, 1029-33.

Villa-Cuesta, E., Holmbeck, M. A. and Rand, D. M. (2014) Rapamycin increases mitochondrial efficiency by mtDNA-dependent reprogramming of mitochondrial metabolism in Drosophila. *Journal of Cell Science,* **127**, 2282-90.

Vladimirova, V., Mikeska, T., Waha, A., Soerensen, N., Xu, J., Reynolds, P. C. and Pietsch, T. (2009) Aberrant methylation and reduced expression of LHX9 in malignant gliomas of childhood. *Neoplasia (New York, N.Y.),* **11**, 700-711.

Wang, S., Xia, B., Qiao, Z., Duan, L., Wang, G., Meng, W., Liu, Z., Wang, Y. and Zhang, M. (2019) Tetramethylpyrazine attenuated bupivacaine-induced neurotoxicity in SH-SY5Y cells through regulating apoptosis, autophagy and oxidative damage. *Drug Design, Development and Therapy,* **13**, 1187-1196.

Wilson, S. I., Shafer, B., Lee, K. J. and Dodd, J. (2008) A molecular program for contralateral trajectory: Rig-1 control by LIM homeodomain transcription factors. *Neuron,* **59**, 413-424.

Wullschleger, S., Loewith, R. and Hall, M. N. (2006) TOR signaling in growth and metabolism. *Cell,* **124**, 471-484.

Xicoy, H., Wieringa, B. and Martens, G. J. M. (2017) The SH-SY5Y cell line in Parkinson's disease research: a systematic review. *Molecular Neurodegeneration,* **12**, 10.

Xu, H., Cao, J., Xu, J., Li, H., Shen, H., Li, X., Wang, Z., Wu, J. and Chen, G. (2019) GATA-4 regulates neuronal apoptosis after intracerebral hemorrhage via the NF-kappaB/Bax/Caspase-3 pathway both in vivo and in vitro. *Exp Neurol,* **315**, 21-31.

Yamazaki, F., Møller, M., Fu, C., Clokie, S. J., Zykovich, A., Coon, S. L., Klein, D. C. and Rath, M. F. (2015) The Lhx9 homeobox gene controls pineal gland development and prevents postnatal hydrocephalus. *Brain Structure & Function,* **220**, 1497-1509.

Yang, G., Francis, D., Krycer, J. R., Larance, M., Zhang, Z., Novotny, C. J., Diaz-Vegas, A., Shokat, K. M. and James, D. E. (2021a) Dissecting the biology of mTORC1 beyond rapamycin. *Science Signaling,* **14**, eabe0161.

Yang, G., Murashige, D. S., Humphrey, S. J. and James, D. E. (2015) A Positive Feedback Loop between Akt and mTORC2 via SIN1 Phosphorylation. *Cell Reports,* **12**, 937-943.

Yang, L., Miao, L., Liang, F., Huang, H., Teng, X., Li, S., Nuriddinov, J., Selzer, M. E. and Hu, Y. (2014) The mTORC1 effectors S6K1 and 4E-BP play different roles in CNS axon regeneration. *Nature Communications,* **5**, 5416.

Yang, W., Pang, D., Chen, M., Du, C., Jia, L., Wang, L., He, Y., Jiang, W., Luo, L., Yu, Z., Mao, M., Yuan, Q., Tang, P., Xia, X., Cui, Y., Jing, B., Platero, A., Liu, Y., Wei, Y., Worley, P. F. and Xiao, B. (2021b) Rheb mediates neuronal-activity-induced mitochondrial energetics through mTORC1-independent PDH activation. *Dev Cell,* **56**, 811-825 e6.

Yu, Y., Yoon, S.-O., Poulogiannis, G., Yang, Q., Ma, X. M., Villén, J., Kubica, N., Hoffman, G. R., Cantley, L. C., Gygi, S. P. and Blenis, J. (2011) Phosphoproteomic analysis identifies Grb10 as an mTORC1 substrate that negatively regulates insulin signaling. *Science (New York, N.Y.),* **332**, 1322-1326.

Zhang, S., Lin, X., Hou, Q., Hu, Z., Wang, Y. and Wang, Z. (2021) Regulation of mTORC1 by amino acids in mammalian cells: A general picture of recent advances. *Animal Nutrition (Zhongguo Xu Mu Shou Yi Xue Hui),* **7**, 1009-1023.

Zhang, Y., Xu, X., Li, W., Miao, H., Huang, S., Zhou, Y., Sun, Y., Li, Z., Guo, Q. and Zhao, L. (2016) Activation of endoplasmic reticulum stress and the extrinsic apoptotic pathway in human lung cancer cells by the new synthetic flavonoid, LZ-205. *Oncotarget,* **7**, 87257-87270.

Zheng, X. F., Florentino, D., Chen, J., Crabtree, G. R. and Schreiber, S. L. (1995) TOR kinase domains are required for two distinct functions, only one of which is inhibited by rapamycin. *Cell,* **82**, 121-130.

Zhuang, X.-X., Wang, S.-F., Tan, Y., Song, J.-X., Zhu, Z., Wang, Z.-Y., Wu, M.-Y., Cai, C.-Z., Huang, Z.-J., Tan, J.-Q., Su, H.-X., Li, M. and Lu, J.-H. (2020) Pharmacological enhancement of TFEB-mediated autophagy alleviated neuronal death in oxidative stress-induced Parkinson's disease models. *Cell Death & Disease,* **11**, 128.

Zinzalla, V., Stracka, D., Oppliger, W. and Hall, M. N. (2011) Activation of mTORC2 by association with the ribosome. *Cell,* **144**, 757-768.

7. Appendix

Appendix 1: Torin1 vs Control differentially expressed upregulated genes (203 genes)

	Ensembl gene ID	log2FoldChange	pvalue	padj	symbol	diffexpressed
1.	ENSG00000004799	1.451953	1.79E-07	2.64E-06	PDK4	UP
2.	ENSG00000006468	1.528477	1.53E-17	1.30E-15	ETV1	UP
3.	ENSG00000006652	1.161588	2.84E-31	1.00E-28	IFRD1	UP
4.	ENSG00000048052	1.099922	7.07E-21	8.90E-19	HDAC9	UP
5.	ENSG00000059378	1.038023	0.000331	0.001971	PARP12	UP
6.	ENSG00000069667	1.062174	4.09E-06	4.24E-05	RORA	UP
7.	ENSG00000079102	1.066641	4.84E-15	2.89E-13	RUNX1T1	UP
8.	ENSG00000081189	1.125769	1.08E-11	3.63E-10	MEF2C	UP
9.	ENSG00000089041	1.031496	2.89E-13	1.31E-11	P2RX7	UP
10.	ENSG00000090447	1.075731	4.51E-16	3.08E-14	TFAP4	UP
11.	ENSG00000100100	1.239385	1.47E-08	2.75E-07	PIK3IP1	UP
12.	ENSG00000101292	1.224675	0.000314	0.001877	PROKR2	UP
13.	ENSG00000101384	1.041545	2.91E-10	7.75E-09	JAG1	UP
14.	ENSG00000104313	1.274657	1.36E-38	7.30E-36	EYA1	UP
15.	ENSG00000104419	1.290232	4.71E-31	1.58E-28	NDRG1	UP
16.	ENSG00000104953	1.189009	0.000226	0.001409	TLE6	UP
17.	ENSG00000106829	1.2846	1.51E-32	5.91E-30	TLE4	UP
18.	ENSG00000107984	1.066731	1.23E-27	3.12E-25	DKK1	UP
19.	ENSG00000108932	1.913509	5.12E-05	0.000388	SLC16A6	UP
20.	ENSG00000109132	1.069872	5.14E-35	2.33E-32	PHOX2B	UP
21.	ENSG00000109323	1.154479	1.56E-12	6.28E-11	MANBA	UP
22.	ENSG00000109452	1.3459	0.004912	0.019463	INPP4B	UP
23.	ENSG00000111644	1.477929	0.003191	0.013616	ACRBP	UP
24.	ENSG00000112038	1.083137	1.24E-09	2.97E-08	OPRM1	UP
25.	ENSG00000113369	1.039682	1.25E-29	3.85E-27	ARRDC3	UP
26.	ENSG00000113851	1.112648	3.48E-17	2.86E-15	CRBN	UP
27.	ENSG00000116183	1.54117	0.000194	0.001234	PAPPA2	UP
28.	ENSG00000117262	1.032741	6.93E-07	8.88E-06	GPR89A	UP
29.	ENSG00000117600	1.02991	4.42E-17	3.54E-15	PLPPR4	UP
30.	ENSG00000117707	1.609934	5.06E-49	8.14E-46	PROX1	UP

31.	ENSG00000118946	1.021364	2.30E-06	2.53E-05	PCDH17	UP
32.	ENSG00000119714	1.023761	2.99E-10	7.91E-09	GPR68	UP
33.	ENSG00000119866	1.103148	1.41E-05	0.000127	BCL11A	UP
34.	ENSG00000121068	1.01967	1.50E-18	1.48E-16	TBX2	UP
35.	ENSG00000121440	1.013451	4.13E-27	9.97E-25	PDZRN3	UP
36.	ENSG00000121897	1.434464	1.73E-18	1.67E-16	LIAS	UP
37.	ENSG00000122691	1.038289	2.01E-25	4.04E-23	TWIST1	UP
38.	ENSG00000124370	1.07944	0.001031	0.005226	MCEE	UP
39.	ENSG00000125772	1.082278	3.48E-11	1.07E-09	GPCPD1	UP
40.	ENSG00000126368	1.186706	8.01E-09	1.61E-07	NR1D1	UP
41.	ENSG00000127311	1.09084	5.44E-07	7.16E-06	HELB	UP
42.	ENSG00000128710	1.035638	2.22E-06	2.47E-05	HOXD10	UP
43.	ENSG00000128849	1.326465	0.008823	0.031591	CGNL1	UP
44.	ENSG00000129422	1.512273	1.02E-31	3.79E-29	MTUS1	UP
45.	ENSG00000131400	1.660266	0.001632	0.007681	NAPSA	UP
46.	ENSG00000133878	1.016773	5.24E-12	1.88E-10	DUSP26	UP
47.	ENSG00000134138	1.203608	8.35E-39	4.83E-36	MEIS2	UP
48.	ENSG00000134899	1.004578	0.000666	0.003608	ERCC5	UP
49.	ENSG00000135914	1.539814	2.47E-05	0.000207	HTR2B	UP
50.	ENSG00000136059	1.391489	1.23E-11	4.08E-10	VILL	UP
51.	ENSG00000136997	1.578147	6.47E-44	6.25E-41	MYC	UP
52.	ENSG00000137801	1.40832	0.013874	0.045666	THBS1	UP
53.	ENSG00000138083	1.272913	9.68E-39	5.39E-36	SIX3	UP
54.	ENSG00000138587	1.028622	1.58E-05	0.000141	MNS1	UP
55.	ENSG00000138621	1.041464	5.72E-06	5.68E-05	PPCDC	UP
56.	ENSG00000139289	1.204224	4.53E-13	2.01E-11	PHLDA1	UP
57.	ENSG00000139793	1.127285	1.56E-12	6.28E-11	MBNL2	UP
58.	ENSG00000141391	1.360367	3.55E-12	1.34E-10	PRELID3A	UP
59.	ENSG00000143355	1.691752	1.80E-21	2.33E-19	LHX9	UP
60.	ENSG00000143578	1.006641	1.36E-14	7.58E-13	CREB3L4	UP
61.	ENSG00000143995	1.145399	5.93E-30	1.87E-27	MEIS1	UP
62.	ENSG00000144460	1.380795	1.62E-05	0.000144	NYAP2	UP
63.	ENSG00000144681	1.07769	3.23E-29	9.18E-27	STAC	UP
64.	ENSG00000145002	1.140315	0.013895	0.045695	FAM86B2	UP
65.	ENSG00000146006	1.351094	1.75E-12	6.97E-11	LRRTM2	UP
66.	ENSG00000149922	1.244687	3.10E-06	3.31E-05	TBX6	UP
67.	ENSG00000150347	1.158567	1.97E-14	1.07E-12	ARID5B	UP
68.	ENSG00000152818	1.072667	3.96E-17	3.21E-15	UTRN	UP
69.	ENSG00000154545	3.121995	0.000222	0.001389	MAGED4	UP
70.	ENSG00000154734	1.428765	9.88E-40	7.15E-37	ADAMTS1	UP
71.	ENSG00000155530	1.769093	0.002605	0.011446	LRGUK	UP
72.	ENSG00000155974	1.512751	2.73E-08	4.77E-07	GRIP1	UP
73.	ENSG00000156804	1.662739	1.18E-08	2.26E-07	FBXO32	UP

74.	ENSG00000157429	1.005891	6.36E-05	0.00047	ZNF19	UP
75.	ENSG00000159387	1.544781	1.20E-15	7.70E-14	IRX6	UP
76.	ENSG00000159915	1.16416	3.72E-07	5.13E-06	ZNF233	UP
77.	ENSG00000162390	1.194111	1.09E-05	0.000101	ACOT11	UP
78.	ENSG00000162407	1.086433	3.87E-25	7.46E-23	PLPP3	UP
79.	ENSG00000162971	1.019699	7.59E-09	1.53E-07	TYW5	UP
80.	ENSG00000163050	1.166743	5.65E-30	1.82E-27	COQ8A	UP
81.	ENSG00000164118	1.089032	6.98E-32	2.66E-29	CEP44	UP
82.	ENSG00000164463	1.01645	8.89E-10	2.19E-08	CREBRF	UP
83.	ENSG00000165029	1.80843	6.16E-06	6.04E-05	ABCA1	UP
84.	ENSG00000165140	1.154257	0.01004	0.035132	FBP1	UP
85.	ENSG00000166046	1.004262	0.000252	0.001548	TCP11L2	UP
86.	ENSG00000166159	1.246145	0.001328	0.006475	LRTM2	UP
87.	ENSG00000166292	1.674184	6.72E-07	8.62E-06	TMEM100	UP
88.	ENSG00000166793	1.053812	1.73E-06	1.99E-05	YPEL4	UP
89.	ENSG00000167081	1.042563	2.17E-29	6.29E-27	PBX3	UP
90.	ENSG00000168264	1.192095	1.89E-45	2.10E-42	IRF2BP2	UP
91.	ENSG00000168348	1.77902	3.92E-79	2.84E-75	INSM2	UP
92.	ENSG00000168405	1.054698	0.015463	0.049876	CMAHP	UP
93.	ENSG00000168491	1.160874	0.002979	0.012851	CCDC110	UP
94.	ENSG00000168916	1.749233	2.99E-65	8.67E-62	ZNF608	UP
95.	ENSG00000169129	1.123541	0.000241	0.001489	AFAP1L2	UP
96.	ENSG00000169554	1.190247	1.44E-30	4.75E-28	ZEB2	UP
97.	ENSG00000169964	1.056326	6.00E-09	1.24E-07	TMEM42	UP
98.	ENSG00000170153	1.042776	3.48E-26	7.62E-24	RNF150	UP
99.	ENSG00000170166	1.200473	0.005267	0.0206	HOXD4	UP
100.	ENSG00000170271	1.796448	2.66E-34	1.17E-31	FAXDC2	UP
101.	ENSG00000170448	1.104971	7.95E-13	3.33E-11	NFXL1	UP
102.	ENSG00000172062	1.097535	0.014426	0.047227	SMN1	UP
103.	ENSG00000172572	1.092339	2.71E-14	1.42E-12	PDE3A	UP
104.	ENSG00000173068	1.190585	0.002004	0.00917	BNC2	UP
105.	ENSG00000173114	1.84584	4.06E-09	8.69E-08	LRRN3	UP
106.	ENSG00000173208	1.228336	5.58E-24	9.08E-22	ABCD2	UP
107.	ENSG00000175097	2.03554	2.26E-23	3.44E-21	RAG2	UP
108.	ENSG00000175155	1.75583	2.67E-39	1.68E-36	YPEL2	UP
109.	ENSG00000176204	1.741547	1.14E-06	1.38E-05	LRRTM4	UP
110.	ENSG00000176933	1.147607	0.002527	0.011172	NA	UP
111.	ENSG00000177103	2.577679	2.22E-05	0.000189	DSCAML1	UP
112.	ENSG00000178381	1.242533	2.65E-13	1.21E-11	ZFAND2A	UP
113.	ENSG00000179270	1.452748	0.000217	0.001359	PCARE	UP
114.	ENSG00000179406	1.17051	7.13E-13	3.01E-11	LINC00174	UP
115.	ENSG00000179978	1.115449	0.001361	0.006606	NA	UP
116.	ENSG00000180660	1.021467	3.60E-33	1.45E-30	MAB21L1	UP

117.	ENSG00000181072	1.384007	0.008779	0.031456	CHRM2	UP
118.	ENSG00000182366	1.697239	3.63E-06	3.80E-05	FAM87A	UP
119.	ENSG00000184226	1.366369	8.08E-10	2.00E-08	PCDH9	UP
120.	ENSG00000184564	1.743457	1.51E-07	2.28E-06	SLITRK6	UP
121.	ENSG00000184898	1.351316	2.03E-11	6.46E-10	RBM43	UP
122.	ENSG00000185158	1.091579	1.39E-11	4.55E-10	LRRC37B	UP
123.	ENSG00000185339	1.316352	5.26E-07	6.95E-06	TCN2	UP
124.	ENSG00000185404	1.06678	0.007694	0.028227	SP140L	UP
125.	ENSG00000188816	1.18107	0.001375	0.006648	HMX2	UP
126.	ENSG00000188818	1.088243	0.012378	0.041594	ZDHHC11	UP
127.	ENSG00000196482	1.181958	5.42E-25	1.02E-22	ESRRG	UP
128.	ENSG00000197054	1.220277	0.001836	0.008501	ZNF763	UP
129.	ENSG00000203709	1.132179	0.002037	0.0093	NA	UP
130.	ENSG00000203865	1.052123	0.004545	0.018269	ATP1A1-AS1	UP
131.	ENSG00000203943	1.031729	0.006946	0.025943	SAMD13	UP
132.	ENSG00000204177	1.212762	0.000281	0.0017	NA	UP
133.	ENSG00000205482	1.708493	0.000722	0.00386	SPDYE18	UP
134.	ENSG00000214439	1.314775	0.000177	0.001141	NA	UP
135.	ENSG00000221883	1.411675	1.86E-05	0.000162	NA	UP
136.	ENSG00000221994	1.01528	0.001808	0.008382	ZNF630	UP
137.	ENSG00000223820	1.352031	0.002645	0.0116	NA	UP
138.	ENSG00000225194	1.347008	0.001263	0.006222	LINC00092	UP
139.	ENSG00000225265	1.141923	2.86E-05	0.000235	TAF1A-AS1	UP
140.	ENSG00000226696	1.121476	0.006385	0.024222	LENG8-AS1	UP
141.	ENSG00000227719	1.981324	2.68E-14	1.41E-12	NA	UP
142.	ENSG00000230409	1.01099	0.001032	0.005232	NA	UP
143.	ENSG00000230715	1.018512	1.50E-05	0.000134	NA	UP
144.	ENSG00000231439	1.220814	0.000143	0.000948	WASIR2	UP
145.	ENSG00000232104	1.096246	0.010967	0.037729	RFX3-DT	UP
146.	ENSG00000232611	1.349134	0.014978	0.048605	NA	UP
147.	ENSG00000232653	1.122169	0.005377	0.020959	GOLGA8N	UP
148.	ENSG00000232821	1.681996	2.12E-10	5.75E-09	NA	UP
149.	ENSG00000237651	1.352254	0.002709	0.011849	C2orf74	UP
150.	ENSG00000240875	1.23575	0.004294	0.017445	LINC00886	UP
151.	ENSG00000241149	1.250123	0.000295	0.001775	ZNF722	UP
152.	ENSG00000241158	1.754211	1.38E-06	1.62E-05	ADAMTS9-AS1	UP
153.	ENSG00000243244	1.147463	3.52E-07	4.88E-06	STON1	UP
154.	ENSG00000243679	1.219083	2.01E-09	4.56E-08	NA	UP
155.	ENSG00000244731	1.200079	0.013598	0.04486	C4A	UP
156.	ENSG00000245556	1.112758	3.32E-07	4.65E-06	SCAMP1-AS1	UP

157.	ENSG00000246859	1.031386	0.000614	0.003368	STARD4-AS1	UP
158.	ENSG00000248905	1.122933	6.63E-16	4.39E-14	FMN1	UP
159.	ENSG00000248971	2.597606	2.75E-05	0.000227	KRT8P46	UP
160.	ENSG00000249859	1.063189	6.28E-06	6.15E-05	PVT1	UP
161.	ENSG00000251634	1.358477	0.014809	0.048184	NA	UP
162.	ENSG00000253661	1.354026	0.0045	0.018116	ZFHX4-AS1	UP
163.	ENSG00000254531	1.183923	4.08E-05	0.000317	FLJ20021	UP
164.	ENSG00000254701	1.010794	0.002778	0.012089	NA	UP
165.	ENSG00000254966	1.293806	0.002975	0.012835	NA	UP
166.	ENSG00000255717	1.206804	1.09E-26	2.51E-24	SNHG1	UP
167.	ENSG00000256064	1.248104	0.011583	0.039394	NA	UP
168.	ENSG00000256594	1.200098	0.008776	0.031454	NA	UP
169.	ENSG00000257027	1.2807	3.53E-06	3.71E-05	NA	UP
170.	ENSG00000257135	1.504812	0.012955	0.043074	NA	UP
171.	ENSG00000259775	1.634637	0.002927	0.01266	NA	UP
172.	ENSG00000259946	2.816772	1.82E-05	0.000159	NA	UP
173.	ENSG00000260236	1.07734	0.001736	0.008107	NA	UP
174.	ENSG00000260404	1.080238	1.09E-12	4.53E-11	NA	UP
175.	ENSG00000260572	1.490922	0.00979	0.034432	NA	UP
176.	ENSG00000260802	2.138455	0.000143	0.000948	SERTM2	UP
177.	ENSG00000262877	1.233955	0.001283	0.006299	NA	UP
178.	ENSG00000264491	1.169196	0.010545	0.036555	NA	UP
179.	ENSG00000265749	1.262297	0.003278	0.013907	NA	UP
180.	ENSG00000269935	1.079662	0.009977	0.034979	NA	UP
181.	ENSG00000270055	1.040022	0.010492	0.036432	NA	UP
182.	ENSG00000271327	1.390424	0.007592	0.027965	NA	UP
183.	ENSG00000272168	1.099082	2.31E-19	2.45E-17	NA	UP
184.	ENSG00000272316	1.102398	0.001928	0.008868	NA	UP
185.	ENSG00000272556	1.100068	3.34E-10	8.78E-09	NA	UP
186.	ENSG00000272849	1.156711	0.004187	0.017079	NA	UP
187.	ENSG00000273080	1.331896	0.005643	0.021855	NA	UP
188.	ENSG00000273142	1.284165	8.71E-12	2.99E-10	NA	UP
189.	ENSG00000273301	1.350564	1.63E-08	3.04E-07	NA	UP
190.	ENSG00000274512	1.07274	9.09E-05	0.000638	TBC1D3	UP
191.	ENSG00000274718	1.30226	8.19E-07	1.03E-05	NA	UP
192.	ENSG00000275038	1.319931	3.13E-06	3.33E-05	NA	UP
193.	ENSG00000276644	1.144881	1.35E-29	4.07E-27	DACH1	UP
194.	ENSG00000278619	1.0455	8.59E-07	1.07E-05	MRM1	UP
195.	ENSG00000279253	1.017453	0.015299	0.049446	NA	UP
196.	ENSG00000279382	1.189684	0.001573	0.007448	NA	UP
197.	ENSG00000279407	1.65532	1.12E-05	0.000103	NA	UP
198.	ENSG00000279555	1.495989	0.005431	0.021145	NA	UP

199.	ENSG00000279873	1.387731	0.012626	0.042281	LINC01126	UP
200.	ENSG00000281706	1.233001	4.87E-05	0.000371	LINC01012	UP
201.	ENSG00000282870	1.051434	0.011585	0.039394	NA	UP
202.	ENSG00000283213	1.523269	0.000165	0.001073	NA	UP
203.	ENSG00000285796	1.126181	0.003637	0.015141	NA	UP

Appendix 2: Torin1 vs Control differentially expressed downregulated genes (251 genes)

	Ensembl gene ID	log2Fold Change	pvalue	padj	symbol	diffexpressed
1.	ENSG00000006327	-1.41778	1.03E-08	2.01E-07	TNFRSF12A	DOWN
2.	ENSG00000022567	-1.53009	8.61E-18	7.79E-16	SLC45A4	DOWN
3.	ENSG00000028277	-1.03686	0.000452	0.002582	POU2F2	DOWN
4.	ENSG00000029153	-1.00192	0.000547	0.003038	BMAL2	DOWN
5.	ENSG00000033100	-1.0058	1.58E-24	2.72E-22	CHPF2	DOWN
6.	ENSG00000034152	-1.047	2.78E-06	3.01E-05	MAP2K3	DOWN
7.	ENSG00000036672	-1.52651	0.000109	0.00075	USP2	DOWN
8.	ENSG00000040608	-1.69579	1.15E-18	1.15E-16	RTN4R	DOWN
9.	ENSG00000060982	-1.08015	7.32E-22	9.81E-20	BCAT1	DOWN
10.	ENSG00000061337	-1.29735	3.28E-22	4.53E-20	LZTS1	DOWN
11.	ENSG00000063176	-1.01436	3.38E-13	1.50E-11	SPHK2	DOWN
12.	ENSG00000065911	-1.26532	4.53E-40	3.45E-37	MTHFD2	DOWN
13.	ENSG00000074276	-1.25286	9.88E-07	1.22E-05	CDHR2	DOWN
14.	ENSG00000081087	-1.16947	3.43E-15	2.06E-13	OSTM1	DOWN
15.	ENSG00000086061	-1.1903	3.06E-35	1.43E-32	DNAJA1	DOWN
16.	ENSG00000086062	-1.39402	8.41E-14	4.13E-12	B4GALT1	DOWN
17.	ENSG00000086506	-1.07978	3.37E-05	0.00027	HBQ1	DOWN
18.	ENSG00000088256	-1.0949	2.28E-23	3.44E-21	GNA11	DOWN
19.	ENSG00000088986	-1.05469	1.10E-24	1.97E-22	DYNLL1	DOWN
20.	ENSG00000090861	-1.17406	2.03E-40	1.63E-37	AARS1	DOWN
21.	ENSG00000099875	-1.15731	3.82E-28	9.87E-26	MKNK2	DOWN
22.	ENSG00000100285	-1.14614	2.65E-20	3.15E-18	NEFH	DOWN
23.	ENSG00000100314	-1.40765	0.011473	0.039132	CABP7	DOWN
24.	ENSG00000100647	-1.02734	2.24E-08	4.05E-07	SUSD6	DOWN
25.	ENSG00000101084	-1.4897	1.97E-16	1.43E-14	RAB5IF	DOWN
26.	ENSG00000101180	-1.34424	3.29E-08	5.67E-07	HRH3	DOWN
27.	ENSG00000101265	-1.72096	0.000996	0.00509	RASSF2	DOWN
28.	ENSG00000101306	-1.71217	0.002716	0.011872	MYLK2	DOWN
29.	ENSG00000101412	-1.01087	3.18E-13	1.43E-11	E2F1	DOWN
30.	ENSG00000101844	-1.20397	0.000143	0.000949	ATG4A	DOWN

31.	ENSG00000101846	-1.15555	0.000358	0.002108	STS	DOWN
32.	ENSG00000102753	-1.08304	3.09E-18	2.93E-16	KPNA3	DOWN
33.	ENSG00000102879	-1.26847	5.11E-12	1.84E-10	CORO1A	DOWN
34.	ENSG00000103257	-2.76397	########	########	SLC7A5	DOWN
35.	ENSG00000103966	-1.3629	7.76E-17	6.01E-15	EHD4	DOWN
36.	ENSG00000105173	-1.31829	1.59E-09	3.68E-08	CCNE1	DOWN
37.	ENSG00000106105	-1.4496	4.33E-47	5.70E-44	GARS1	DOWN
38.	ENSG00000106992	-1.08598	0.014526	0.047466	AK1	DOWN
39.	ENSG00000109062	-1.12763	2.59E-18	2.48E-16	NHERF1	DOWN
40.	ENSG00000109066	-1.46846	1.50E-25	3.06E-23	TMEM104	DOWN
41.	ENSG00000110619	-1.08586	6.30E-29	1.72E-26	CARS1	DOWN
42.	ENSG00000112033	-1.07089	8.70E-19	8.80E-17	PPARD	DOWN
43.	ENSG00000112715	-1.24571	2.54E-27	6.24E-25	VEGFA	DOWN
44.	ENSG00000113739	-1.4235	2.56E-16	1.82E-14	STC2	DOWN
45.	ENSG00000114648	-1.21708	3.23E-13	1.45E-11	KLHL18	DOWN
46.	ENSG00000114757	-2.27151	1.88E-05	0.000164	PEX5L	DOWN
47.	ENSG00000115884	-1.2049	4.49E-34	1.91E-31	SDC1	DOWN
48.	ENSG00000115902	-1.63782	7.25E-41	6.56E-38	SLC1A4	DOWN
49.	ENSG00000116237	-1.65047	5.81E-52	1.05E-48	ICMT	DOWN
50.	ENSG00000117016	-1.22649	1.21E-39	7.96E-37	RIMS3	DOWN
51.	ENSG00000117318	-1.304	2.03E-06	2.28E-05	ID3	DOWN
52.	ENSG00000117394	-1.00317	3.98E-17	3.21E-15	SLC2A1	DOWN
53.	ENSG00000117461	-1.31558	1.31E-25	2.79E-23	PIK3R3	DOWN
54.	ENSG00000118513	-1.17809	0.000267	0.001627	MYB	DOWN
55.	ENSG00000118894	-1.06024	5.01E-07	6.64E-06	EEF2KMT	DOWN
56.	ENSG00000119547	-1.25908	1.91E-09	4.37E-08	ONECUT2	DOWN
57.	ENSG00000120937	-1.188	0.01234	0.041512	NPPB	DOWN
58.	ENSG00000123395	-1.05394	2.39E-09	5.32E-08	ATG101	DOWN
59.	ENSG00000124762	-1.85241	1.04E-77	5.00E-74	CDKN1A	DOWN
60.	ENSG00000125508	-1.18559	0.004063	0.016635	SRMS	DOWN
61.	ENSG00000125878	-1.16084	0.002452	0.010891	TCF15	DOWN
62.	ENSG00000126803	-1.81543	2.65E-24	4.45E-22	HSPA2	DOWN
63.	ENSG00000126882	-1.61317	3.85E-05	0.000303	FAM78A	DOWN
64.	ENSG00000127423	-1.59926	6.00E-06	5.90E-05	AUNIP	DOWN
65.	ENSG00000128011	-1.07786	1.41E-12	5.77E-11	LRFN1	DOWN
66.	ENSG00000128165	-1.39501	3.10E-12	1.18E-10	ADM2	DOWN
67.	ENSG00000128203	-1.39179	5.10E-12	1.84E-10	ASPHD2	DOWN
68.	ENSG00000128228	-1.9859	3.08E-22	4.29E-20	SDF2L1	DOWN
69.	ENSG00000128266	-1.0264	3.10E-20	3.59E-18	GNAZ	DOWN
70.	ENSG00000128594	-2.58223	1.26E-06	1.50E-05	LRRC4	DOWN
71.	ENSG00000128965	-2.97812	8.34E-29	2.24E-26	CHAC1	DOWN
72.	ENSG00000129911	-1.05611	3.59E-16	2.50E-14	KLF16	DOWN
73.	ENSG00000130054	-1.27284	1.24E-08	2.36E-07	NALF2	DOWN

74.	ENSG00000130584	-1.14461	6.45E-07	8.33E-06	ZBTB46	DOWN
75.	ENSG00000130766	-1.60033	2.64E-22	3.74E-20	SESN2	DOWN
76.	ENSG00000131094	-1.0253	1.93E-15	1.20E-13	C1QL1	DOWN
77.	ENSG00000131148	-1.0148	2.10E-09	4.74E-08	EMC8	DOWN
78.	ENSG00000131323	-1.15947	1.22E-14	6.83E-13	TRAF3	DOWN
79.	ENSG00000131467	-1.06658	2.35E-28	6.18E-26	PSME3	DOWN
80.	ENSG00000132002	-1.19259	1.66E-19	1.83E-17	DNAJB1	DOWN
81.	ENSG00000132819	-1.02013	2.30E-16	1.65E-14	RBM38	DOWN
82.	ENSG00000133069	-1.04471	1.94E-15	1.20E-13	TMCC2	DOWN
83.	ENSG00000134317	-1.85718	0.000248	0.001527	GRHL1	DOWN
84.	ENSG00000134590	-1.04977	4.26E-27	1.01E-24	RTL8C	DOWN
85.	ENSG00000134684	-1.12422	1.13E-31	4.10E-29	YARS1	DOWN
86.	ENSG00000135069	-1.40137	5.06E-45	5.24E-42	PSAT1	DOWN
87.	ENSG00000135127	-1.18394	8.58E-11	2.48E-09	BICDL1	DOWN
88.	ENSG00000135472	-1.1848	2.57E-17	2.14E-15	FAIM2	DOWN
89.	ENSG00000135617	-1.27623	4.31E-06	4.44E-05	PRADC1	DOWN
90.	ENSG00000135709	-2.16333	1.76E-14	9.72E-13	KIAA0513	DOWN
91.	ENSG00000137492	-1.1934	7.86E-23	1.16E-20	THAP12	DOWN
92.	ENSG00000138073	-1.10708	7.71E-22	1.02E-19	PREB	DOWN
93.	ENSG00000138166	-1.39336	0.000163	0.001059	DUSP5	DOWN
94.	ENSG00000138623	-1.356	4.66E-07	6.21E-06	SEMA7A	DOWN
95.	ENSG00000139514	-1.03204	4.03E-31	1.39E-28	SLC7A1	DOWN
96.	ENSG00000139645	-1.03064	1.91E-17	1.61E-15	ANKRD52	DOWN
97.	ENSG00000140044	-1.90601	3.40E-08	5.83E-07	JDP2	DOWN
98.	ENSG00000140157	-1.07136	4.86E-18	4.48E-16	NIPA2	DOWN
99.	ENSG00000140406	-1.03726	9.27E-18	8.27E-16	TLNRD1	DOWN
100.	ENSG00000140557	-1.2143	1.53E-17	1.30E-15	ST8SIA2	DOWN
101.	ENSG00000140743	-1.23847	7.81E-13	3.28E-11	CDR2	DOWN
102.	ENSG00000140961	-1.2017	0.004418	0.017864	OSGIN1	DOWN
103.	ENSG00000141682	-1.35881	1.96E-21	2.51E-19	PMAIP1	DOWN
104.	ENSG00000141854	-1.06826	0.001922	0.008843	MISP3	DOWN
105.	ENSG00000143590	-1.14905	7.96E-06	7.63E-05	EFNA3	DOWN
106.	ENSG00000143753	-1.19248	1.62E-26	3.67E-24	DEGS1	DOWN
107.	ENSG00000143942	-1.18925	0.01494	0.048506	CHAC2	DOWN
108.	ENSG00000145990	-1.31583	0.001045	0.005285	GFOD1	DOWN
109.	ENSG00000147526	-1.26737	1.30E-06	1.54E-05	TACC1	DOWN
110.	ENSG00000148411	-1.22424	5.05E-06	5.09E-05	NACC2	DOWN
111.	ENSG00000150667	-1.44357	0.007201	0.026742	FSIP1	DOWN
112.	ENSG00000151012	-2.81128	6.71E-19	6.89E-17	SLC7A11	DOWN
113.	ENSG00000152056	-2.43953	2.73E-05	0.000226	AP1S3	DOWN
114.	ENSG00000152969	-1.15442	0.013564	0.044759	JAKMIP1	DOWN
115.	ENSG00000153879	-1.17528	2.90E-22	4.08E-20	CEBPG	DOWN
116.	ENSG00000154813	-1.01746	1.58E-12	6.32E-11	DPH3	DOWN

117.	ENSG00000156381	-1.34977	3.56E-26	7.68E-24	ANKRD9	DOWN
118.	ENSG00000157240	-1.1104	2.70E-16	1.89E-14	FZD1	DOWN
119.	ENSG00000158470	-1.07869	1.83E-29	5.39E-27	B4GALT5	DOWN
120.	ENSG00000160113	-1.0289	2.40E-22	3.47E-20	NR2F6	DOWN
121.	ENSG00000160200	-1.29666	2.80E-05	0.000231	CBS	DOWN
122.	ENSG00000160785	-1.05372	1.68E-19	1.83E-17	SLC25A44	DOWN
123.	ENSG00000162073	-1.46897	4.49E-27	1.05E-24	PAQR4	DOWN
124.	ENSG00000162104	-1.00519	0.000158	0.001034	ADCY9	DOWN
125.	ENSG00000162302	-1.13576	7.53E-10	1.88E-08	RPS6KA4	DOWN
126.	ENSG00000162878	-1.24435	7.15E-06	6.92E-05	PKDCC	DOWN
127.	ENSG00000163376	-1.32589	0.000426	0.002455	KBTBD8	DOWN
128.	ENSG00000163485	-1.01942	0.011578	0.039389	ADORA1	DOWN
129.	ENSG00000163686	-1.13554	6.04E-08	9.86E-07	ABHD6	DOWN
130.	ENSG00000164045	-1.43092	1.10E-23	1.75E-21	CDC25A	DOWN
131.	ENSG00000164938	-1.09787	5.99E-18	5.49E-16	TP53INP1	DOWN
132.	ENSG00000165389	-1.1185	3.00E-15	1.82E-13	SPTSSA	DOWN
133.	ENSG00000165886	-1.0124	4.01E-08	6.79E-07	UBTD1	DOWN
134.	ENSG00000166002	-1.57376	0.000797	0.004192	SMCO4	DOWN
135.	ENSG00000166123	-1.69055	2.24E-65	8.09E-62	GPT2	DOWN
136.	ENSG00000166289	-1.15721	4.62E-05	0.000354	PLEKHF1	DOWN
137.	ENSG00000166986	-1.43716	3.04E-53	7.34E-50	MARS1	DOWN
138.	ENSG00000167106	-1.23163	4.73E-16	3.22E-14	EEIG1	DOWN
139.	ENSG00000167114	-1.23984	7.30E-21	9.03E-19	SLC27A4	DOWN
140.	ENSG00000167244	-1.02644	5.03E-06	5.07E-05	IGF2	DOWN
141.	ENSG00000167552	-1.23505	1.69E-33	7.00E-31	TUBA1A	DOWN
142.	ENSG00000168209	-1.60314	7.09E-14	3.53E-12	DDIT4	DOWN
143.	ENSG00000168389	-2.53725	1.60E-22	2.34E-20	MFSD2A	DOWN
144.	ENSG00000168398	-1.12927	0.004972	0.019648	BDKRB2	DOWN
145.	ENSG00000168496	-1.01647	1.66E-16	1.23E-14	FEN1	DOWN
146.	ENSG00000168906	-1.40872	7.62E-36	3.68E-33	MAT2A	DOWN
147.	ENSG00000169184	-1.41271	0.001317	0.006436	MN1	DOWN
148.	ENSG00000169981	-1.17063	7.87E-10	1.96E-08	ZNF35	DOWN
149.	ENSG00000169991	-2.60254	2.43E-07	3.49E-06	IFFO2	DOWN
150.	ENSG00000170340	-1.30248	2.65E-16	1.87E-14	B3GNT2	DOWN
151.	ENSG00000170468	-1.27876	1.36E-12	5.57E-11	RIOX1	DOWN
152.	ENSG00000170871	-1.97828	8.81E-53	1.82E-49	KIAA0232	DOWN
153.	ENSG00000171388	-2.13762	0.000166	0.001076	APLN	DOWN
154.	ENSG00000171450	-1.2727	2.65E-25	5.19E-23	CDK5R2	DOWN
155.	ENSG00000171621	-1.0642	0.007213	0.026767	SPSB1	DOWN
156.	ENSG00000171786	-1.60546	0.004503	0.01812	NHLH1	DOWN
157.	ENSG00000171793	-1.26538	7.25E-25	1.33E-22	CTPS1	DOWN
158.	ENSG00000172115	-1.45827	1.58E-46	1.90E-43	CYCS	DOWN
159.	ENSG00000172183	-1.49767	0.002879	0.012474	ISG20	DOWN

160.	ENSG00000172216	-2.07162	1.25E-24	2.18E-22	CEBPB	DOWN
161.	ENSG00000172458	-1.02511	0.000105	0.00072	IL17D	DOWN
162.	ENSG00000172780	-1.429	0.001348	0.006554	RAB43	DOWN
163.	ENSG00000173110	-1.76525	0.001321	0.006446	HSPA6	DOWN
164.	ENSG00000173436	-1.01324	0.000722	0.003862	MICOS10	DOWN
165.	ENSG00000174306	-1.06005	2.42E-08	4.31E-07	ZHX3	DOWN
166.	ENSG00000174574	-1.07267	1.24E-23	1.94E-21	AKIRIN1	DOWN
167.	ENSG00000174996	-1.01445	5.64E-19	5.84E-17	KLC2	DOWN
168.	ENSG00000175283	-1.30299	6.17E-14	3.09E-12	DOLK	DOWN
169.	ENSG00000175348	-1.05266	2.38E-10	6.40E-09	TMEM9B	DOWN
170.	ENSG00000176396	-1.1542	1.79E-11	5.82E-10	EID2	DOWN
171.	ENSG00000177875	-1.03287	2.42E-08	4.31E-07	CCDC184	DOWN
172.	ENSG00000178623	-1.34224	0.002336	0.010447	GPR35	DOWN
173.	ENSG00000178718	-1.03358	2.46E-14	1.31E-12	RPP25	DOWN
174.	ENSG00000179918	-1.22334	2.60E-25	5.15E-23	SEPHS2	DOWN
175.	ENSG00000180423	-1.01157	0.001589	0.007513	HARBI1	DOWN
176.	ENSG00000181061	-1.0724	1.84E-14	1.01E-12	HIGD1A	DOWN
177.	ENSG00000181773	-1.18185	0.000193	0.001233	GPR3	DOWN
178.	ENSG00000181817	-1.15116	2.08E-11	6.60E-10	LSM10	DOWN
179.	ENSG00000182175	-1.0433	1.96E-05	0.000169	RGMA	DOWN
180.	ENSG00000182199	-1.06104	3.70E-24	6.08E-22	SHMT2	DOWN
181.	ENSG00000182481	-1.10638	6.36E-36	3.18E-33	KPNA2	DOWN
182.	ENSG00000182544	-1.09965	1.14E-10	3.24E-09	MFSD5	DOWN
183.	ENSG00000183682	-1.84708	0.001265	0.006226	BMP8A	DOWN
184.	ENSG00000184207	-1.08018	5.10E-10	1.31E-08	PGP	DOWN
185.	ENSG00000184602	-1.5876	4.24E-39	2.56E-36	SNN	DOWN
186.	ENSG00000184678	-1.10222	0.000551	0.003055	H2BC21	DOWN
187.	ENSG00000184986	-1.47543	7.94E-12	2.76E-10	TMEM121	DOWN
188.	ENSG00000185115	-1.02131	2.19E-12	8.60E-11	NSMCE3	DOWN
189.	ENSG00000185340	-1.16697	1.68E-13	7.92E-12	GAS2L1	DOWN
190.	ENSG00000185838	-1.01686	7.90E-07	9.95E-06	GNB1L	DOWN
191.	ENSG00000186283	-1.12026	7.69E-16	5.03E-14	TOR3A	DOWN
192.	ENSG00000186350	-1.1071	8.66E-12	2.99E-10	RXRA	DOWN
193.	ENSG00000186594	-2.01504	3.86E-09	8.31E-08	MIR22HG	DOWN
194.	ENSG00000188229	-1.31699	9.22E-49	1.33E-45	TUBB4B	DOWN
195.	ENSG00000188486	-1.07656	4.61E-29	1.28E-26	H2AX	DOWN
196.	ENSG00000188763	-1.45356	9.82E-12	3.31E-10	FZD9	DOWN
197.	ENSG00000196517	-3.3239	9.93E-15	5.70E-13	SLC6A9	DOWN
198.	ENSG00000196581	-1.44506	4.11E-09	8.74E-08	AJAP1	DOWN
199.	ENSG00000196843	-1.38737	3.16E-05	0.000255	ARID5A	DOWN
200.	ENSG00000196850	-1.10572	5.25E-15	3.12E-13	PPTC7	DOWN
201.	ENSG00000196972	-1.01844	0.012355	0.041544	SMIM10L2B	DOWN
202.	ENSG00000197019	-1.46013	0.000693	0.003727	SERTAD1	DOWN

203.	ENSG00000197451	-1.41634	9.16E-41	7.80E-38	HNRNPAB	DOWN
204.	ENSG00000197798	-1.51533	1.53E-15	9.74E-14	FAM118B	DOWN
205.	ENSG00000198018	-1.1867	4.05E-09	8.69E-08	ENTPD7	DOWN
206.	ENSG00000198431	-1.21447	1.15E-37	5.97E-35	TXNRD1	DOWN
207.	ENSG00000198435	-1.43014	1.00E-10	2.86E-09	NRARP	DOWN
208.	ENSG00000198736	-1.09575	1.46E-12	5.92E-11	MSRB1	DOWN
209.	ENSG00000198835	-1.72596	0.000533	0.002973	GJC2	DOWN
210.	ENSG00000198855	-1.64494	7.09E-07	9.05E-06	FICD	DOWN
211.	ENSG00000198934	-1.01712	2.52E-07	3.60E-06	MAGEE1	DOWN
212.	ENSG00000198948	-1.64637	5.28E-06	5.28E-05	MFAP3L	DOWN
213.	ENSG00000203993	-1.34447	1.25E-13	5.98E-12	ARRDC1-AS1	DOWN
214.	ENSG00000204103	-1.21661	0.014229	0.046634	MAFB	DOWN
215.	ENSG00000204388	-1.46297	6.75E-13	2.87E-11	HSPA1B	DOWN
216.	ENSG00000204389	-1.71095	6.55E-12	2.31E-10	HSPA1A	DOWN
217.	ENSG00000205670	-2.63732	5.68E-05	0.000425	SMIM11	DOWN
218.	ENSG00000211584	-1.16496	3.53E-11	1.08E-09	SLC48A1	DOWN
219.	ENSG00000214226	-1.19736	0.000998	0.005097	C17orf67	DOWN
220.	ENSG00000215301	-1.24248	1.11E-39	7.66E-37	DDX3X	DOWN
221.	ENSG00000216285	-1.23367	0.012485	0.041874	NA	DOWN
222.	ENSG00000226328	-1.16561	0.000209	0.001319	NUP50-DT	DOWN
223.	ENSG00000238227	-1.08184	6.55E-22	8.86E-20	TMEM250	DOWN
224.	ENSG00000241360	-1.65207	3.94E-19	4.16E-17	PDXP	DOWN
225.	ENSG00000247095	-1.67261	4.74E-06	4.80E-05	MIR210HG	DOWN
226.	ENSG00000248498	-1.7058	0.00014	0.000933	NA	DOWN
227.	ENSG00000254858	-1.71332	5.33E-15	3.15E-13	MPV17L2	DOWN
228.	ENSG00000256663	-1.12401	5.76E-05	0.00043	NA	DOWN
229.	ENSG00000259330	-1.91714	1.65E-27	4.12E-25	INAFM2	DOWN
230.	ENSG00000261061	-1.0489	0.003478	0.014591	NA	DOWN
231.	ENSG00000261342	-2.32735	2.49E-12	9.60E-11	NA	DOWN
232.	ENSG00000261578	-1.52688	3.26E-09	7.12E-08	NA	DOWN
233.	ENSG00000262454	-1.41144	0.013533	0.044685	MIR193BHG	DOWN
234.	ENSG00000262919	-1.19693	7.04E-11	2.06E-09	CCNQ	DOWN
235.	ENSG00000264278	-1.44263	0.01006	0.035169	ZNF236-DT	DOWN
236.	ENSG00000265282	-1.0681	0.005989	0.022966	NA	DOWN
237.	ENSG00000265763	-1.07461	0.012663	0.042369	ZNF488	DOWN
238.	ENSG00000265806	-1.71815	0.004201	0.017126	MIR4292	DOWN
239.	ENSG00000271303	-1.26478	2.48E-05	0.000208	SRXN1	DOWN
240.	ENSG00000272077	-1.31078	5.19E-06	5.20E-05	NA	DOWN
241.	ENSG00000272899	-1.20344	4.40E-05	0.000339	ATP6V1FNB	DOWN
242.	ENSG00000273270	-1.07823	1.98E-15	1.22E-13	NA	DOWN
243.	ENSG00000273604	-1.12997	8.86E-15	5.11E-13	EPOP	DOWN
244.	ENSG00000275063	-1.07152	0.010325	0.03598	LOC102723407	DOWN

245.	ENSG00000276023	-1.19232	2.09E-08	3.81E-07	DUSP14	DOWN
246.	ENSG00000276043	-1.14995	6.22E-20	7.03E-18	UHRF1	DOWN
247.	ENSG00000277147	-1.18848	0.011439	0.039055	NA	DOWN
248.	ENSG00000279108	-1.23544	0.005177	0.020306	NA	DOWN
249.	ENSG00000279207	-1.41741	2.32E-11	7.36E-10	NA	DOWN
250.	ENSG00000279348	-1.20565	9.71E-05	0.000674	NA	DOWN
251.	ENSG00000279821	-1.34765	0.009917	0.034786	NA	DOWN

Appendix 3: RapaLink-1 vs Control differentially expressed upregulated genes (128 genes)

	Ensembl gene ID	log2FoldChange	p-value	padj	symbol	diff.expressed
1.	ENSG00000006652	0.783643	1.76E-16	8.83E-14	IFRD1	UP
2.	ENSG00000007392	0.601118	1.38E-07	1.77E-05	LUC7L	UP
3.	ENSG00000025708	0.691943	0.000478	0.011376	TYMP	UP
4.	ENSG00000080947	0.727138	0.003694	0.045773	NA	UP
5.	ENSG00000088340	0.600894	0.001447	0.024648	FER1L4	UP
6.	ENSG00000092094	0.693229	4.11E-06	0.000322	OSGEP	UP
7.	ENSG00000099869	0.64715	0.003153	0.040928	IGF2-AS	UP
8.	ENSG00000100263	0.613971	1.14E-05	0.00072	RHBDD3	UP
9.	ENSG00000102878	0.702123	8.30E-05	0.003259	HSF4	UP
10.	ENSG00000102890	0.990805	0.000386	0.009817	ELMO3	UP
11.	ENSG00000104899	0.805485	1.92E-19	1.16E-16	AMH	UP
12.	ENSG00000105771	0.63523	1.30E-06	0.000122	SMG9	UP
13.	ENSG00000107984	0.653897	2.69E-11	8.54E-09	DKK1	UP
14.	ENSG00000109758	1.026371	0.002223	0.032331	HGFAC	UP
15.	ENSG00000109927	0.767085	0.001589	0.026359	TECTA	UP
16.	ENSG00000111664	0.897259	0.003973	0.047942	GNB3	UP
17.	ENSG00000114841	0.629411	0.001316	0.023201	DNAH1	UP
18.	ENSG00000114857	0.649577	8.81E-10	2.36E-07	NKTR	UP
19.	ENSG00000115129	0.740164	6.15E-06	0.000438	TP53I3	UP
20.	ENSG00000116001	0.675313	1.14E-10	3.26E-08	TIA1	UP
21.	ENSG00000117480	0.65741	0.001533	0.025667	FAAH	UP
22.	ENSG00000117569	0.655406	3.66E-07	4.16E-05	PTBP2	UP
23.	ENSG00000117616	0.646151	4.12E-05	0.001921	RSRP1	UP
24.	ENSG00000120738	1.243543	1.20E-11	4.02E-09	EGR1	UP
25.	ENSG00000126522	0.613816	6.30E-05	0.002686	ASL	UP
26.	ENSG00000127863	0.644369	1.67E-11	5.44E-09	TNFRSF19	UP
27.	ENSG00000127920	0.676927	0.00326	0.041688	GNG11	UP
28.	ENSG00000131797	0.68705	0.00138	0.02374	NA	UP
29.	ENSG00000132522	0.693131	0.001513	0.025475	GPS2	UP
30.	ENSG00000132773	0.714784	1.52E-05	0.000915	TOE1	UP
31.	ENSG00000134343	0.666834	0.001512	0.025475	ANO3	UP
32.	ENSG00000135205	0.89397	0.001922	0.029602	CCDC146	UP
33.	ENSG00000135502	0.730599	0.000983	0.018935	SLC26A10P	UP
34.	ENSG00000136059	0.938951	1.17E-05	0.000737	VILL	UP
35.	ENSG00000136997	0.698578	4.59E-09	1.04E-06	MYC	UP

36.	ENSG00000139289	0.609461	0.000216	0.006477	PHLDA1	UP
37.	ENSG00000139292	0.664224	1.34E-14	5.99E-12	LGR5	UP
38.	ENSG00000140398	0.851409	0.00019	0.005926	NEIL1	UP
39.	ENSG00000140451	0.616254	0.000114	0.0041	PIF1	UP
40.	ENSG00000141391	0.734072	0.000708	0.015057	PRELID3A	UP
41.	ENSG00000147119	0.757244	1.35E-07	1.75E-05	CHST7	UP
42.	ENSG00000148357	0.610308	5.36E-06	0.000391	HMCN2	UP
43.	ENSG00000148824	1.065547	9.65E-05	0.003603	MTG1	UP
44.	ENSG00000152117	0.67633	1.69E-06	0.000148	SMPD4BP	UP
45.	ENSG00000153443	0.631838	2.00E-05	0.001124	UBALD1	UP
46.	ENSG00000156398	0.670168	0.003107	0.040805	SFXN2	UP
47.	ENSG00000159387	0.760825	0.000287	0.007955	IRX6	UP
48.	ENSG00000160072	0.676925	3.78E-08	6.07E-06	ATAD3B	UP
49.	ENSG00000160766	0.751907	0.000295	0.008092	NA	UP
50.	ENSG00000161010	0.661724	2.60E-06	0.000216	MRNIP	UP
51.	ENSG00000162004	0.970398	1.40E-05	0.000868	CCDC78	UP
52.	ENSG00000166140	0.638972	6.67E-05	0.002801	ZFYVE19	UP
53.	ENSG00000167302	0.847585	9.18E-06	0.000611	TEPSIN	UP
54.	ENSG00000168348	1.103896	8.69E-30	1.05E-26	INSM2	UP
55.	ENSG00000168830	0.668021	0.00339	0.043151	HTR1E	UP
56.	ENSG00000170049	0.648909	0.000572	0.013061	KCNAB3	UP
57.	ENSG00000171045	0.731691	5.37E-05	0.002372	TSNARE1	UP
58.	ENSG00000173137	0.835715	0.00016	0.005283	ADCK5	UP
59.	ENSG00000175265	0.773541	0.00028	0.007808	GOLGA8A	UP
60.	ENSG00000178381	0.838924	8.20E-07	8.31E-05	ZFAND2A	UP
61.	ENSG00000178623	0.952975	0.00075	0.015621	GPR35	UP
62.	ENSG00000181274	0.732254	9.28E-07	9.25E-05	FRAT2	UP
63.	ENSG00000182685	0.703022	0.0041	0.049139	BRICD5	UP
64.	ENSG00000182983	0.653629	0.000322	0.008608	ZNF662	UP
65.	ENSG00000185262	0.600636	1.93E-07	2.35E-05	UBALD2	UP
66.	ENSG00000185339	0.805736	0.003421	0.043465	TCN2	UP
67.	ENSG00000186166	0.778192	0.000168	0.005454	CENATAC	UP
68.	ENSG00000187634	0.950458	0.000221	0.00655	SAMD11	UP
69.	ENSG00000188234	0.815887	1.13E-05	0.00072	AGAP4	UP
70.	ENSG00000196296	0.695798	0.000852	0.017092	ATP2A1	UP
71.	ENSG00000196421	0.790184	0.003652	0.045582	C20orf204	UP
72.	ENSG00000196656	1.010014	4.75E-08	7.35E-06	NA	UP
73.	ENSG00000197182	1.26721	1.66E-07	2.08E-05	MIRLET7BHG	UP
74.	ENSG00000197308	0.700318	0.000222	0.006567	GATA3-AS1	UP
75.	ENSG00000197774	0.735192	0.000618	0.013711	EME2	UP
76.	ENSG00000197818	0.683678	2.61E-05	0.001411	SLC9A8	UP
77.	ENSG00000198563	0.646081	1.03E-11	3.54E-09	DDX39B	UP
78.	ENSG00000198695	0.877625	1.21E-23	9.70E-21	ND6	UP

79.	ENSG00000198712	0.868541	2.38E-35	4.79E-32	COX2	UP
80.	ENSG00000198727	0.941906	5.92E-35	8.92E-32	CYTB	UP
81.	ENSG00000198763	0.989252	4.22E-44	5.09E-40	ND2	UP
82.	ENSG00000198786	0.852367	6.55E-30	8.78E-27	ND5	UP
83.	ENSG00000198804	0.840413	5.17E-35	8.90E-32	COX1	UP
84.	ENSG00000198886	0.858094	2.94E-36	8.86E-33	ND4	UP
85.	ENSG00000198888	0.927607	1.28E-39	7.69E-36	ND1	UP
86.	ENSG00000198899	0.896415	4.56E-36	1.10E-32	ATP6	UP
87.	ENSG00000198938	0.874224	4.76E-37	1.91E-33	COX3	UP
88.	ENSG00000204149	0.685018	2.52E-05	0.001376	AGAP6	UP
89.	ENSG00000204172	0.845813	0.000145	0.004918	AGAP9	UP
90.	ENSG00000204305	0.775902	0.001365	0.023604	AGER	UP
91.	ENSG00000204316	0.785177	0.002119	0.031547	MRPL38	UP
92.	ENSG00000204859	0.677705	1.41E-06	0.000128	ZBTB48	UP
93.	ENSG00000209082	1.172682	4.72E-05	0.002137	NA	UP
94.	ENSG00000210082	0.725362	2.21E-27	1.90E-24	NA	UP
95.	ENSG00000210140	0.850386	9.30E-17	4.88E-14	NA	UP
96.	ENSG00000210144	0.667961	0.000385	0.009817	NA	UP
97.	ENSG00000211459	0.609608	3.69E-18	2.12E-15	NA	UP
98.	ENSG00000212694	0.692851	0.000393	0.009939	LINC01089	UP
99.	ENSG00000212907	0.855067	3.06E-29	3.33E-26	ND4L	UP
100	ENSG00000213903	0.74218	0.00119	0.021737	LTB4R	UP
101	ENSG00000214176	0.656209	0.000793	0.016295	NA	UP
102	ENSG00000221978	0.619286	6.69E-11	2.02E-08	CCNL2	UP
103	ENSG00000224660	0.807817	0.0003	0.008182	SH3BP5-AS1	UP
104	ENSG00000225630	0.960991	1.78E-19	1.13E-16	MTND2P28	UP
105	ENSG00000225756	0.949796	6.35E-12	2.25E-09	DBH-AS1	UP
106	ENSG00000227063	0.621733	0.003261	0.041688	NA	UP
107	ENSG00000227719	1.443909	4.97E-09	1.11E-06	NA	UP
108	ENSG00000228253	1.174258	6.40E-11	1.98E-08	ATP8	UP
109	ENSG00000230630	0.609575	0.002111	0.031533	NA	UP
110	ENSG00000233016	0.601096	1.14E-06	0.000111	SNHG7	UP
111	ENSG00000234912	0.893029	0.000359	0.009298	SNHG20	UP
112	ENSG00000237973	1.162819	1.60E-15	7.42E-13	MTCO1P12	UP
113	ENSG00000243716	0.703615	6.52E-09	1.37E-06	NPIPB5	UP
114	ENSG00000246859	0.705945	6.61E-09	1.37E-06	STARD4-AS1	UP
115	ENSG00000248527	1.049485	3.31E-29	3.33E-26	MTATP6P1	UP
116	ENSG00000250979	0.836622	5.75E-05	0.002494	NA	UP
117	ENSG00000253230	1.098541	2.61E-08	4.44E-06	MIR124-1HG	UP
118	ENSG00000258947	0.680572	0.000423	0.010492	TUBB3	UP
119	ENSG00000258986	0.75259	5.64E-08	8.51E-06	TMEM179	UP
120	ENSG00000259031	1.138927	8.33E-05	0.003261	NA	UP
121	ENSG00000259865	0.680275	0.002699	0.036802	NA	UP

122	ENSG00000260518	0.780648	0.001463	0.024768	NA	UP
123	ENSG00000261326	0.882288	0.003937	0.047708	NA	UP
124	ENSG00000264112	1.007789	2.06E-12	8.27E-10	NA	UP
125	ENSG00000269858	0.928696	0.000952	0.018574	EGLN2	UP
126	ENSG00000271533	1.0691	0.00019	0.005926	NA	UP
127	ENSG00000279382	1.276266	3.92E-05	0.001865	NA	UP
128	ENSG00000284976	0.759151	2.61E-08	4.44E-06	LOC122513141	UP

Appendix 4: RapaLink-1 vs Control differentially expressed downregulated genes (41 genes)

	Ensembl gene ID	log2FoldChange	p-value	padj	symbol	diff.expressed
1.	ENSG00000006283	-0.65672	0.000175	0.005602	CACNA1G	DOWN
2.	ENSG00000065060	-0.64453	9.27E-09	1.80E-06	BLTP3A	DOWN
3.	ENSG00000070669	-0.82665	0.002086	0.031364	ASNS	DOWN
4.	ENSG00000090861	-0.65349	3.79E-17	2.08E-14	AARS1	DOWN
5.	ENSG00000095596	-0.62431	2.51E-07	2.94E-05	CYP26A1	DOWN
6.	ENSG00000100234	-0.72903	8.78E-08	1.20E-05	TIMP3	DOWN
7.	ENSG00000103257	-0.88812	8.89E-28	8.24E-25	SLC7A5	DOWN
8.	ENSG00000106105	-0.75406	4.45E-22	3.36E-19	GARS1	DOWN
9.	ENSG00000113739	-1.09256	4.51E-12	1.75E-09	STC2	DOWN
10.	ENSG00000119138	-0.89894	0.000207	0.006296	KLF9	DOWN
11.	ENSG00000128165	-0.94563	4.00E-07	4.50E-05	ADM2	DOWN
12.	ENSG00000128283	-0.61031	0.004035	0.048506	CDC42EP1	DOWN
13.	ENSG00000128965	-2.26869	1.51E-21	1.07E-18	CHAC1	DOWN
14.	ENSG00000129244	-0.82236	4.21E-05	0.001951	ATP1B2	DOWN
15.	ENSG00000130766	-0.71683	2.09E-08	3.76E-06	SESN2	DOWN
16.	ENSG00000135069	-0.82846	2.01E-20	1.35E-17	PSAT1	DOWN
17.	ENSG00000136010	-0.70502	1.18E-05	0.000742	ALDH1L2	DOWN
18.	ENSG00000140044	-0.93058	0.001453	0.024691	JDP2	DOWN
19.	ENSG00000141682	-0.62034	8.85E-07	8.89E-05	PMAIP1	DOWN
20.	ENSG00000148200	-0.69896	0.003017	0.039924	NR6A1	DOWN
21.	ENSG00000149527	-0.72268	2.62E-09	6.08E-07	PLCH2	DOWN
22.	ENSG00000151012	-0.96484	3.85E-05	0.001848	SLC7A11	DOWN
23.	ENSG00000151136	-0.65461	7.41E-05	0.003018	ABTB3	DOWN

24.	ENSG00000151718	-0.63599	0.000249	0.007127	WWC2	DOWN
25.	ENSG00000160179	-0.6688	0.000703	0.014972	ABCG1	DOWN
26.	ENSG00000162433	-0.68261	5.24E-06	0.000388	AK4	DOWN
27.	ENSG00000162772	-0.67406	1.42E-05	0.000873	ATF3	DOWN
28.	ENSG00000163629	-0.61181	4.29E-06	0.000331	PTPN13	DOWN
29.	ENSG00000164070	-0.65082	6.54E-08	9.50E-06	HSPA4L	DOWN
30.	ENSG00000168209	-1.53791	2.24E-16	1.08E-13	DDIT4	DOWN
31.	ENSG00000168918	-0.68035	2.56E-06	0.000214	INPP5D	DOWN
32.	ENSG00000171368	-0.62092	0.000429	0.010584	TPPP	DOWN
33.	ENSG00000172216	-0.98944	4.34E-08	6.79E-06	CEBPB	DOWN
34.	ENSG00000175928	-0.69108	0.000372	0.009563	LRRN1	DOWN
35.	ENSG00000176438	-0.67026	0.001121	0.021024	SYNE3	DOWN
36.	ENSG00000196517	-0.89424	0.00184	0.028884	SLC6A9	DOWN
37.	ENSG00000198756	-0.9001	7.10E-05	0.002952	COLGALT2	DOWN
38.	ENSG00000204131	-0.77045	0.000277	0.007737	NHSL2	DOWN
39.	ENSG00000230383	-0.64494	0.002157	0.031825	RPL6P19	DOWN
40.	ENSG00000255650	-0.73799	0.003141	0.040928	FAM222A-AS1	DOWN
41.	ENSG00000270533	-1.00402	0.000816	0.01658	NA	DOWN

Appendix 5: Table displaying the names of the common genes from both datasets.

(Supplementary table for the Venn Diagram)

	R vs C and T vs C common upregulated genes	**R vs C and T vs C common downregulated regulated genes**	**R vs C upregulated and T vs C downregulated common genes**
1.	IFRD1	AARS1	GPR35
2.	DKK1	SLC7A5	
3.	VILL	GARS1	
4.	MYC	STC2	
5.	PHLDA1	ADM2	
6.	PRELID3A	CHAC1	
7.	IRX6	SESN2	
8.	INSM2	PSAT1	
9.	ZFAND2A (AIRAP)	JDP2	
10.	TCN2	PMAIP1	
11.	ENSG00000227719	SLC7A11	
12.	STARD4-AS1	DDIT4	
13.	TEC	CEBPB	
14.		SLC6A9	